Copyright Warning & Restrictions

The copyright law of the United States (Title 17, United States Code) governs the making of photocopies or other reproductions of copyrighted material.

Under certain conditions specified in the law, libraries and archives are authorized to furnish a photocopy or other reproduction. One of these specified conditions is that the photocopy or reproduction is not to be "used for any purpose other than private study, scholarship, or research." If a, user makes a request for, or later uses, a photocopy or reproduction for purposes in excess of "fair use" that user may be liable for copyright infringement,

This institution reserves the right to refuse to accept a copying order if, in its judgment, fulfillment of the order would involve violation of copyright law.

Please Note: The author retains the copyright while the New Jersey Institute of Technology reserves the right to distribute this thesis or dissertation

Printing note: If you do not wish to print this page, then select "Pages from: first page # to: last page #" on the print dialog screen

68-16,973

LOVENGUTH, Ronald Francis, 1941-
BOILING HEAT TRANSFER IN THE PRESENCE OF ELECTRIC FIELDS.

Newark College of Engineering, D. Eng.Sc., 1968
Engineering, chemical

University Microfilms, Inc., Ann Arbor, Michigan

BOILING HEAT TRANSFER IN THE PRESENCE OF ELECTRIC FIELDS

BY

RONALD F. LOVENGUTH

A DISSERTATION

PRESENTED IN PARTIAL FULFILLMENT OF

THE REQUIREMENTS FOR THE DEGREE

OF

DOCTOR OF ENGINEERING SCIENCE

AT

NEWARK COLLEGE OF ENGINEERING

Newark, New Jersey

1968

APPROVAL OF DISSERTATION

BOILING HEAT TRANSFER IN THE

PRESENCE OF ELECTRIC FIELDS

BY

RONALD F. LOVENGUTH

FOR

DEPARTMENT OF CHEMICAL ENGINEERING

NEWARK COLLEGE OF ENGINEERING

BY

FACULTY COMMITTEE

APPROVED: _____ CHAIRMAN

_____

_____

_____

_____

NEWARK, NEW JERSEY

JUNE, 1968

ABSTRACT

The effects of a non-uniform, radial, D.C. electric field on the natural convection and nucleate boiling regimes in saturated pool boiling and on the peak heat flux phenomenon were determined for trichlorotrifluoroethane, carbon tetrachloride, dichloromonofluoromethane and chloroform using as a heat transfer surface a 0.02 inch diameter platinum wire.

Bubble departure diameters for the nucleate boiling region were measured by photographic means as a function of the electric field intensity at the heat transfer surface.

The application of an electric field was found to have a significant effect on the natural convection mode of heat transfer and also the peak heat flux phenomenon. Three fold increases in the peak heat flux are not uncommon. The high dielectric constant fluids exhibit a greater increase in heat transfer per unit electric stress.

The experimental increases in the peak heat flux phenomenon were quantitatively and mechanistically explained by the model of an electrically stabilized Helmholtz-Taylor hydrodynamic condition.

The use of an "equivalent electric field" postulation was found to be useful for interpreting data obtained using non-uniform electric fields.

Complete boiling curves were obtained for the four fluids as a function of the electric field intensity at the heat transfer surface.

ACKNOWLEDGEMENTS

The author wishes to acknowledge the assistance, guidance, and direction given to him by Dr. Deran Hanesian during the course of this dissertation.

The author would also like to thank Mr. Anthony La Sala and Mr. Louis Guino for their help in constructing the experimental apparatus which was used in this work.

The author also expresses his sincere appreciation to his wife for her assistance and encouragement which made the completion of this dissertation possible.

The financial assistance afforded the author through the reception of both a National Defense Education Act and American Cyanamid Fellowship during the course of his studies is also sincerely acknowledged.

TABLE OF CONTENTS

TABLE OF CONTENTS Cont'd.

LIST OF FIGURES

LIST OF FIGURES Cont'd

LIST OF FIGURES Cont'd

LIST OF TABLES

CHAPTER I

INTRODUCTION

Scope and Purpose of Investigation

The effect of electrostatic fields on boiling heat transfer was brought to the author's attention by a publication of Markels and Durfee[14] which described the action of applied voltage on the pool boiling characteristics of water and isopropanol. In their work, effects were noted for the nucleate and film boiling regimes. There were also large increases in the peak heat flux. A further literature study in this area showed that other authors[3,5] had also investigated these effects; but neither a suitable explanation of the mechanisms involved nor an adequate quantitative prediction of the observed effects was offered. Of particular interest to this author, was the effect on the peak heat flux phenomenon. This phenomenon was by far the most dramatic and the most important effect. In some cases a five-fold increase was recorded with the applied voltage seemingly the only limitation. Subsequently, a program was developed to investigate the subject in more detail by experiment. In this respect, the recommendations of Choi[5] were followed with regard to studying the effect of an electrostatic field on high dielectric constant fluids. In addition to supplementing the sparse experimental data on this subject, the author hoped, that perhaps a quantitative expression for the peak heat

flux might evolve, either through a theoretical, semi-theoretical or an empirical approach. To this end, Choi's experimental apparatus[5] was chosen because of its availability, reliability, and simplicity. The initial overall plan of the investigation was then:

(1) to acquire additional data on the effects of electrostatic fields on boiling heat transfer to varying dielectric constant fluids.

(2) to attempt to define quantitatively the effects observed on the normal boiling curve, particularly the peak heat flux.

(3) to obtain visual observations of the boiling process, in particular, bubble shapes.

Literature Survey

Extensive reviews on the various regimes associated with boiling heat transfer are to be found in the literature[16, 19, 24, 11]. The list of references is large, mainly due to the complexities of the mechanisms involved, and to the various methods employed to increase heat transfer in any one of the three regimes. One of these methods is the application of electric fields. A review[2] has recently been compiled concerning this method.

Initially it is important to recognize the electrical forces and fluid interactions associated with increases in heat

transfer. Regarding this aspect, Pohl[18] described certain phenomenon occuring in dielectric liquids as a result of impressed fields. The observed effects were related to two electrical forces which he termed "dielectrophoresis" and "electrophoresis". Dielectrophoresis was defined as the tendency of matter to become polarized and move to regions of highest field strength. This effect requires a non-uniform electric field. The term electrophoresis was described as the electrostatic attraction of charged particles for charged electrodes. This effect operates in both uniform and in non-uniform electric fields.

Surface interactions of fluids stressed by electric fields have been theoretically and experimentally described by Melcher[15]. These effects, termed electrohydrodynamic (EHD) surface waves, are similar to the familar capillary and gravity waves discussed in hydrodynamic texts. Several types of these wave form interactions have been investigated by other authors[6,12,13] both experimentally and theoretically. Depending on the electrical field geometry and on the presence or absence of free charges or currents at the fluid interface, the electric field may either stabilize or destabilize a fluid interface.

Specific increases in heat transfer have been noted by Senftleben and Braun[21] who studied free convection of gases from a heated wire placed in the center of a horizontal cylinder. Appli-

cation of an electric field between the wire and the cylinder resulted in heat transfer increases of nearly fifty per cent, depending upon whether or not the gas was paraelectric (molecules that carry a permanent dipole). Schmidt and Leidenfrost[20] studied the natural convection of non-conducting oils (parafin, beeswax, castor oil) in strong electric fields. The increases reported were shown to result from the formation of charged "balls" of fluid, with the resulting electrostatic bulk forces contributing to the observed heat transfer increases.

In the case of saturated pool boiling heat transfer, Bonjour et al.[3] reported that impressed fields caused increased heat transfer coefficients to boiling fluids, particularly in the natural convection zone and at the peak heat flux. The geometry of their experiment consisted of a pair of parallel wires with an impressed A.C. voltage between them. The increase in heat transfer was attributed to the phenomenon of dielectrophoresis.

Later Choi[5] corroborated Bonjour's results. He employed a cylindrical geometry and a direct current voltage. He studied the fluid trichlorotrifluoroethane ("Freon 113"). He also attributed the increases in the different regimes to the dielectrophoresis force. Choi postulated an electrical gravity equivalent to account for these effects. He accomplished this by dividing the volume force associated with dielectrophoresis by the liquid density of the fluid.

As mentioned previously, Markels and Durfee[14] ascertained the effects of applied voltage on pool boiling of isopropanol and water for a steam heated tube. They attributed the heat transfer increases, mainly the peak heat flux, to the increased wetting of the tube surface and the voltage drop across the region of vapor formation (condenser effect).

Recently, Victor Asch[1] showed that pool boiling heat transfer to trichlorotrifluoroethane and the attendent increase in the peak heat flux was the result of electrophoresis, not of dielectrophoresis. He studied the effect of both A.C. and D.C. fields on the peak heat flux of trichlorotrifluoroethane.

In all of the works reported above, only Choi[5] with his theory of an equivalent gravity field, based on the "Dielectrophoretic force effect", offered a mechanistic interpretation and a quantitative expression for the observed effects on the peak heat flux phenomenon. To date, there is no accurate picture of the mechanism involved, nor is there a predictor equation for the increase in the peak heat flux by the action of an electric field.

This study is then another effort to ascertain the mechanism of the phenomena involved, and to offer a quantitative equation to predict the increase in the peak heat flux of various fluids with an attendent electric field.

CHAPTER II

THEORY

Boiling Heat Transfer Curve

The study of boiling heat transfer begins with an understanding of the now rather generalized boiling heat transfer curve.

The different regimes shown in Figure 1 (AB, BC, CD, and DE) represent different heat transfer mechanisms. Region AB is the natural convection zone. Nucleate boiling, or the formation of bubbles at the heater surface, begins at point B and continues to point C. At low heat fluxes, bubbles grow at preferred sites on the heater surface. As the wall temperature increases, more nucleation sites are activated and the heating surface becomes covered with bubbles. Point C is a critical point. Here the bubbles are so numerous that they coalesce and partially blanket the surface with a vapor film. With wires, this usually results in a condition called "burnout" because the onset of film boiling brings about a decrease in the overall heat transfer coefficient resulting in a rapid accumulation of heat in the wire which is usually sufficient to melt the wire. In the region CD, called the transition state, both nucleate boiling and film

FIGURE 1

BOILING HEAT TRANSFER CURVE

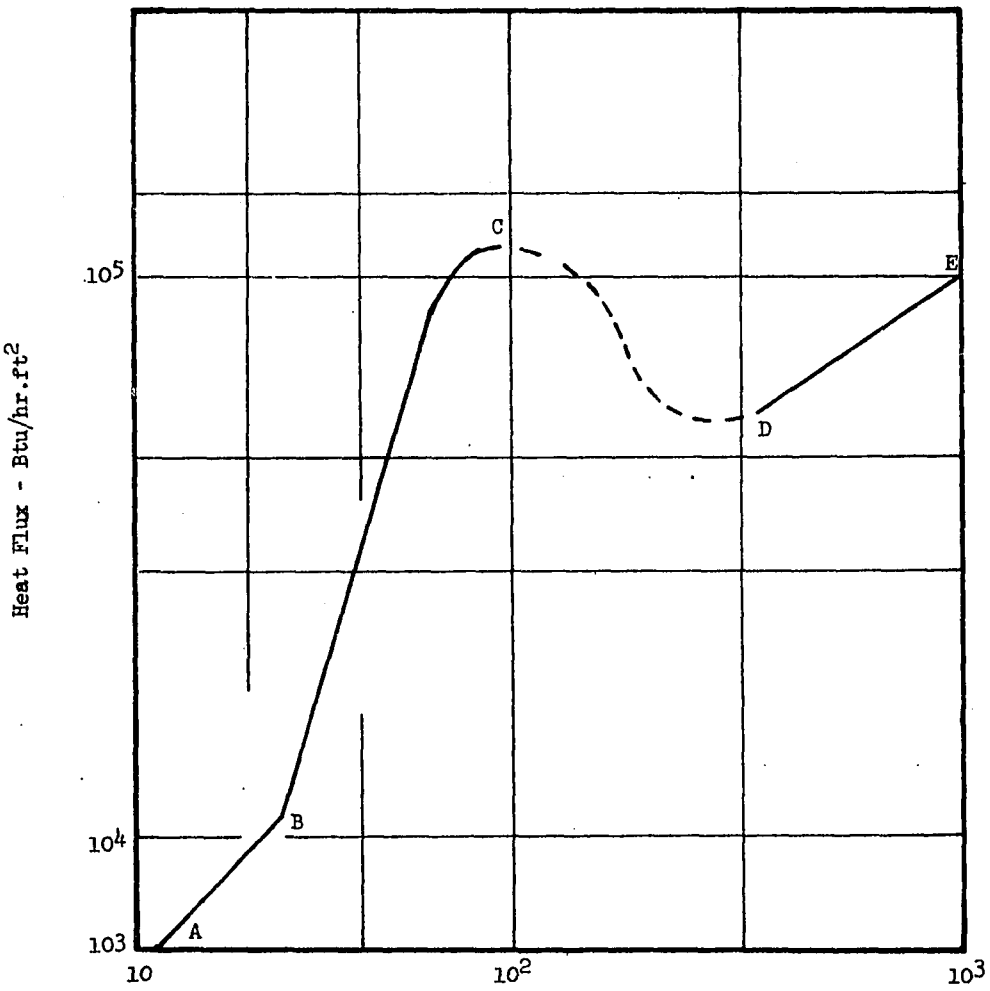

boiling are evident on sections of the heater surface. This region is usually studied by the use of condensing vapors as a source of heat due to the rapid transition from point C to point D experienced by the wires. Region DE, the film boiling range, is characterized by a total vapor film covering the heating surface with bubble formation at the vapor-liquid interface. The wall temperatures are correspondingly very high.

From an engineering standpoint, the prediction of the peak heat flux (point C) is important in order to define the limit of actual operating conditions (nucleate boiling regime). Points to the right of the critical heat flux result in decreased efficiency in operations and in possible damage to heaters as in the case of wires. Therefore a prediction of the critical heat flux from physical data of the fluid without recourse to actual experimentation has been the object of many researchers. The following paragraphs will show the prediction of the critical heat flux and its subsequent increase by an electric field based on a hydrodynamic approach.

Hydrodynamic Model for Peak Heat Flux

As early as 1951, Kutateladze[9] suggested that hydrodynamic conditions were responsible for the peak heat flux phenomenon.

By dimensional analysis he derived the following expression,

$$\frac{(Q/A)_{max}}{h_v \rho_v} = 0.16 \left[\frac{\sigma g (\rho_L - \rho_v)}{\rho_v^2}\right]^{1/4} \quad (1)$$

the constant (0.16) being fitted from experimental data. In the English system of units the use of g_c will make Equation 1 dimensionally equal.

A few years later, Zuber and Tribus[26] specified that the specific fluid mechanisms responsible for the peak heat flux phenomenon were the combined Helmholtz-Taylor instabilities. They derived the following equation:

$$\frac{(Q/A)_{max}}{h_v \rho_v} = 0.13 \left[\frac{\sigma g (\rho_L - \rho_v)}{\rho_v^2}\right]^{1/4} \left[\frac{\rho_L}{\rho_L + \rho_v}\right]^{1/2} \quad (2)$$

the value 0.13 is a theoretical constant resulting from the Helmholtz-Taylor analysis. Recently Moisses and Berenson[16] produced another expression based on a similar Helmholtz-Taylor analysis:

$$\frac{(Q/A)_{max}}{h_v \rho_v} = 0.18 \left[\frac{\sigma g (\rho_L - \rho_v)}{\rho_v^2}\right]^{1/4} \left[\frac{1 + \left(\frac{\rho_v}{\rho_L}\right)^2}{1 + 2\left(\frac{\rho_v}{\rho_L}\right)^2 + \frac{\rho_v}{\rho_L}}\right]^{1/2} \quad (3)$$

The constant here (0.18) was fitted from experimental data. The last term in Equation 3 is usually about 1.0 at atmospheric conditions.

The following prediction of the critical heat flux is based upon the criterion of a Helmholtz-Taylor instability.

The derivation of Zuber[25] will be presented here.

When two immiscible fluids flow adjacent to each other along an interface as pictured in Figure 2, a maximum relative velocity exists above which a small disturbance will amplify and grow, and thus distort the flow. This phenomenon is known as a Helmholtz instability. According to Lamb[10] and to Zuber[25], the velocity of propagation C, of a surface wave along a vertical vapor jet of upward velocity V_g, with an accompanying downward liquid velocity V_l, is as follows, where σ is the surface tension, and ρ_l and ρ_v are the liquid and vapor densities, respectively:

$$C^2 = \left(\frac{N}{M}\right)^2 = \frac{\sigma M}{\rho_l + \rho_v} - \frac{\rho_l \rho_v}{(\rho_l + \rho_v)^2}\left[V_g - V_l\right]^2 \qquad (4)$$

The wave number M equals $2\pi/\lambda$, and the wave angular frequency N equals $2\pi/\lambda \times C$ equals MC.

The condition for a stable jet is that the wave angular frequency N be real.

$$C^2 = \left(\frac{N}{M}\right)^2 > 0 \qquad (5)$$

FIGURE 2

IDEALIZED FLOW MODEL FOR PEAK HEAT FLUX CONDITION
HELMHOLTZ-TAYLOR INSTABILITY ANALYSIS[25]

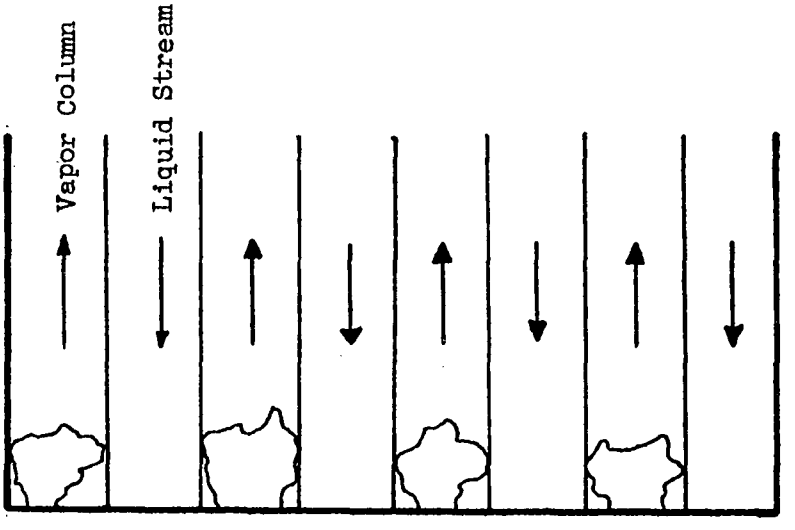

Equation 4 then gives:

$$\frac{\sigma M}{\rho_L+\rho_V} > \frac{\rho_L\rho_V}{(\rho_L+\rho_V)^2}\left[V_g - V_L\right]^2 \qquad (6)$$

If these terms are equated, Vg becomes Vg max for the Helmholtz analysis. For a steady state condition the equation of continuity gives:

$$\rho_L V_L + \rho_V V_g = 0 \qquad (7)$$

Substituting Equation 7 into Equation 6 then gives:

$$V_{g_{max}} = \left[\frac{\sigma M \rho_L}{\rho_V(\rho_L+\rho_V)}\right]^{1/2} \qquad (8)$$

The spacing of vapor release points is determined by the wave number for Taylor instability[25] of a liquid layer of semi-infinite extent lying over a lighter fluid which is also of semi-infinite extent. This maximum wave number is given below as follows by Zuber[25]:

$$M = \frac{2\pi}{\lambda} = \left|\frac{g(\rho_L-\rho_V)}{\sigma}\right|^{1/2} \qquad (9)$$

Finally, substituting Equation 9 into Equation 8 gives:

$$V_{g_{max}} = \left[\frac{\sigma g(\rho_L-\rho_V)}{\rho_V^2}\right]^{1/4}\left[\frac{\rho_L}{\rho_L+\rho_V}\right]^{1/2} \qquad (10)$$

Zuber relates the critical heat flux to the maximum gas velocity as follows: (From latent heat flow to vapor generated)

$$\left(\frac{Q}{A}\right)_{max} = \frac{\pi}{24} h_v \rho_v (V_{g_{max}}) \tag{11}$$

Equation 11, when coupled with the result of Equation 10 gives:

$$\frac{(Q/A)_{max}}{h_v \rho_v} = \frac{\pi}{24}\left[\frac{\sigma g(\rho_l - \rho_v)}{\rho_v^2}\right]^{1/4}\left[\frac{\rho_l}{\rho_l + \rho_v}\right]^{1/2} \tag{12}$$

This then is the predictor equation for the peak heat flux based on the Helmholtz-Taylor hydrodynamic instability analysis.

Electric Field Effect - Electrohydrodynamic Approach

It is postulated that the hydrodynamic model of the peak heat flux as previously discussed will be the same physically with the introduction of the electric field. There is evidence for this physical model based on previous work by Markels and Durfee[7].

> "Several correlations of the (Q/A) data . . . . with temperature difference, electrical voltage and current, and fluid properties were attempted but proved unsuccessful. The primary difficulty appears to be that the shape of the normal (Q/A) vs. ΔT curve persisted even at 10,000 volts. This characteristic shape is undoubtedly due to hydrodynamic functions."

Melcher[15] has shown that an electric field placed parallel to an interface has the effect of raising the wave angular frequency for waves of a given wavenumber M. Melcher's equation neglecting gravity and assuming infinite distance from external bounderies (these are the same assumptions made by Zuber in his analysis of the zero electric field case) is:

$$C^2 = \left(\frac{N}{M}\right)^2 = \frac{\sigma M}{\rho_2+\rho_1} + \frac{(\epsilon-\epsilon_0)^2 E^2}{(\epsilon+\epsilon_0)\rho_2} \qquad (13)$$

In Melcher's terminology this equation is referred to as an EH-II wave (EH being electrohydrodynamic). This equation is exactly analogous to Equation 4 with the fluids at rest. Initially it is assumed that the effects are additive, that the electric term in the above equation may be added to the two terms of Equation 4. This analysis then produces a Kelvin-Helmholtz instability equation which relates the stability of a wave under electric stress to the surface tension, relative velocity, and electric field. The following equation is then proposed for two fluids in relative motion coupled with an impressed parallel electric field:

$$C^2 = \left(\frac{N}{M}\right)^2 = \frac{\sigma M}{\rho_2+\rho_1} + \frac{(\epsilon-\epsilon_0)^2 E^2}{(\epsilon+\epsilon_0)\rho_2} - \frac{\rho_2\rho_1}{(\rho_2+\rho_1)^2}\left[V_g - V_2\right]^2 \qquad (14)$$

Proceeding as before; the condition for stability being that the wave angular frequency be real.

$$C^2 = \left(\frac{N}{M}\right)^2 > 0 \tag{5}$$

Equation 14 then gives:

$$\frac{\sigma M}{\rho_L + \rho_V} + \frac{(\varepsilon - \varepsilon_0)^2 E^2}{(\varepsilon + \varepsilon_0)\rho_L} > \frac{\rho_L \rho_V}{(\rho_L + \rho_V)^2}\left[V_g - V_L\right]^2 \tag{15}$$

Equating the two parts of Equation 15, Vg becomes Vgmax. Applying the continuity equation as before, namely that the total material reaching the wire equals the material leaving the wire, gives:

$$\rho_V V_g = -\rho_L V_L \tag{7}$$

The result of the Taylor instability analysis is:

$$M = \left|\frac{g(\rho_L - \rho_V)}{\sigma}\right|^{1/2} \tag{9}$$

Melcher[15] states that the wavenumber remains unchanged with the addition of the field intensity. Combining then Equations 15, 9, and 7 gives the critical vapor velocity in the presence of an electric field, namely:

$$V_{g_{max}} = \left[\left[\frac{\sigma^{1/2} g^{1/2} (\rho_L - \rho_V)^{1/2}}{\rho_V}\right]\left[\frac{\rho_L}{\rho_L + \rho_V}\right] + \frac{(\varepsilon - \varepsilon_0)^2 E^2}{(\varepsilon + \varepsilon_0)\rho_V}\right]^{1/2} \tag{16}$$

Substituting Equation 16 into Equation 11 results in the following equation for the critical heat flux:

$$\frac{(Q/A)_{max}}{h_v \rho_v} = C_1 \left[\frac{\sigma^{1/2} g^{1/2} (\rho_L - \rho_v)^{1/2}}{\rho_v} \left(\frac{\rho_L}{\rho_L + \rho_v} \right) + \frac{(\varepsilon - \varepsilon_0)^2 E^2}{\rho_v (\varepsilon + \varepsilon_0)} \right]^{1/2} \tag{17}$$

The electrical term may be placed in an alternate form since $\varepsilon = K\varepsilon_0$, where K equals the dielectric constant of the fluid, as shown below:

$$\frac{(\varepsilon - \varepsilon_0)^2 E^2}{(\varepsilon + \varepsilon_0)\rho_v} = \frac{\varepsilon_0 (K-1)^2 E^2}{\rho_v (K+1)} \tag{18}$$

Equation 17 may be rewritten:

$$\frac{(Q/A)_{max}}{h_v \rho_v} = C_1 \left| \frac{\sigma^{1/2} g^{1/2} (\rho_L - \rho_v)^{1/2}}{\rho_v} \left(\frac{\rho_L}{\rho_L + \rho_v} \right) + \frac{\varepsilon_0 (K-1)^2 E^2}{\rho_v (K+1)} \right|^{1/2} \tag{19}$$

Equation 19 predicts that the influence of a parallel electric field will be to increase the critical heat flux. Specifically, the electric field has the effect of increasing the relative velocity at which the Kelvin-Helmholtz instability occurs. The equation predicts a linear relationship between E and the peak heat flux when the electric term in Equation 19 is much greater than the non electric term. At low values of E deviation from linearity will occur. The original hydrodynamic model is still present since Equation 19 reduces to Equation 12 at zero electric field.

The above derivation has assumed that the dispersion equation (Equation 14) is applicable to a Kelvin-Helmholtz instability. An analogous solution[4] for the case of a parallel magnetic field yields an equivalent description; that is, that the Kelvin-Helmholtz instability will be suppressed by the action of a parallel magnetic field. It is further assumed that the electric field intensity is both constant and uniform; for non-uniform electric fields an average value of E (electric field intensity) might be sufficient for constant heat transfer system geometries.

Non-Uniform Electric Fields - Equivalent Field Postulation

Equation 19, as described and derived above, was based on the fact that a uniform D.C. electric field was stressing the vapor-liquid interface at the critical heat flux. It was noted in the assumptions above that perhaps an average or "equivalent electric field" could be postulated to account for the different electric geometry of non-uniform electric fields. This postulation arises because E_s (the electric field intensity at the heat transfer surface) is a maximum value for any given voltage difference for most non-uniform electric field geometries. Furthermore, E_s is not representative of the electric field intensities existing in the

immediate vicinity of the heat transfer surface. $E_{eq.}$ could then be defined as some average value between E_s and zero. Based on the above reasoning, an equivalent electric field intensity for non-uniform electric fields and constant heat transfer geometries was defined as:

$$E_{eq.} = C_o E_s \tag{20}$$

where $E_{eq.}$ = Equivalent electric field intensity (non-uniform electric fields),

where E_s = Electric field intensity at heat transfer surface,

where C_o = Constant factor, $(1 > C_o > 0)$

Equation 19 may then be rewritten for non-uniform electric fields as follows:

$$\frac{(Q/A)_{max}}{h_v \rho_v} = C_1 \left[\frac{\sigma^{1/2} g^{1/2} (\rho_L - \rho_v)^{1/2}}{\rho_v} \left(\frac{\rho_L}{\rho_L + \rho_v} \right) + \frac{\varepsilon_o (K-1)^2 (C_o E_s)^2}{\rho_v (K+1)} \right]^{1/2} \tag{21}$$

The increase in the peak heat flux in the presence of an electric field may now be obtained by differentiating Equation 21, where C, equals 0.18 based on experimental data[19].

$$\frac{d(Q/A)_{max}}{dE_s} = 0.18 h_v \rho_v \left[A + BE_s^2 \right]^{-1/2} \left[BE_s \right] \tag{21a}$$

where $$A = \frac{\sigma^{1/2} g^{1/2} (\rho_L - \rho_V)^{1/2}}{\rho_V} \left(\frac{\rho_L}{\rho_L + \rho_V} \right)$$

and $$B = \frac{\epsilon_0 (K-1)^2 C_0^2}{\rho_V (K+1)}$$

Equation 21a shows that as the electric term BE_s^2 becomes large relative to the A term the rate of increase of the peak heat flux approaches a constant value, as shown below:

$$\frac{d(q/A)_{max}}{dE_s} \cong 0.18 h_v \rho_V (B^{1/2}) \qquad (22)$$

This limiting rate on the peak heat flux increase in the presence of an electric field suggests that Equation 21 can be modified to an alternate form. In effect the hypothesis is made that the increase in the peak heat flux by the action of a non-uniform electric field can be quantitatively defined by Equation 22.

The final semi-theoretical equation proposed to estimate the peak heat flux of any fluid in the presence of a non-uniform electric field is obtained by integration of Equation 22 and allowing the constant of integration to be equal to the zero field peak heat flux given by Zuber[25]. This gives:

$$\frac{(q/A)_{max}}{h_v \rho_V (0.18)} = \left[\frac{\sigma^{1/2} g^{1/2} (\rho_L - \rho_V)^{1/2}}{\rho_V} \left(\frac{\rho_L}{\rho_L + \rho_V} \right) \right]^{1/2} + \left[\frac{\epsilon_0 (K-1)^2 C_0^2 E_s^2}{\rho_V (K+1)} \right]^{1/2} \qquad (23)$$

CHAPTER III

EXPERIMENTAL SYSTEM

Equipment Design

The overall design of the experimental system was governed by the following considerations:

1. a need for a reliable method for data collection in all three regimes of boiling: free convection, nucleate boiling, and film boiling.
2. a need for an electric field for which the electrical characteristics were well known mathematically.
3. a need for visual and photographic observation of the boiling phenomena, particularly the nucleate boiling regime.
4. a need of fool-proof safety features for the experimental apparatus because of the presence of high voltages and currents.

Experimental Apparatus and Instrumentation

Since Choi's[5] experimental design was available, and because with it the considerations discussed above were available with a minimum of material and parts, his experimental apparatus, with certain modifications, was chosen for this study of the effect of an electric field on boiling heat transfer. Figure 3 is a schematic

FIGURE 3

TEST SECTION SCHEMATIC

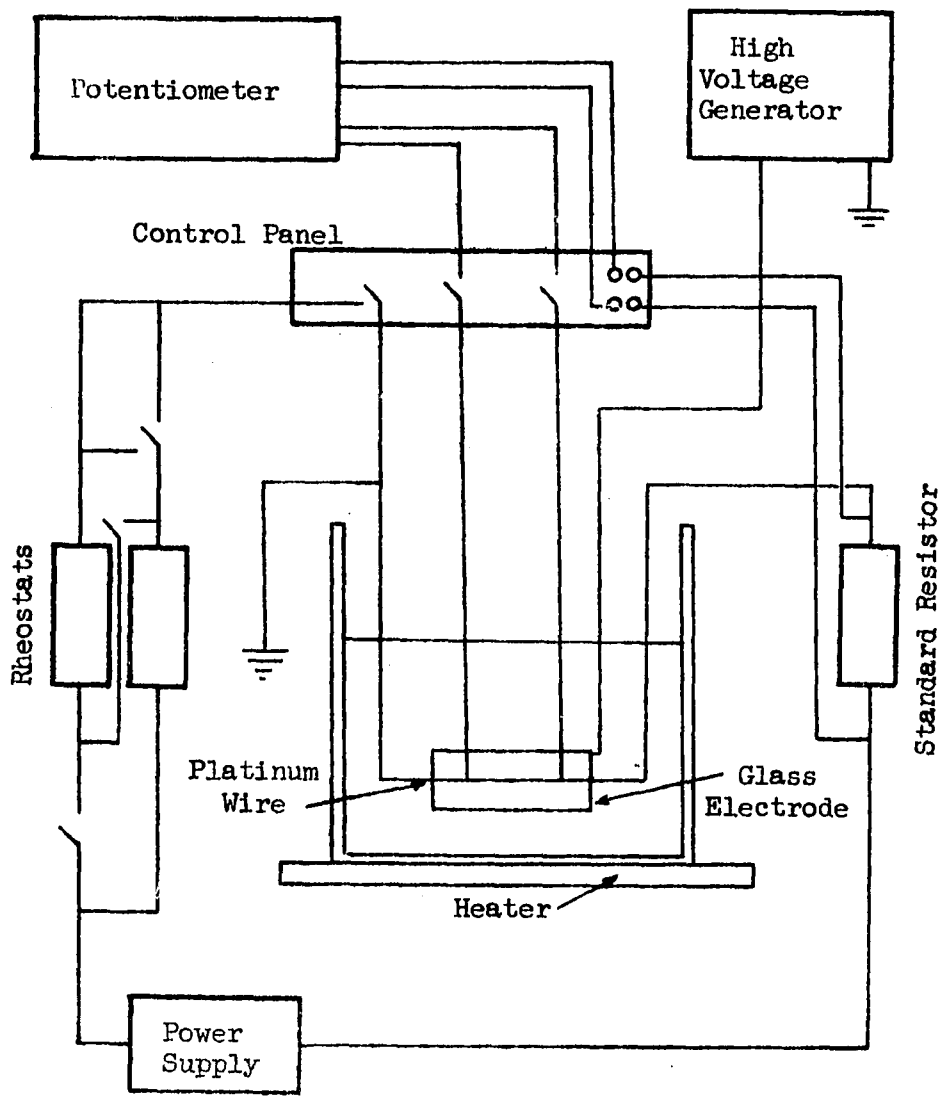

FIGURE 4

TEST SECTION ASSEMBLY

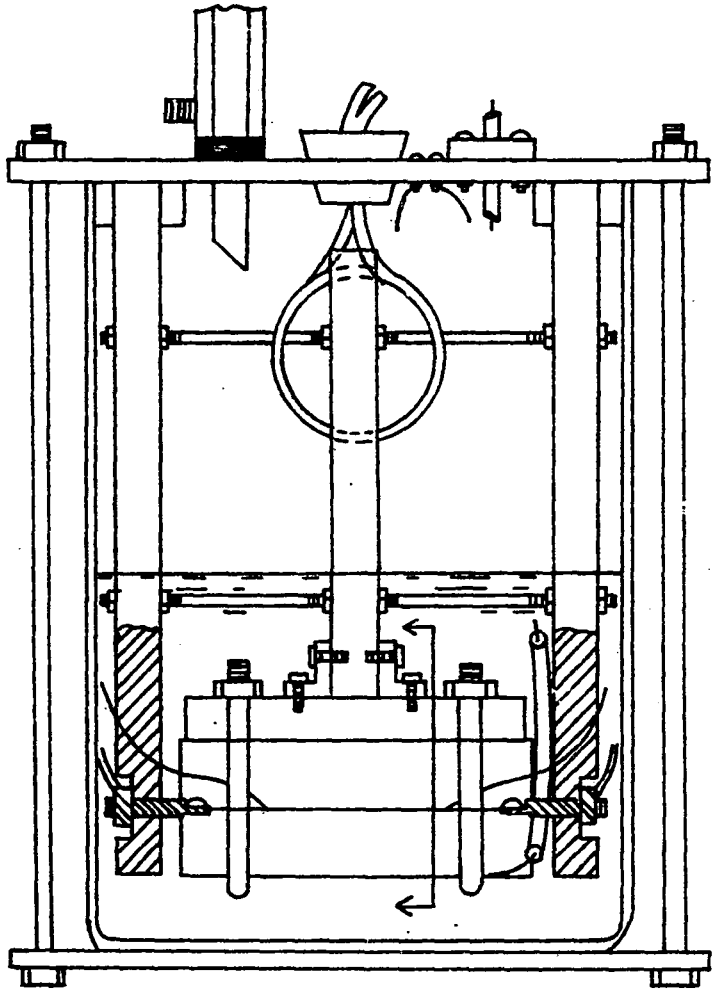

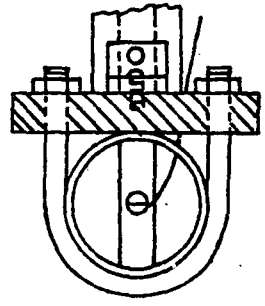

EQUIPMENT SPECIFICATIONS FOR FIGURE 5

a. Leeds & Northrup Potentiometer Facility, K-3, No. 7553.

b. Moseley Autograf, X-Y Recorder, Model 135.

c. Simpson Meter, (0-5 kv) Model 260, Series 5P.

d. Forsythe Laboratory Resistors - (42 amp capacity), No. 82965-2 Cenco.

e. 12 Volt Storage Batteries (4).

f. Leeds & Northrup Precision Resistor, 0.01 ohm, air cooled, No. 4361.

g. Beckman High Voltage Insulation Tester, Model 4000 DC.

FIGURE 5

ELECTRICAL CIRCUIT DIAGRAM

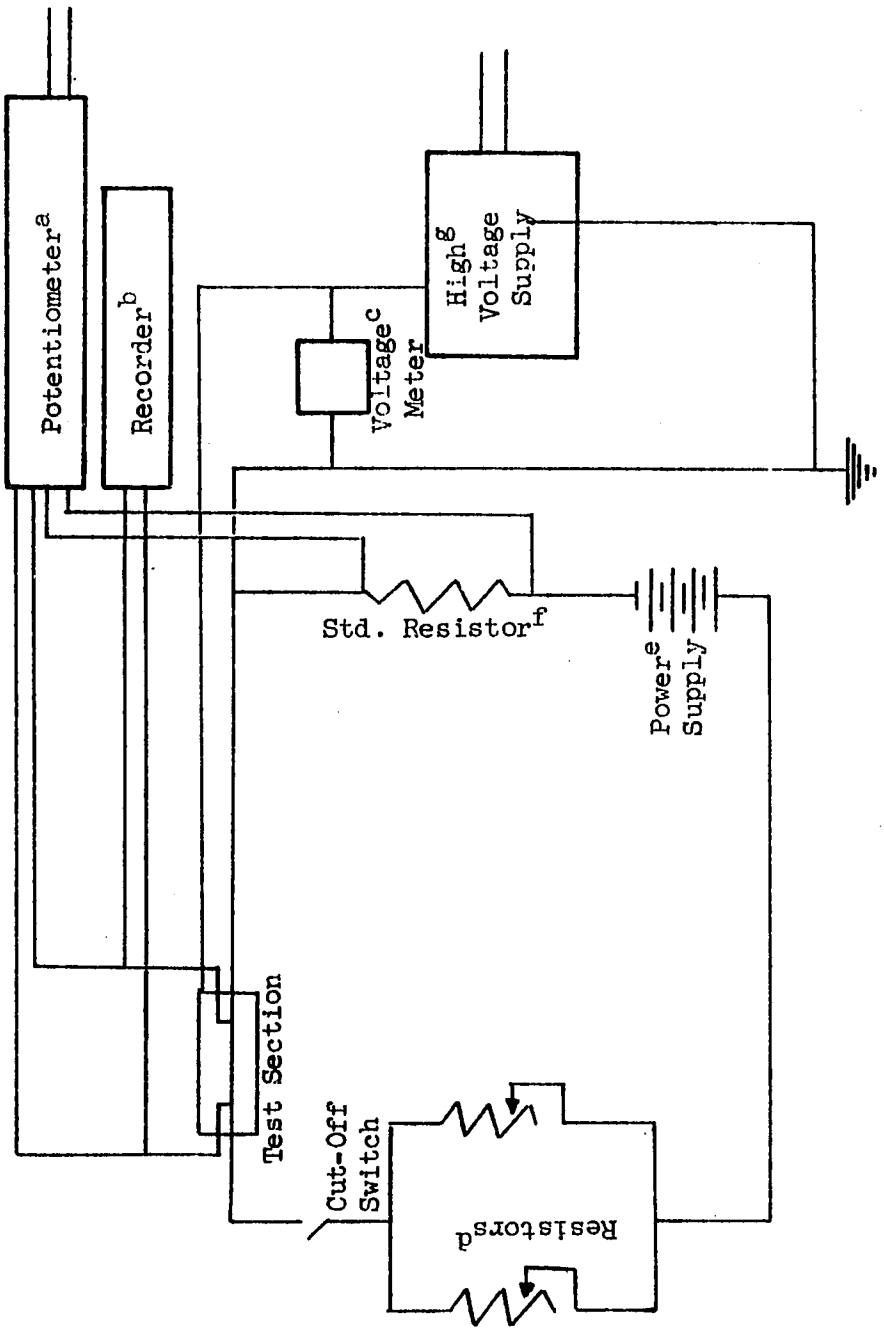

of the test section. Figure 4 is a sketch of the modified overall test section assembly. Figure 5 is an electrical circuit diagram for the system.

Test Section

The heat transfer surface was a platinum wire, 0.0201 inches ± .0002 inches in diameter. The platinum wire also served as a convenient resistance thermometer. Knowing the resistance of the wire, the temperature of the surface could be found from the well-known Callender equation for platinum resistance thermometers. Platinum voltage leads of 0.01 inch diameter were spot welded at a distance of about two inches on the large 0.0201 inch diameter wire. This two inch section of the 0.0201 inch diameter platinum wire between the voltage potential leads was then the test section for the data recorded in this study. The ends of the 0.0201 inch diameter platinum wire (outside the test section) were doubled over and spot welded together. This double wire end was then spot welded to the end of a threaded $\frac{1}{4}$ inch brass rod. The brass platinum weld was then covered with solder to insure and complete the fastening. The use of a double platinum thickness at the outside of the test section was devised in order to prevent premature film boiling from occuring at the platinum brass connection. Premature film boiling was a problem encountered in early fabrications with only a single wire connection, especially when the normal peak heat

flux was surpassed with the application of the electric field. The test wires were calibrated in accordance with the usual standard practices of platinum resistance thermometry[22]. The platinum was chemically pure, resistance grade, thermocouple wire purchased from Englehardt Industries of Newark, New Jersey. The wires were fully annealed in an electric muffle furnace before use, and they were calibrated at the ice and steam points. The Callender equation which relates resistance to temperature was programmed for digital computer use, and temperatures from resistance readings were calculated by use of the computer. This procedure eliminated any errors associated with reading a graph.

The high tension electrode was identical to the one employed by Choi[5]. It was an electrically conducting pyrex tube, 4 inches long and 1.5 inches in diameter. The conducting film was coated on the inside of the tube and was transparent. The tubes were specially prepared by the Corning Glass Works. The heating wire was located in the center of the tube and acted as ground for the high voltage unit.

All supports for the unit were constructed of teflon, brass, aluminum, or stainless steel; this construction allowed for a greater temperature operating range of the test section assembly, and chemical inertness for varying test fluid properties. The tube supports and the wire ends were adjustable to enable exact alignment of the high

voltage tube and the heating wire. Two 1 foot, 3/8" diameter glass condensers, and a 1/4" diameter copper tube (12" length coiled), were used to condense the vapor generated during a run.

The test section was immersed in the fluid to be studied in a specially constructed rectangular pyrex glass box. The glass container was constructed with flat, polished, borosilicate pyrex glass which was distortion free. This allowed clear pictures to be taken of the boiling process. The rectangular glass container was clamped between a 1/2" teflon plate at the top, and a 1/4" aluminum plate at the bottom, by six threaded rods. A natural rubber gasket sealed the glass edges at the top to the teflon plate. Ventilation was provided through the glass condensers. The current leads, the voltage leads, and the high voltage electrode, were brought through the appropriate connections which were drilled through the teflon top plate. These connections were permanently placed there to facilitate easy removal of the test section apparatus.

General System

The glass container holding the test section was placed on a flat plate 750 watt heater. The temperature of the fluid was kept constant at the boiling point by the proper adjustment of the heater output. A storage bank of four 12 volt batteries (in parallel) pro-

duced the current for the heating wire. Since the maximum current drawn for the heating wire during the tests was approximately 50 amperes, two Forsythe water cooled resistors with an 80 ampere capacity were used to vary the current in the system.

A Beckman High Voltage insulation tester, with a capacity of 40 thousand volts, was used as the high voltage source. All of the equipment was grounded, and the high voltage and heater assembly units were doubly grounded. The end of the high voltage lead was stripped of the normal lucite insulation and wrapped with teflon tape with a sufficient thickness to insulate the wire, and at the same time, to provide a reaction-free surface for the fluids studied.

The measurement circuit is shown in Figure 3. The current was measured by a voltage drop across a Leeds and Northrup 0.01 ohm, air cooled precision resistor in series with the heating wire. The voltage drop across the test section was measured directly with the Leeds and Northrup precision potentiometer. The high voltage was measured with a Simpson Meter for the low ranges (less than 5KV.) and the Beckman unit voltage meter was used for the higher voltages. The voltage drop across the test section and the current through the wire near the peak heat flux, and at the peak heat flux, were measured by a Mosely-Autograph X-Y recorder.

The readings of the X-Y recorder were checked at each current and voltage reading during a run by the Leeds and Northrup precision

potentiometer to insure correct readings near the peak heat flux, and at the peak heat flux. A knife switch was provided to prevent burnout of the wire by shutting off the current when the peak heat flux condition was reached. This was usually ascertained by the noise of the X-Y recorder going off scale because of the sudden increase in the resistance of the wire.

Test Conditions and Procedures

Four fluids were studied experimentally in this work. They were trichlorotrifluoroethane ("Freon 113"), carbon tetrachloride, chloroform, and dichloromonofluoromethane ("Freon 21"). All were chemically pure grades. All of the fluids, except dichloromonofluoromethane, were reused after proper distillation. The fluid trichlorotrifluoroethane was tested to insure that the apparatus was functioning properly, and that the data taken were reliable. Data were taken for selected free convection, nucleate boiling, and peak heat flux conditions, for both no electric field and electric field cases. The agreement between measured values and those of Choi[5] for the peak heat flux are shown on Table 1. Agreement was considered excellent. In most cases, duplicate runs were made for the peak heat flux points to test reproducibility. Agreement between duplicating runs never varied more than 3 to 4 per cent.

Wires - New platinum wire assemblies were used after each run. The potential taps and the double thickness ends were spot-

TABLE 1

PEAK HEAT FLUX COMPARISON

FREON 113

Applied Voltage Between Test Section & Cylinder Electrode kv	Electric Field Intensity at Heater Surface E_S kv/cm	Peak Heat Flux Choi[5] Btu/hr.ft^2	Peak Heat Flux This Study Btu/hr. ft^2
0	0	88,500	89,000
5.25	47.4	149,000	144,000
10.5	95.4	192,000	203,000
15.0	136.3	-	260,000

welded together, and the entire assembly was annealed in the electric furnace for several hours. After annealing, the platinum wire assembly was carefully spot-welded and soldered to the 1/4" threaded brass ends.

Temperature Calibration - The test section was calibrated at the ice and the steam points for each new batch of wires.

Steady State Attainment - A run was started when the test fluid had been at its boiling point for at least two hours. This was confirmed by the passing of a small current through the test section, and by the reading of a sensitive thermometer immersed in the boiling fluid. The boiling points of the four fluids which were tested did not vary more than 0.1°C during a run. At least ten minutes were allowed for attainment of steady state conditions at the free convection and low nucleate boiling points. Heat fluxes close to the expected peak heat fluxes were recorded after only five minutes between current adjustments.

Data Collection and Pictures - Complete boiling curves up to the peak heat flux were recorded for the fluids studied for both the normal condition and for the various voltage levels. In the course of a run, pictures were taken during nucleate boiling conditions to ascertain the effect of an electric field on bubble departure size. The bubble pictures were taken with a Nikon F Photomic T camera

coupled with a bellows extension and a F2.8 lens for close-up photography. Shutter speed was kept constant at 1/1000 of a second for the majority of the pictures. Light was provided by two 500 watt flood lamps positioned on either side of the boiling apparatus. The camera was equipped with a polaroid attachment, so that the pictures could be developed at once to insure proper picture and lighting conditions.

CHAPTER IV

EXPERIMENTAL RESULTS

Analysis of Results

The effect of an electric field on the peak heat flux in boiling heat transfer as derived in Chapter II for non-uniform electric fields is shown below:

$$\frac{(Q/A)_{max}}{h_{fg}\rho_v(0.18)} = \left[\frac{\sigma^{1/2}g^{1/2}(\rho_l-\rho_v)^{1/2}}{\rho_v}\left(\frac{\rho_l}{\rho_l+\rho_v}\right)\right]^{1/2} + \left[\frac{\varepsilon_o(K-1)^2C_o^2E_s^2}{\rho_v(K+1)}\right]^{1/2} \quad (23)$$

This equation requires the evaluation of one empirical constant, C_o, the constant (0.18) being taken from the literature.[19] In order to determine a value for C_o, the experimental peak heat flux data for the first system studied, trichlorotrifluoroethane ("Freon 113"), was analyzed with respect to the second term in Equation 23, (this data was in excellent agreement with Choi's previous work). The peak heat flux data for trichlorotrifluoroethane was plotted as a function of the electric field strength at the wire surface to yield the increase in the peak heat flux by the action of a non-uniform electric field. (Figure 6.) Since the second term in Equation 23 gives the expected increase in the peak heat flux with the application of an electric field, a value for C_o was obtained

FIGURE 6

PEAK HEAT FLUX INCREASE OF TRICHLORO-
TRIFLUOROETHANE WITH AN ELECTRIC FIELD

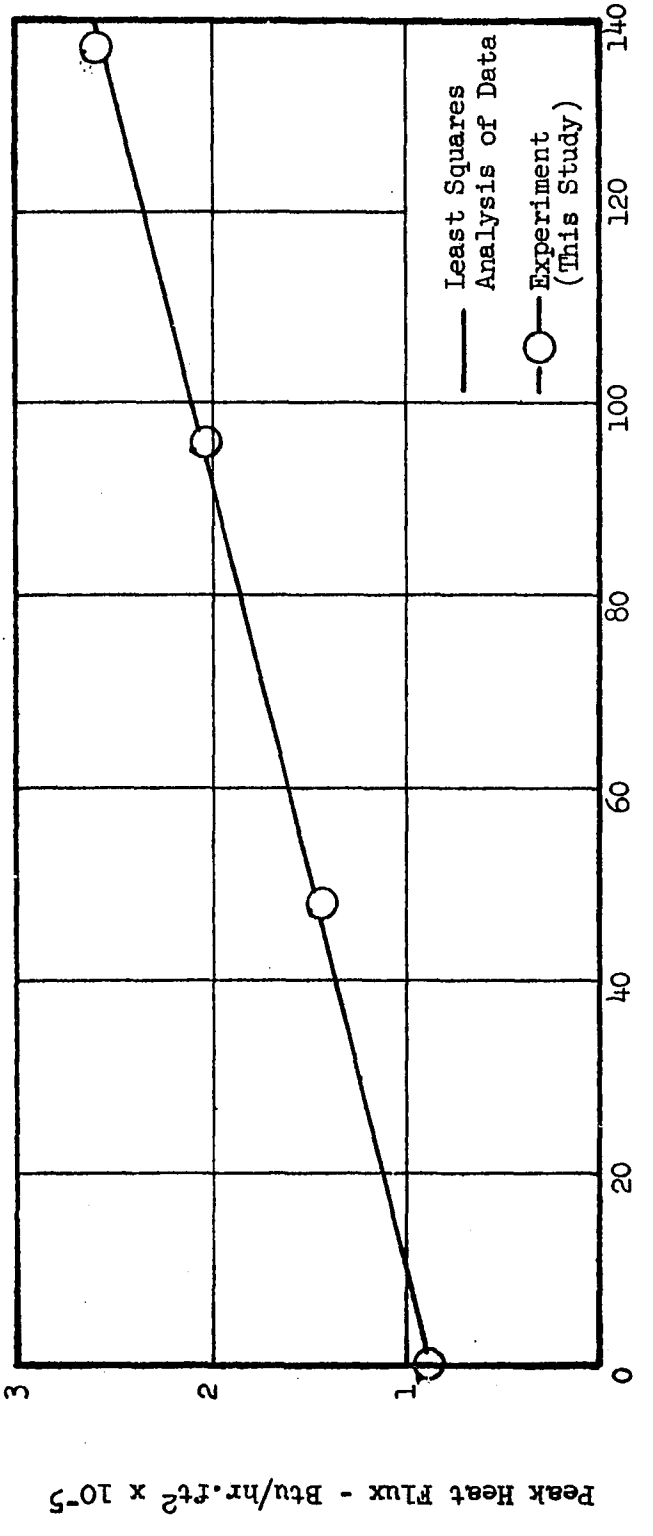

by equating the increase in the peak heat flux (Figure 6) to the second term in Equation 23, as shown below:

$$\frac{\Delta(Q/A)_{max}}{h_v \rho_v} = 0.18 \left[\frac{\varepsilon_o (K-1)^2 (C_o E_s)^2}{\rho_v (K+1)} \right]^{\frac{1}{2}} \qquad (22)$$

where $\Delta(Q/A)$ max = experimental increase in peak heat flux for trichlorotrifluoroethane by electric field as determined by least squares analysis.

where C_o = empirical constant as defined by Equation 20.

and h_v = latent heat of vaporization

ρ_v = vapor density

ε_o = inductive capacity of free space (vacuum)

K = dielectric constant, dimensionless

E_s = electrical field intensity

Since the only unknown in Equation 22 is C_o, it can readily be evaluated. By this approach, a value for C_o, of 0.235 was obtained for the fluid trichlorotrifluoroethane and for the geometric arrangement as described in Chapter III. This value of C_o (0.235) was subsequently used for all other fluids tested.

It might be noted that for a surface electric field intensity of 137 kv/cm for trichlorotrifluoroethane the rate of increase of the peak heat flux as given by Equation 21a is 90% of that predicted by Equation 22.

The first term in Equation 23 represents the familiar Kutateladze-Zuber[9,25] analysis or predictor equation for the normal peak heat flux condition, and the second term represents the expected increase for the specific case of a non-uniform D.C. electric field. In order to further test the validity of the assumptions and modifications which led to Equation 23, several other fluids, in addition to the aforementioned trichlorotrifluroethane, were studied to test the parameters associated with the electric field term of Equation 23. They were specifically, carbon tetrachloride, chloroform, and dichloromonofluromethane ("Freon 21").

Thermodynamic and Electrical Parameters

Equation 23 predicts that the latent heat of vaporization h_v and the fluid vapor density ρ_v, are prime factors for both the "normal" and the electric field cases. For electric field effects in particular, the additional effect of the dielectric constant should be very important. For the four fluids studied, trichlorotrifluroethane, carbon tetrachloride, chloroform, and dichloromonofluromethane, the thermodynamic term associated with the electrical term $(h\rho_v^{0.5})$ was relatively constant (Table 2) with a maximum variation of 30%. This is in direct contrast to the almost 400% increase exhibited by the observed and predicted peak

TABLE 2

VARIATION OF THE THERMODYNAMIC TERM
ASSOCIATED WITH THE ELECTRICAL FIELD TERM OF EQUATION 22

Fluid	+ Latent Heat of Vaporization Btu/lb	+ Vapor Density lb/ft.3	$h_v \rho_v$	$h_v \rho_v^{0.5}$
Dichloro-monofluoromethane	63.09	0.464	29.27	43.0
Trichloro-trifluoroethane	104.15	0.285	29.62	55.4
Carbon Tetrachloride	83.5	0.340	28.39	48.7
Cloroform	106.3	0.272	28.80	55.4

+ Evaluated at Normal Boiling Point

heat flux values for the above four fluids for any one particular electric field intensity. Hence, the primary factor or term accounting for the observed and predicted variations in the peak heat flux for these four fluids was the electric, and not the thermodynamic term. Subsequent increases in the peak heat flux would be approximately proportional to the dielectric constant factor. The dielectric constants for the above four fluids varied from 2.10 for carbon tetrachloride (evaluated at the boiling point) to 5.65 for dichloromonofluoromethane.

Comparison of Theory and Experiment (D.C. Fields)

The observed and predicted increases in the peak heat flux as determined respectively by experiment and Equation 23 for the four fluids listed above are shown in graphical form in Figures 7, 8, 9, and 10. A subsequent graph, Figure 11, compares the generalized equation (Equation 22) with the actually observed peak heat flux increases. In all cases experiment and theory were found to give good agreement. As predicted, larger values of applied voltage or electric field strength were required for the lower dielectric constant fluids (carbon tetrachloride and trichlorotrifluroethane) in order to sustain or maintain the same increases in the peak heat flux with higher dielectric constant fluids such as, chloroform and dichloromonofluromethane (Figure 12).

FIGURE 7

PEAK HEAT FLUX VARIATION OF TRICHLORO-
TRIFLUORO-ETHANE WITH AN ELECTRIC FIELD

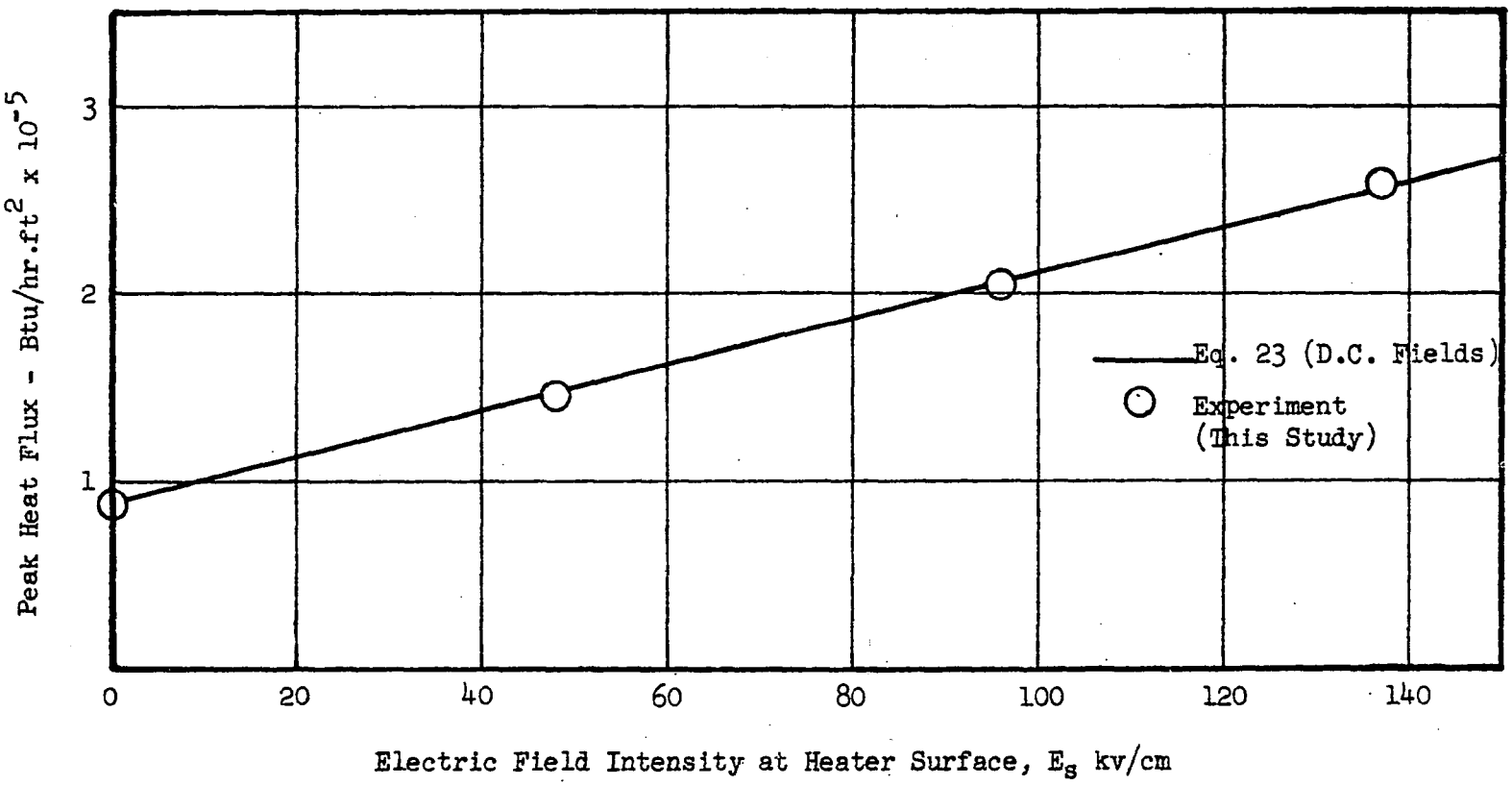

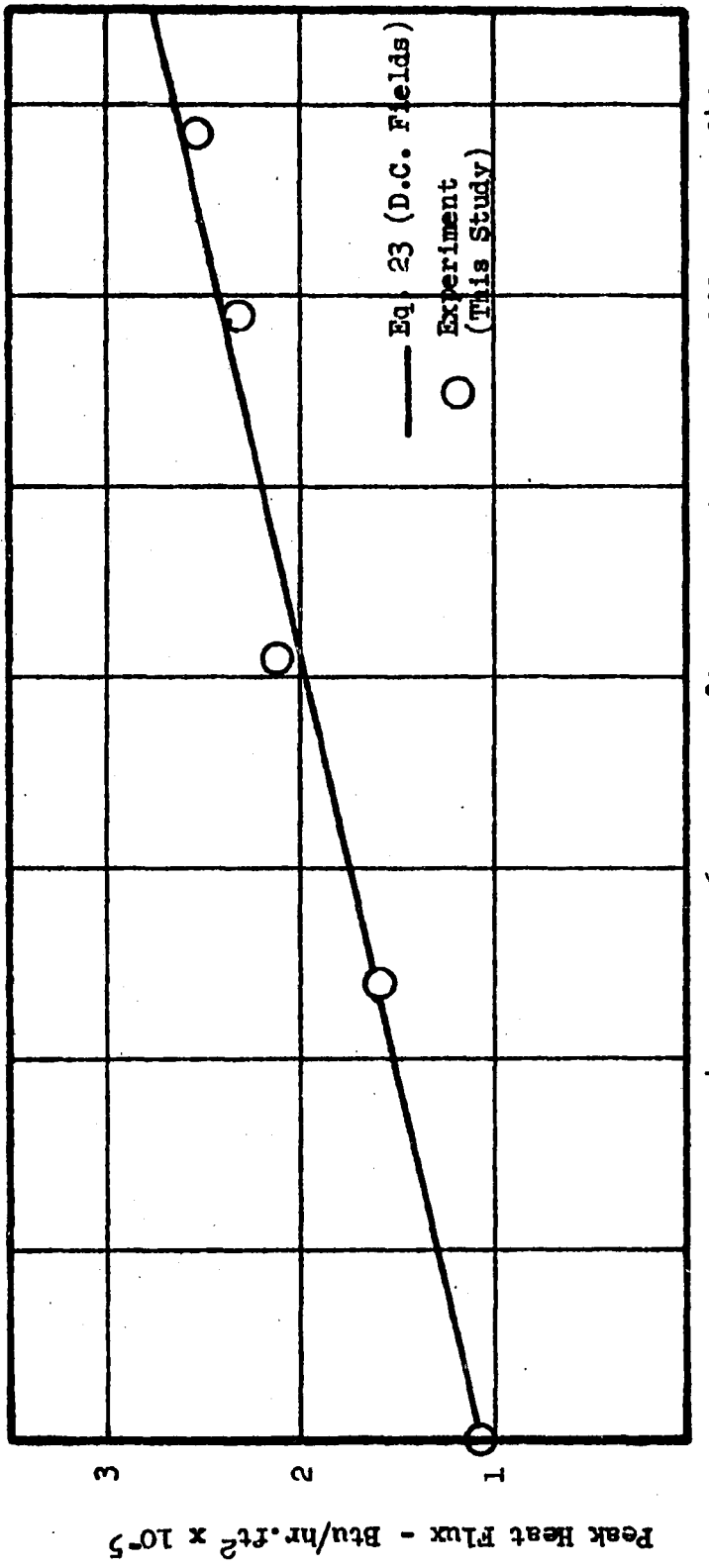

FIGURE 8

PEAK HEAT FLUX VARIATION OF CARBON TETRACHLORIDE WITH AN ELECTRIC FIELD

FIGURE 9

PEAK HEAT FLUX VARIATION OF
CHLOROFORM WITH AN ELECTRIC FIELD

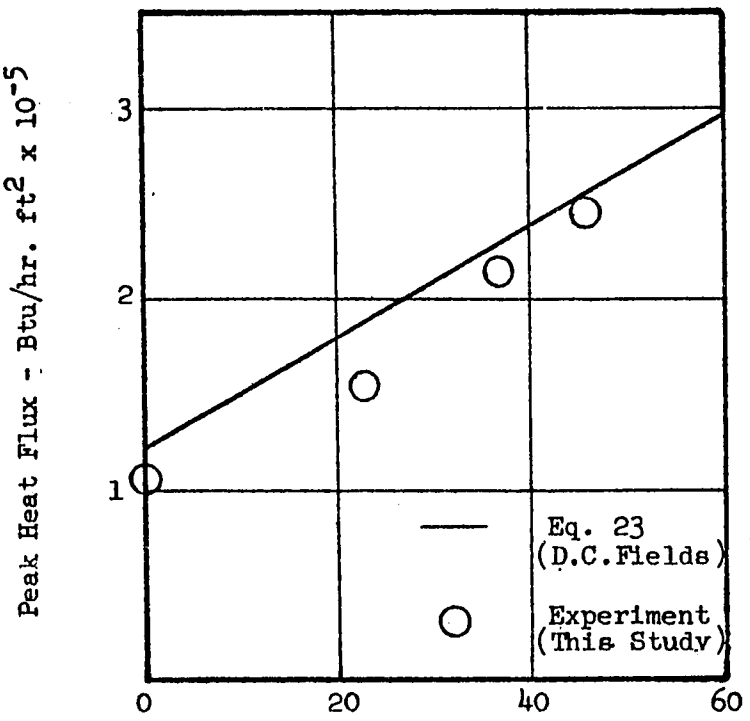

FIGURE 10

PEAK HEAT FLUX VARIATION OF
DICHLOROMONOFLUOROMETHANE
WITH AN ELECTRIC FIELD

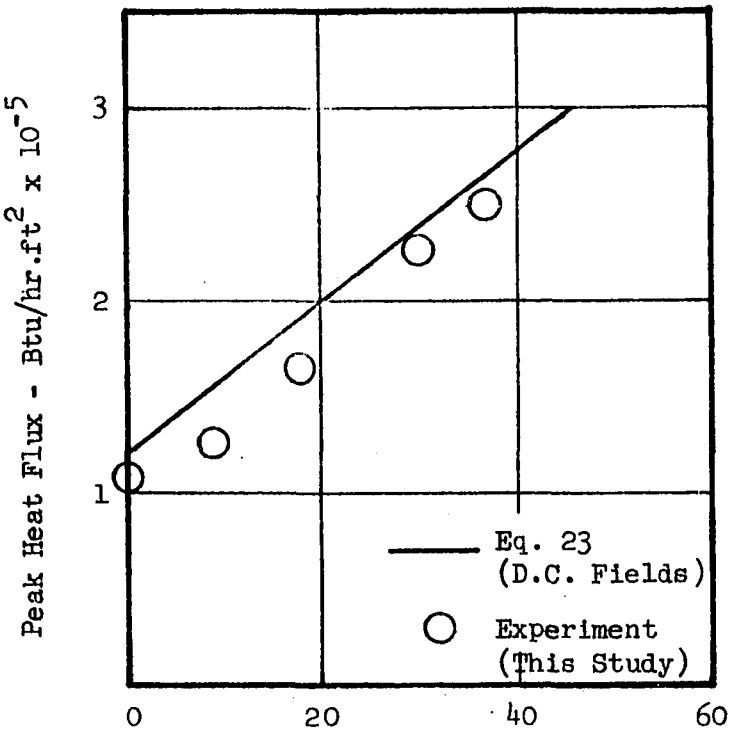

FIGURE 11

COMPARISON OF EXPERIMENTAL
INCREASE IN PEAK HEAT FLUX
WITH THE THEORETICAL PREDICTION
(D.C. FIELDS) OF EQUATION 22

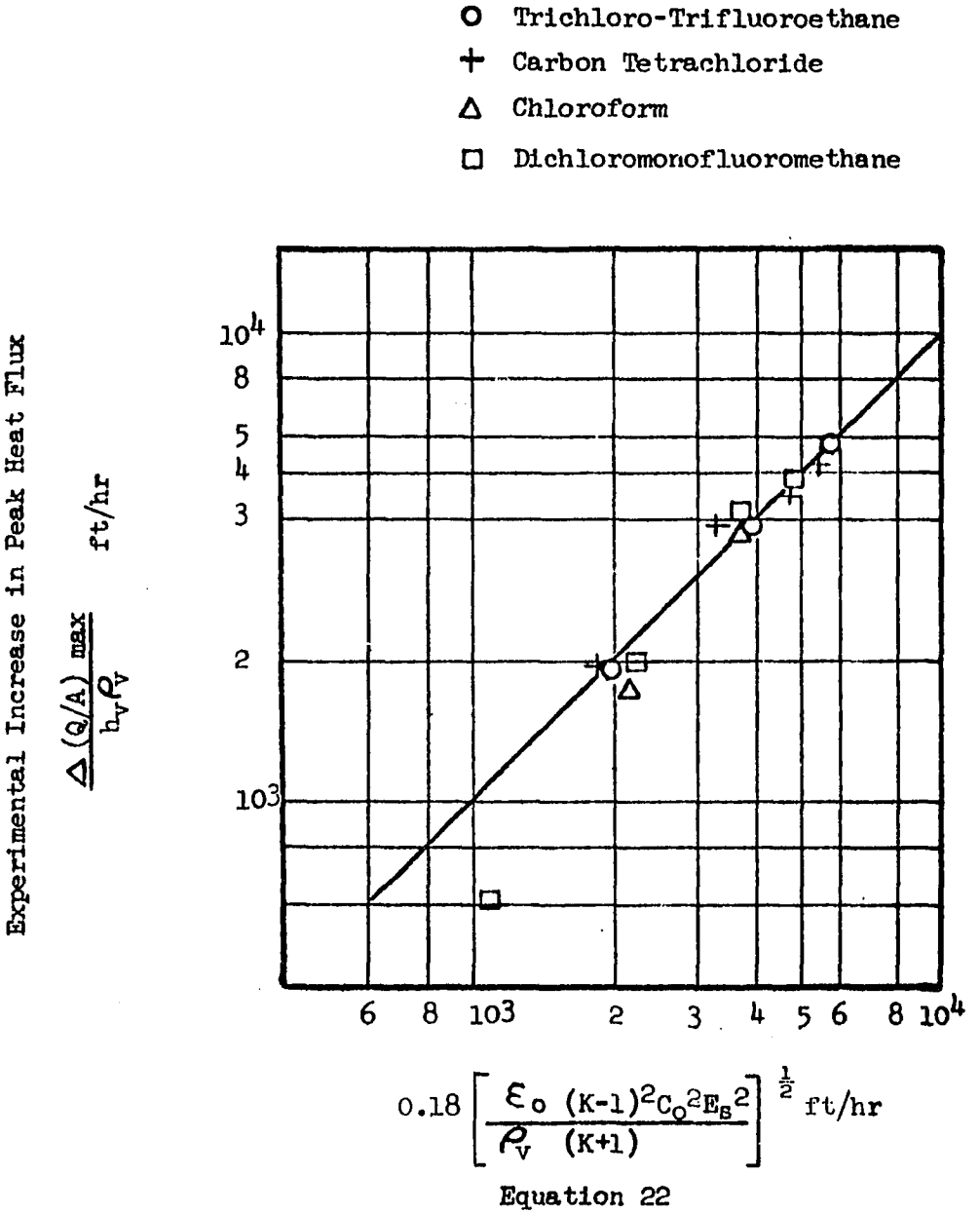

Equation 22

FIGURE 12

PREDICTED INCREASES IN PEAK HEAT FLUX WITH
APPLICATION OF AN ELECTRIC FIELD FROM EQUATION 23

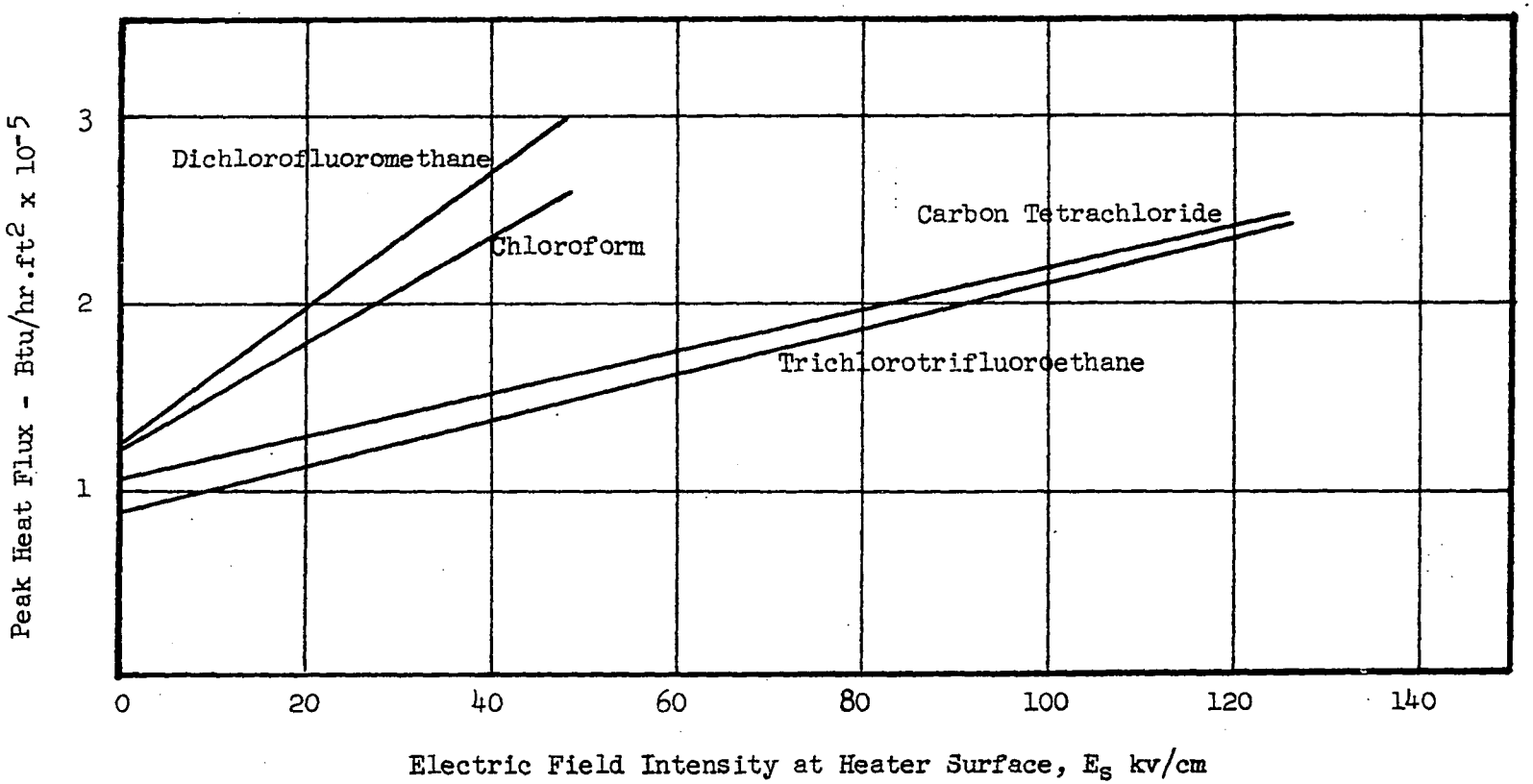

A.C. Fields (60 cycle)

The scant literature references[1,14] for the effect of both A.C. and D.C. electric fields in boiling heat transfer and in particular the peak heat flux indicate that impressed A.C. fields are not as effective as D.C. fields. This was well demonstrated by the recent work of Asch[1] who showed experimentally that impressed non-uniform A.C. fields were approximately 40 to 50 per cent less effective on the peak heat flux than non-uniform D.C. fields for the specific case of the fluid trichlorotrifluoroethane. Since trichlorotrifluoroethane was the fluid upon which the equivalent electric field strength was based in this work, as a first approximation one might say that for non-uniform A.C. fields and heat transfer geometries similar to that employed in this study (namely tubes and wires), a value of the equivalent electric field strength should be approximately one half the value determined for equivalent geometry D.C. fields. This new defined constant for non-uniform A.C. fields is shown below:

$$C_n \cong \frac{C_o}{2} \qquad (24)$$

where C_n = equivalent field strength coefficient for A.C. fields

where C_o = equivalent field strength coefficient for D.C. fields.

This new value of the equivalent field strength coefficient might now be substituted into Equation 23 to evaluate and predict the effect of non-uniform A.C. fields on the peak heat flux phenomenon.

Comparison of Theory and Experiment (A.C. Fields)

The effect of non-uniform A.C. fields on the peak heat flux for liquid nitrogen, benzene, toluene, hexane, dichlorodifluromethane (Freon 12), ethyl ether and water was reported by Bonjour et al[3]. These experimenters, as mentioned previously, employed a parallel wire electric geometry for their study; and in this respect their apparatus is quite similar to the heat transfer geometry of this work. A comparison of the predicted normal peak heat flux and of the subsequent peak heat flux increases with the experimentally determined values is given by Figures 13 through 19. The equivalent field strength coefficient for A.C. fields as defined above, C_n, was substituted into Equation 23 to give the predicted increases in the peak heat flux. The agreement of the predicted increases with the experimental data is good. The agreement for water is particularly striking. The fluids tested by Bonjour et al[3], and

FIGURE 13

PEAK HEAT FLUX VARIATION OF LIQUID NITROGEN WITH AN ELECTRIC FIELD

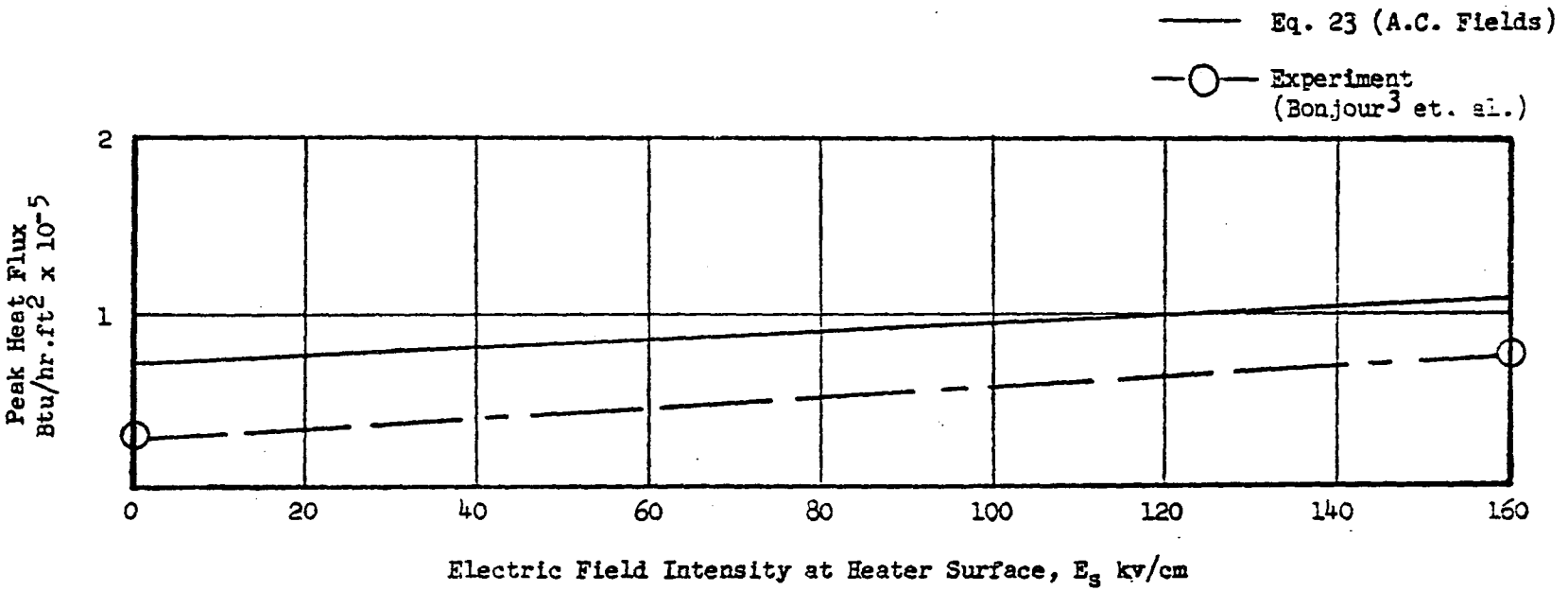

FIGURE 14

PEAK HEAT FLUX VARIATION OF
HEXANE WITH AN ELECTRIC FIELD

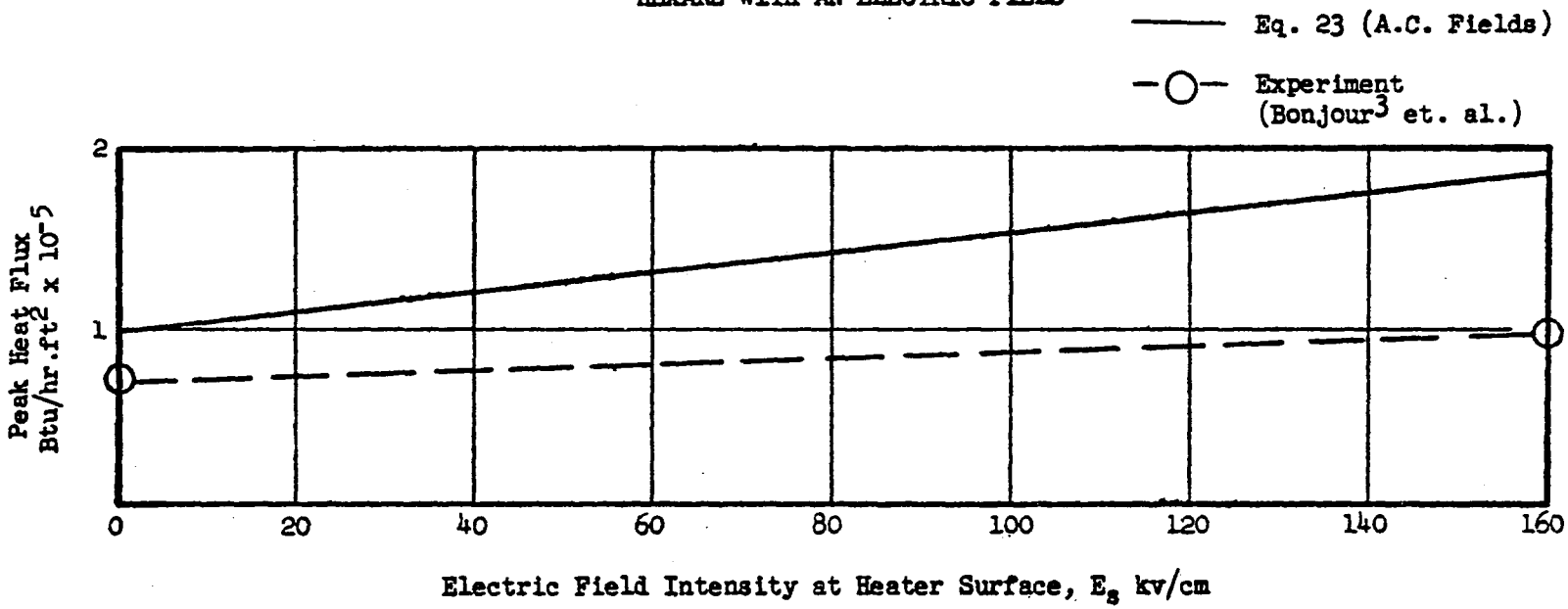

FIGURE 15

PEAK HEAT FLUX VARIATION OF
BENZENE WITH AN ELECTRIC FIELD

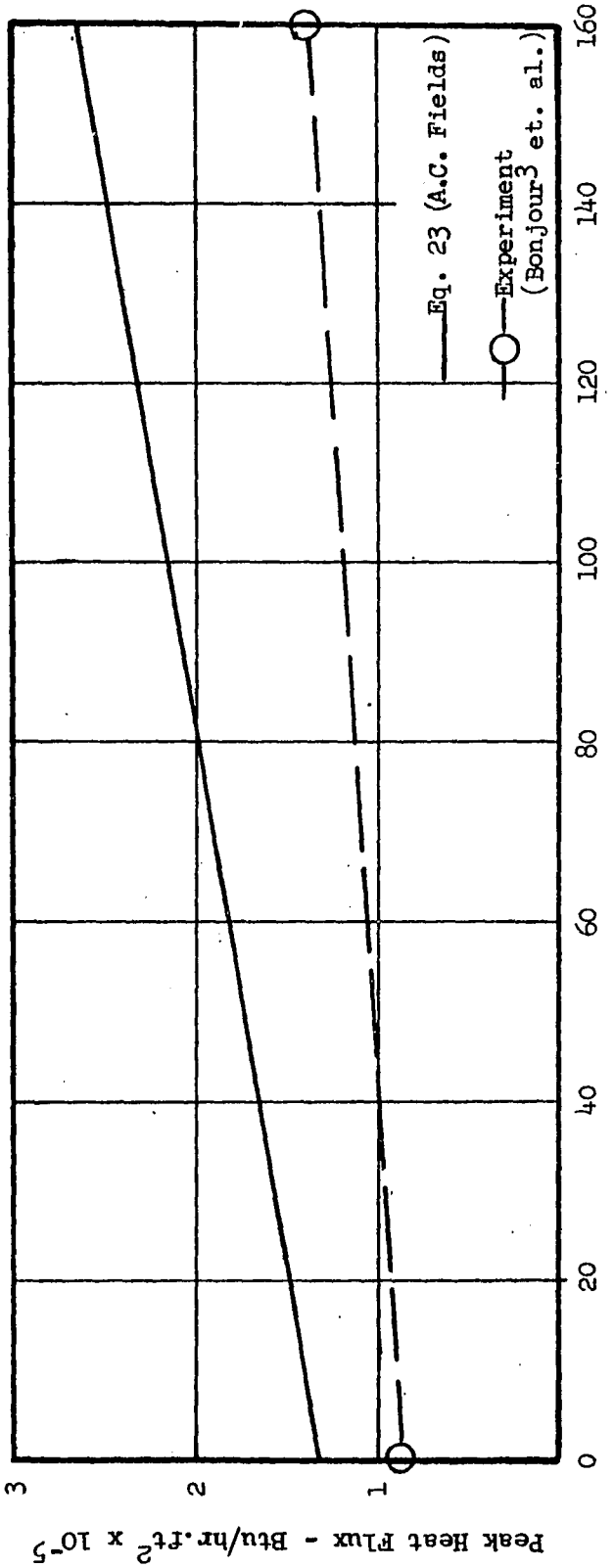

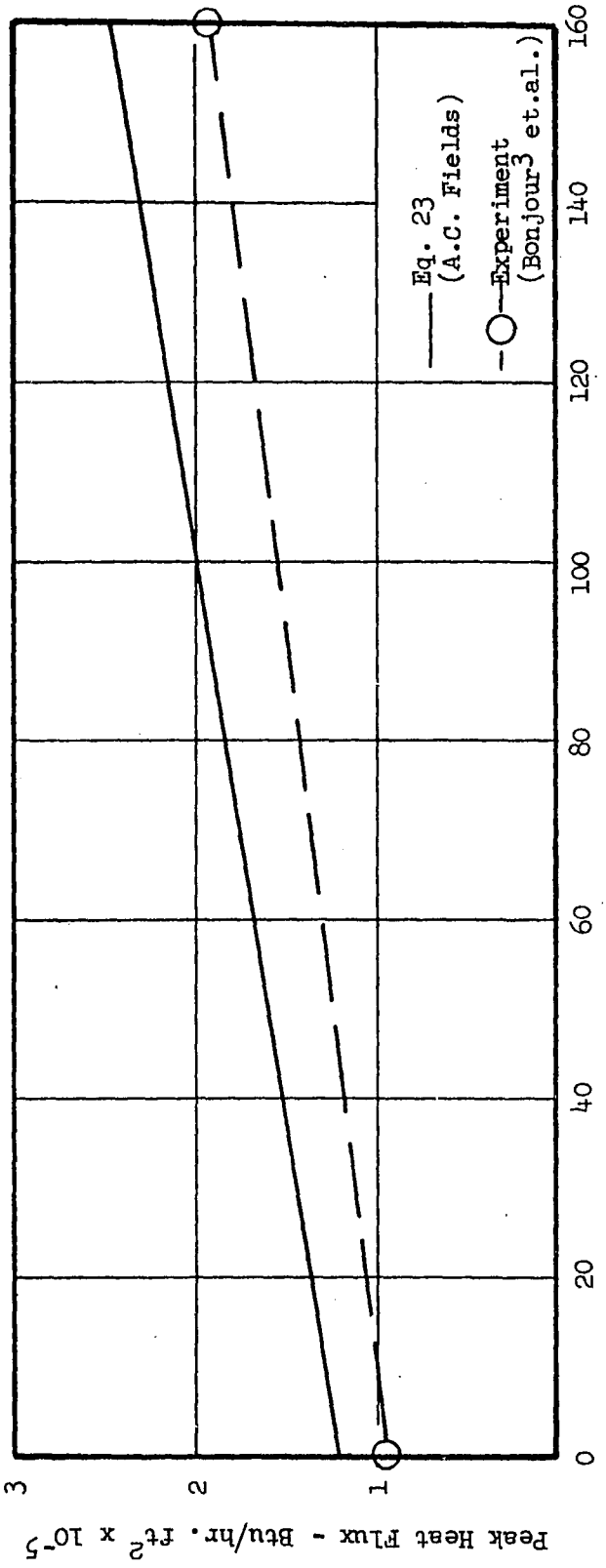

FIGURE 16

PEAK HEAT FLUX VARIATION OF
TOLUENE WITH AN ELECTRIC FIELD

FIGURE 17

PEAK HEAT FLUX VARIATION OF DICHLORO-
DIFLUOROMETHANE (FREON 12) WITH AN ELECTRIC FIELD

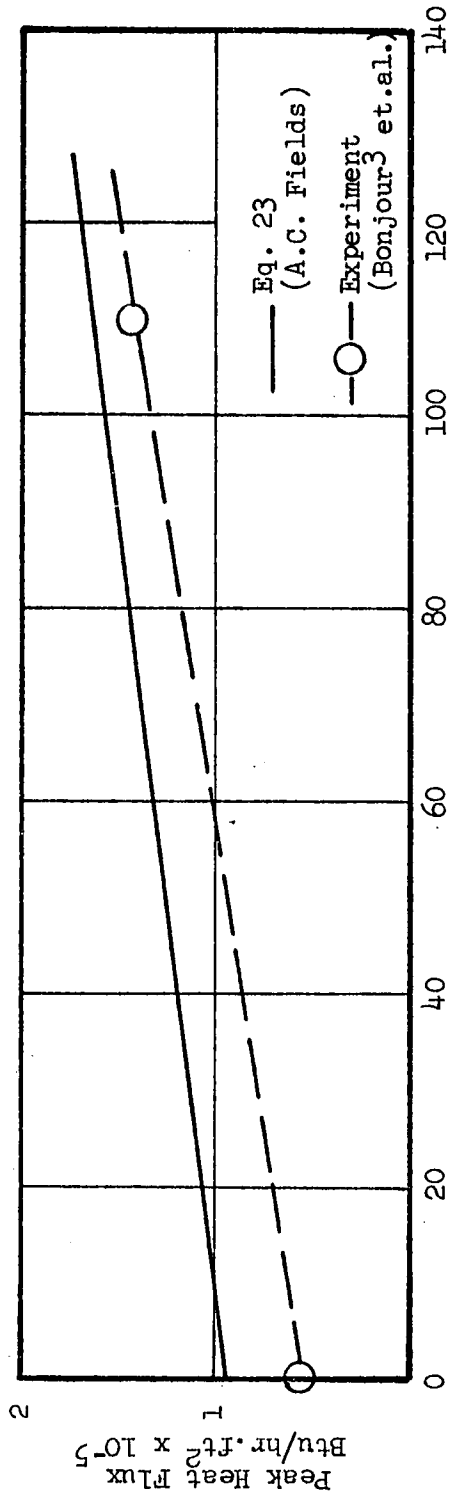

FIGURE 18

PEAK HEAT FLUX VARIATION OF
ETHYL ETHER WITH AN ELECTRIC FIELD

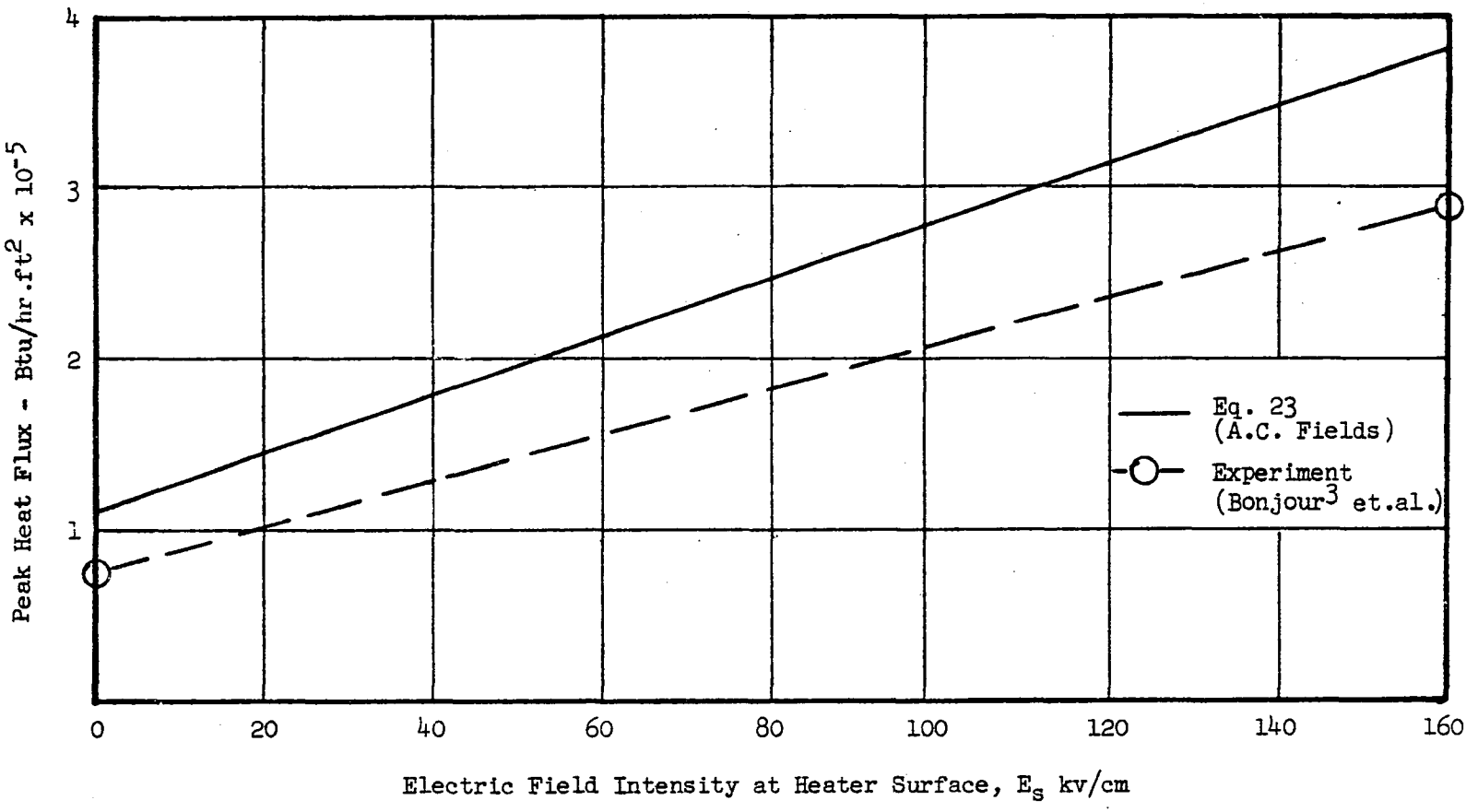

FIGURE 19

PEAK HEAT FLUX VARIATION OF
WATER WITH ELECTRIC FIELD

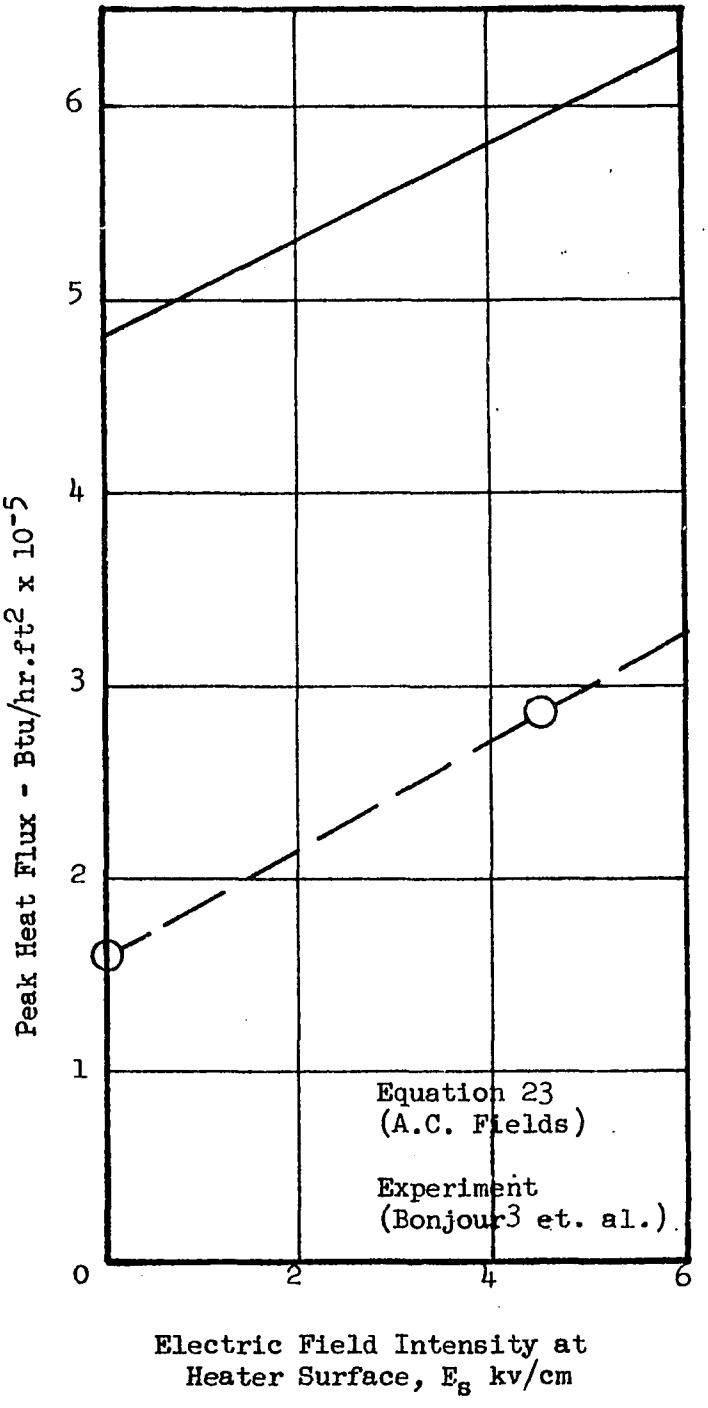

FIGURE 20

COMPARISON OF EXPERIMENTAL[3] INCREASE IN PEAK HEAT FLUX WITH THE THEORETICAL PREDICTION (A.C. FIELDS) OF EQUATION 22

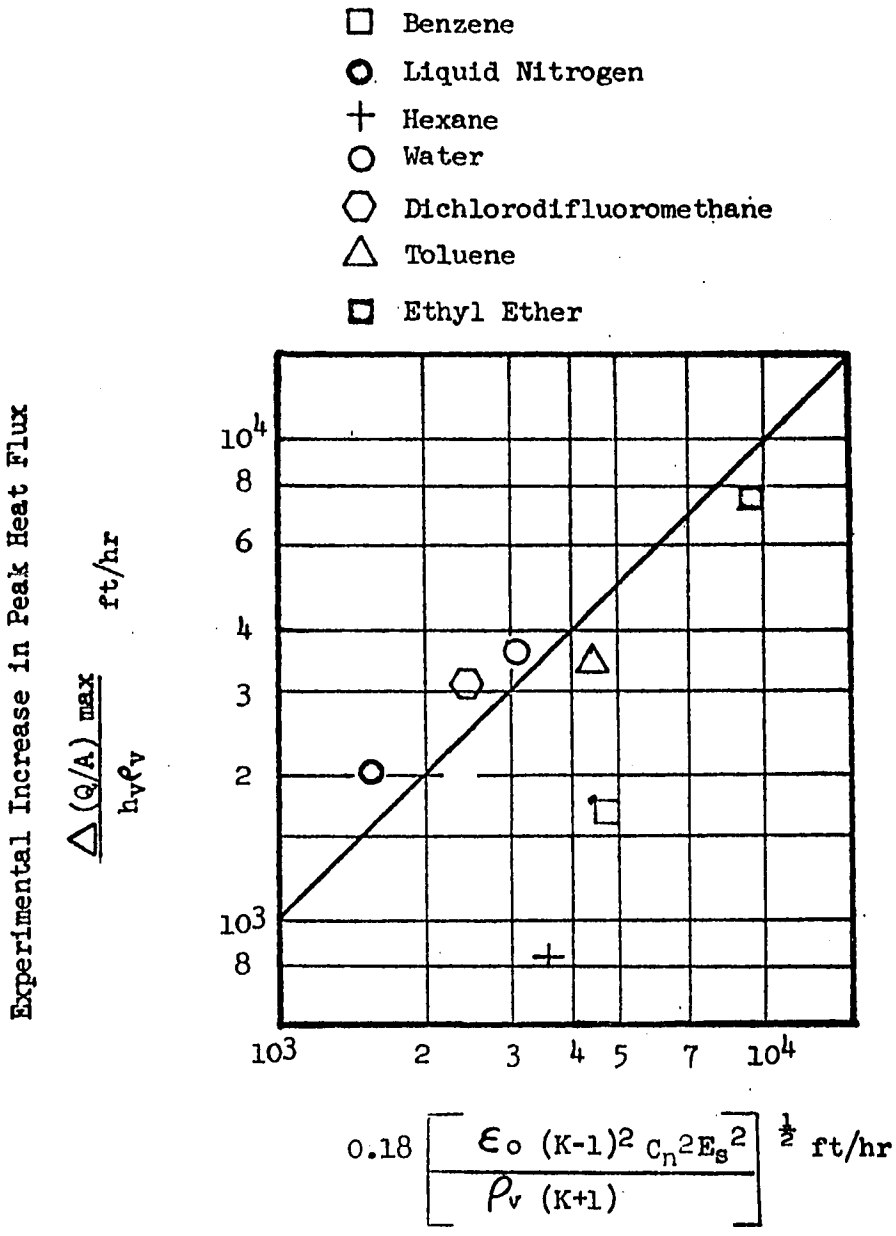

Equation 22

tested here, have a dielectric constant range of approximately 2 to 55.

Markels and Durfee[14] have investigated the effect of D.C. fields on the peak heat flux for isopropanol, and A.C. fields for water. Data on absolute electric field strengths at the heater surface is lacking[27] due to the particular geometry of the heat transfer system. However, comparisons between the relative slopes or increases in the respective peak heat fluxes can be made from the experimental data with the relative slopes as predicted by Equation 23. This comparison is made contingent on the premise that the voltage values reported are directly related to the electric field strength at the heater surface. The theoretically predicted increases are shown by Figure 21. Table 3 compares the experimental increases with the theoretical predictions. Again the agreement is good. It might be noted that the heat transfer surface in the work of Markels and Durfee[14] was a steam tube as contrasted to the wire surface used in this thesis.

Natural Convection Effects

The effect of an electric field on natural convection in boiling heat transfer as observed in this study is shown in Figures 25 through 28. At constant heat fluxes in this region the application of an electric field reduces the heat transfer

FIGURE 21

PREDICTED PEAK HEAT FLUX INCREASES
FROM EQUATION 23 FOR WATER AND
ISOPROPANOL WITH AN ELECTRIC FIELD

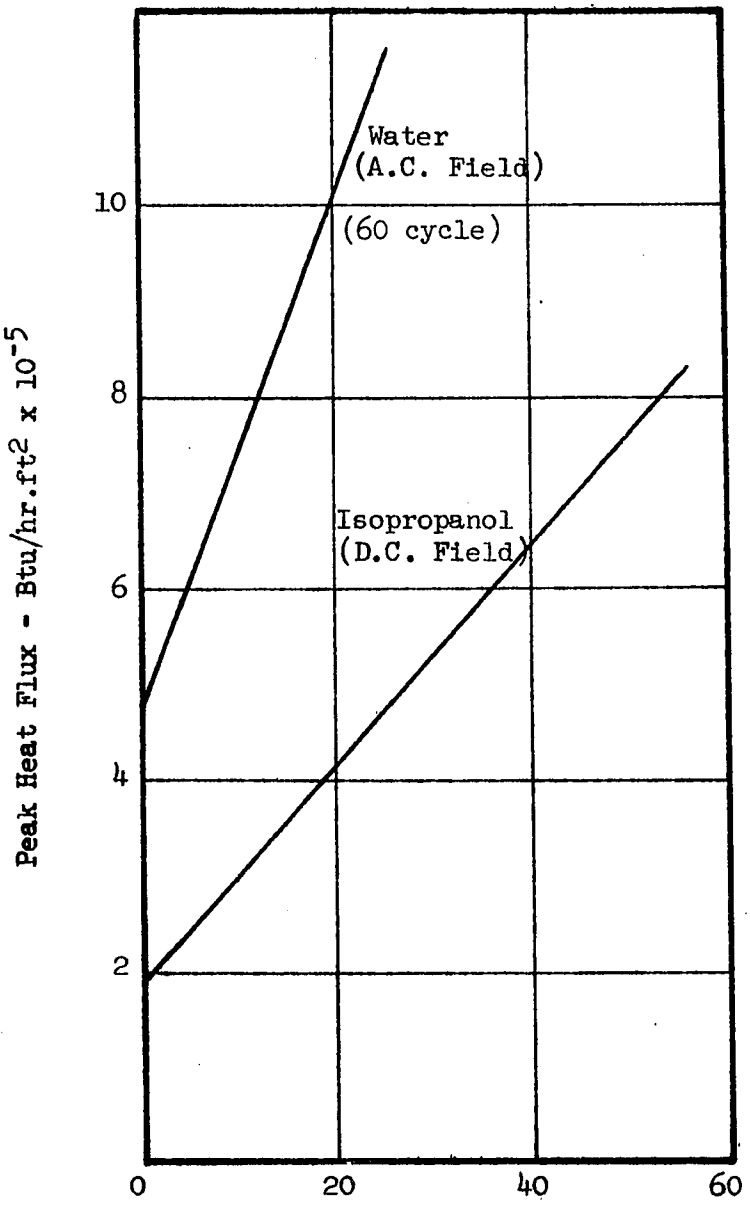

TABLE 3

COMPARISON OF PEAK HEAT FLUX I"CREASES FROM TUBE DATA OF MARKELS AND DURFEE[14] WITH EQUATION 22

Voltage Reading kv	Fluid Under Test	Experimental Increase In Normal Peak Heat Flux Btu/hr. ft^2 (Markels & Durfee[14])	Experimental Ratio of Peak Heat Flux Increases[14]	Predicted Increase Ratio in Peak Heat Flux From Equation 22.
1	Water (A.C.)	70,000	---	---
	Isopropanol (D.C.)			
2	Water (A.C.)	150,000	2.06	2.17
	Isopropanol (D.C.)	73,000		

FIGURE 22

BOILING HEAT TRANSFER CURVE
FOR CARBON TETRACHLORIDE WITH AN
ATTENDENT ELECTRIC FIELD (D.C. FIELD)

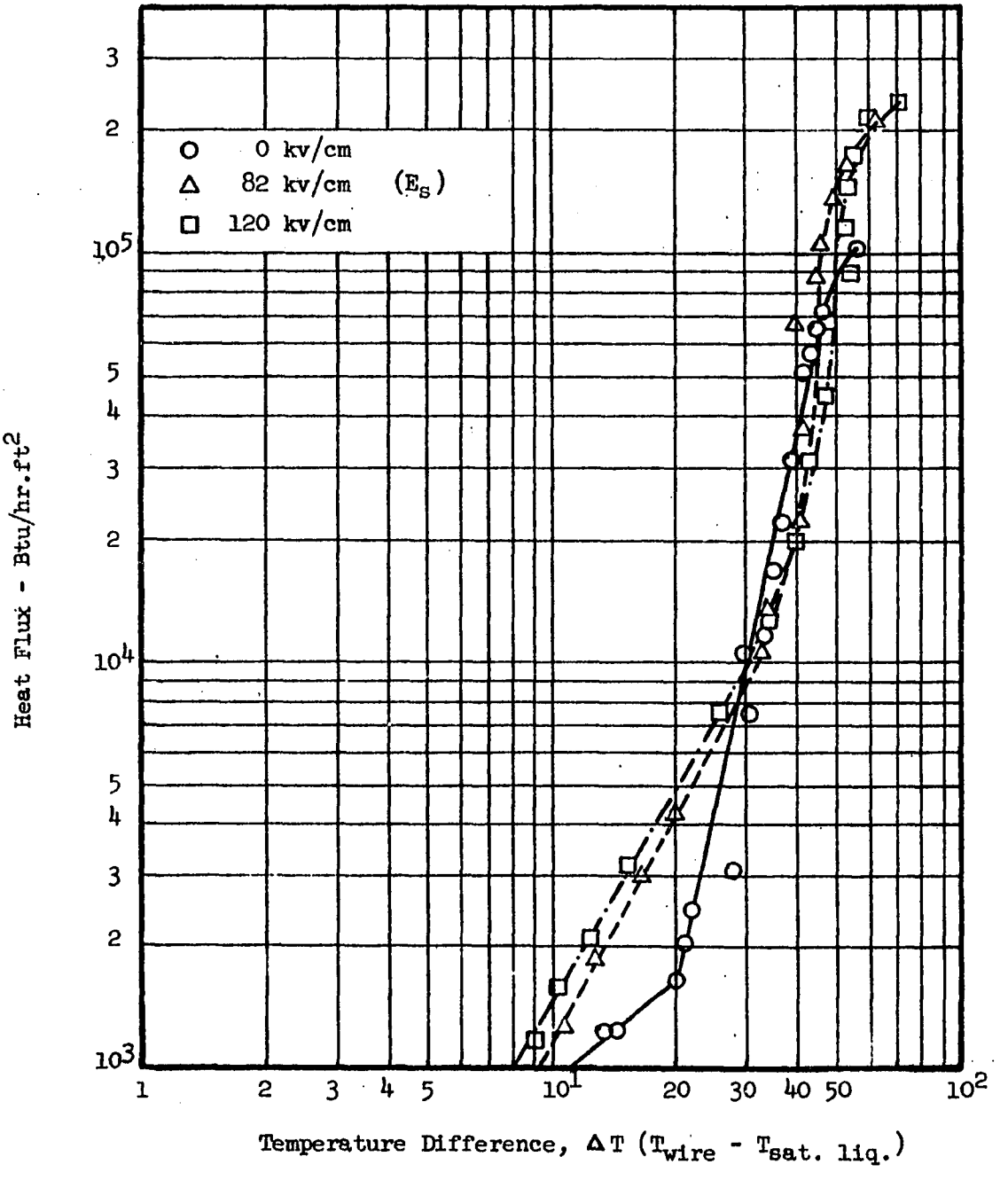

FIGURE 23

BOILING HEAT TRANSFER CURVE FOR
DICHLOROMONOFLUOROMETHANE WITH AN
ATTENDENT ELECTRIC FIELD (D.C. FIELD)

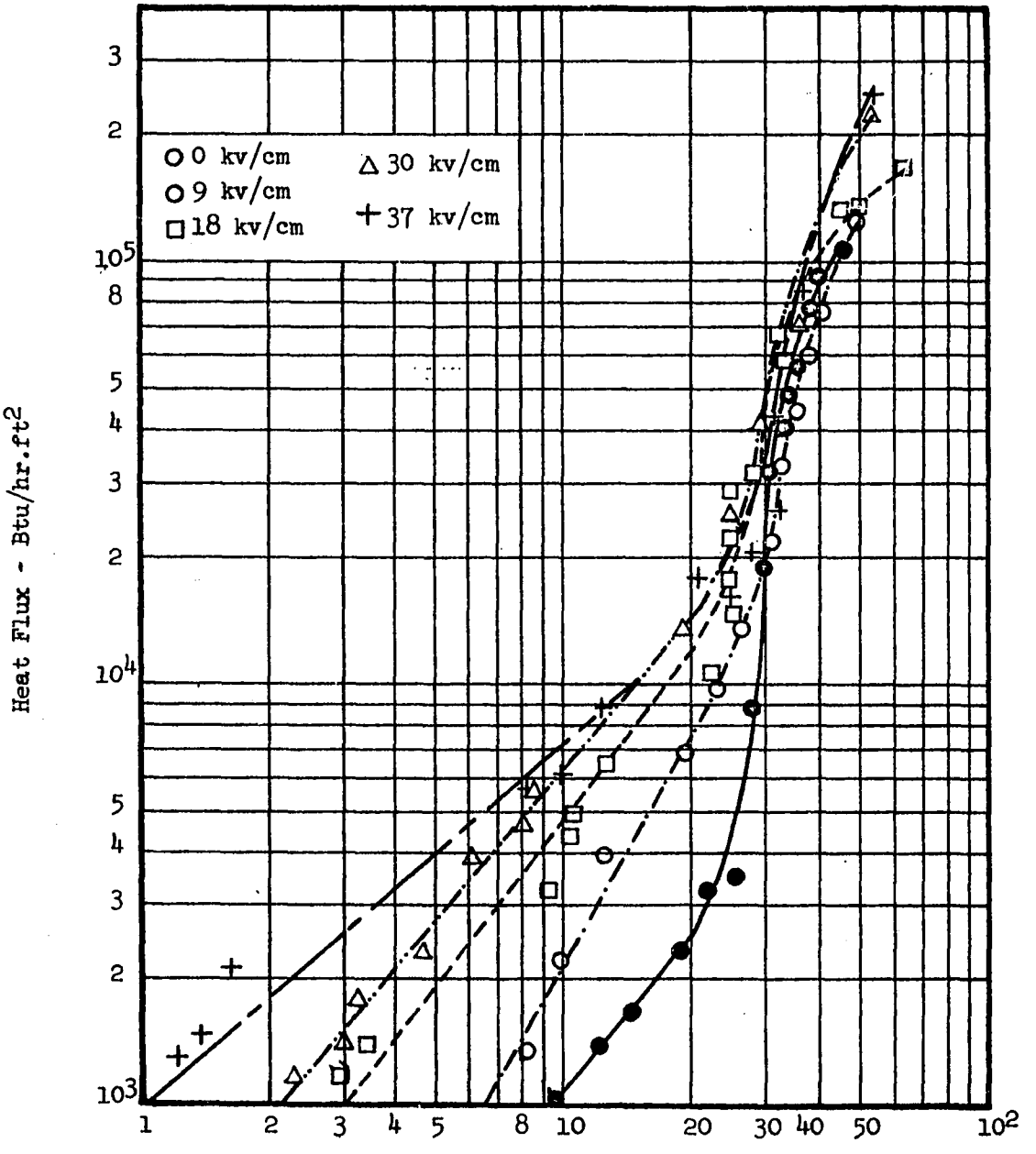

FIGURE 24

BOILING HEAT TRANSFER CURVE FOR CHLOROFORM
WITH AN ATTENDENT ELECTRIC FIELD (D.C. FIELD)

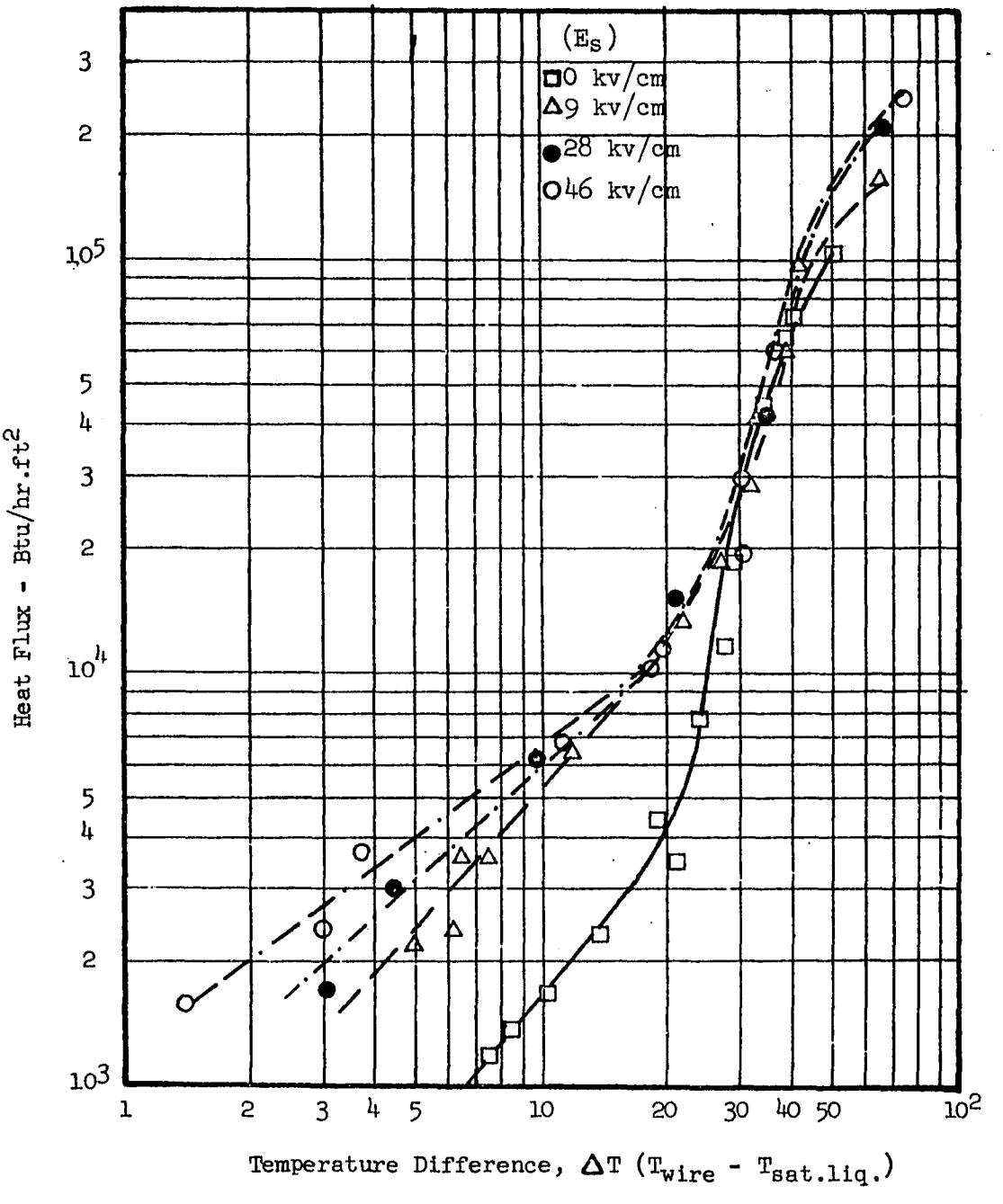

FIGURE 25

BOILING HEAT TRANSFER CURVE FOR TRICHLOROTRIFLUORO-ETHANE WITH AN ATTENDENT ELECTRIC FIELD (D.C. FIELD)

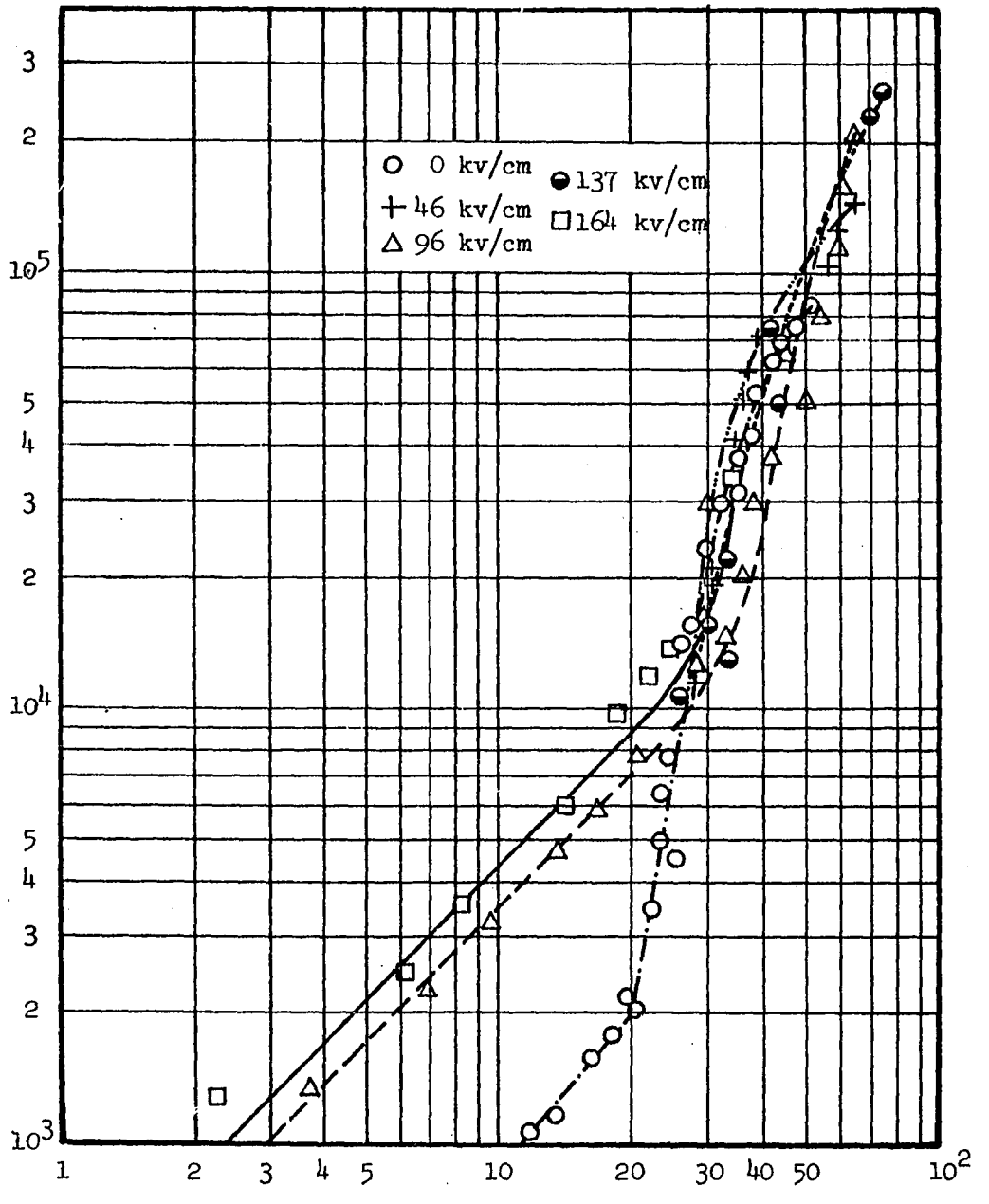

surface temperature. As noted in Chapter I, the electrical forces associated with polarized and charged matter might best account for this phenomenon. Choi's[5] definition of an equivalent gravity field based on the above electrical forces might be expected to best quantitatively account for these effects.

Nucleate Boiling Region

The effect of an electric field on nucleation and nucleate boiling is negligible. In all of the fluids studied in this work, nucleation for all electric field strengths occurred at approximately 20 to 25 degrees of superheat. At appropriate heat fluxes (1.5×10^4 Btu/hr.ft^2) the application of an electric field will transform nucleate boiling into the natural convection mode of heat transfer. Above this heat flux value small temperature differences are seen to exist with the application of the electric field. At very high nucleate boiling rates the reverse condition of an increase in required temperature develops. An adequate explanation of this phenomenon and of the low range of the nucleate boiling zone in the presence of electric forces has not yet been offered.

CHAPTER V

BUBBLE SHAPES

Bubble Size

Bubbles leaving a heat transfer surface exhibit various bubble departure sizes. Bubbles are seen to leave a surface having diameter ratios of approximately 2.0, depending on the nucleating characteristics of the heat transfer surface. Although an exact correspondence of bubble departure size with heat flux is not possible, a particular heat transfer surface and a fluid do exhibit a range of most probable departure diameters and these values can be put to profitable analysis.

Electric Field Effects

The effect of a non-uniform electric field on bubble departure size is:

A. To reduce the bubble departure size

B. To increase the frequency of bubble departure

For strong electric fields these effects can be quite pronounced. Bubble departure sizes in this study were determined by photographing various portions of the nucleate boiling range for the four fluids studied and physically measuring the range of departure sizes for selected bubbles. As mentioned above, for any one heat flux, the depar-

ture bubble diameters exhibit a scatter of range of sizes and an attempt was therefore made to average out the various recorded departure sizes. This was accomplished by recording departure bubble sizes for a given heat flux and then averaging the sum of these various bubble sizes for any one given picture. These results are summarized in Figures 22 through 25, and in Tables 4 through 7.

It was observed from these results that a similar effect on the bubble departure size was experienced for all four fluids, and that the product of the bubble departure size and the electric field intensity at the heater surface was approximately a constant as shown in Table 8 for a field exceeding 10 kv/cm.

Bubble Departure Hypothesis

The following conclusions regarding the electric field effects on bubble shapes may now be offered. They are: one, that the product of the electric field intensity at the heater surface and the average bubble departure size is nearly constant for the fluids tested, and two, that the size and frequency of bubble departure might be expressed as the product of the frequency and the departure bubble diameter squared. This second conclusion is based on the following assumptions and reasoning.

FIGURE 26

BUBBLE DEPARTURE DIAMETER AS A
FUNCTION OF ELECTRIC FIELD INTENSITY AT
HEATER SURFACE FOR TRICHLORO-TRIFLUOROETHANE

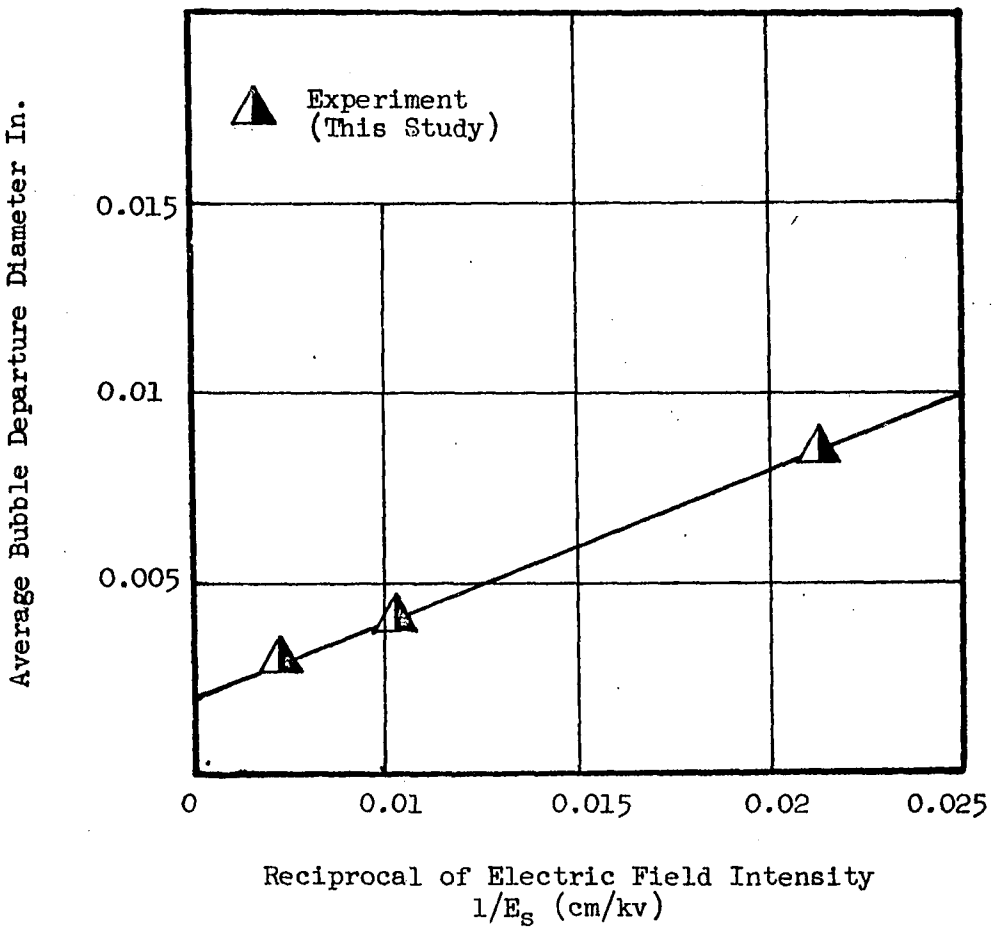

FIGURE 27

BUBBLE DEPARTURE DIAMETER AS A FUNCTION OF ELECTRIC FIELD INTENSITY AT HEATER SURFACE FOR CARBON TETRACHLORIDE

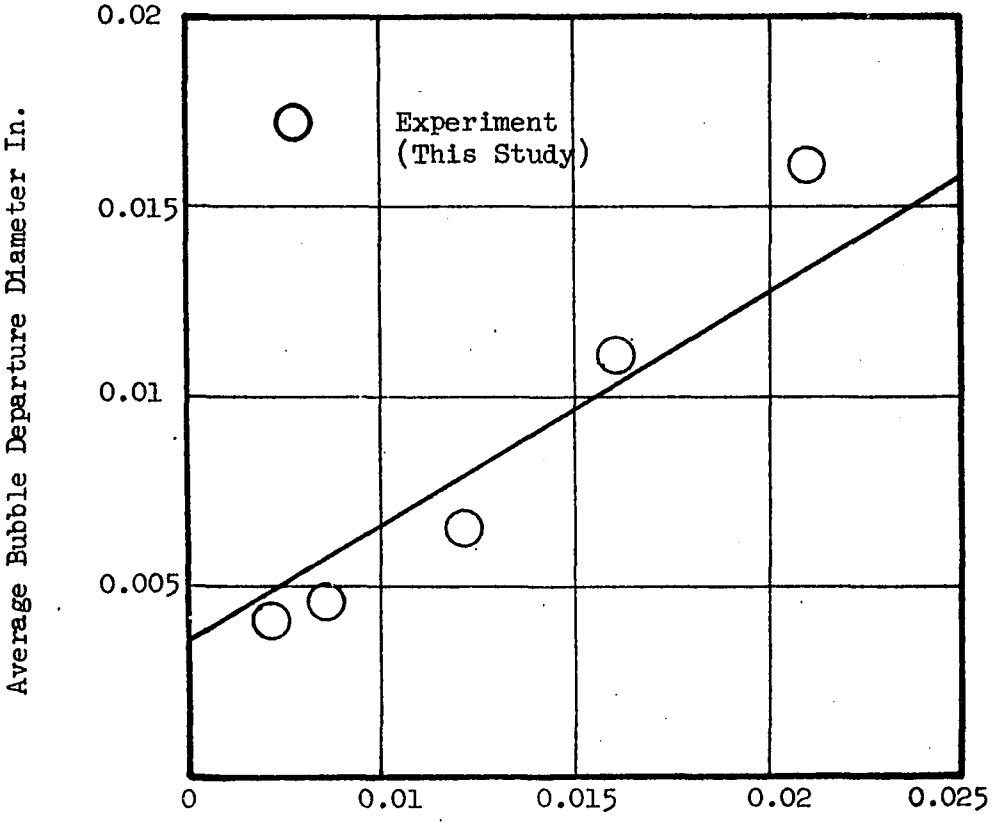

FIGURE 28

BUBBLE DEPARTURE DIAMETER AS A
FUNCTION OF ELECTRIC FIELD INTENSITY AT
HEATER SURFACE FOR DICHLOR-MONOFLUOROMETHANE

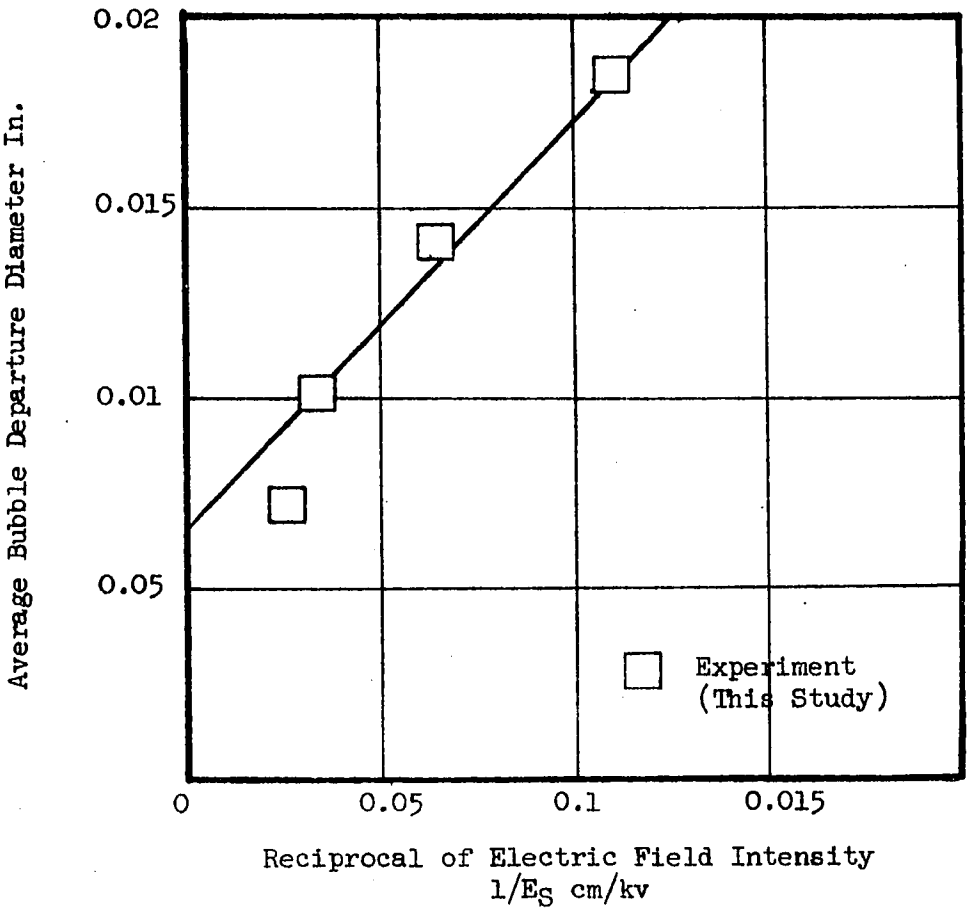

TABLE 4

BUBBLE DEPARTURE DIAMETER RANGE FOR TRICHLORO-TRIFLUOROETHANE AS A FUNCTION OF ELECTRIC FIELD INTENSITY AT HEATER SURFACE

Electric Field Intensity At Heater Surface (E_s) kv/cm	Run Number	Measured Bubble Departure Diameters (in.)
0	6	0.020-0.030
	7	0.02-0.03
	10	0.02-0.03
	17	0.02-0.03
	24	0.02-0.03
	22	0.020-0.025
	12	0.020-0.025
46	12A	0.005-0.01
	18	0.007-0.01
	23	0.01
	24	0.01
92	7A	0.005
	4	0.005
	12B	0.002-0.005
137	12C	0.002-0.004
	6B	0.002
183	12D	0.001-0.002
	8A	0.002-0.003

TABLE 5

BUBBLE DEPARTURE DIAMETER RANGE FOR CARBON TETRACHLORIDE
AS A FUNCTION OF ELECTRIC FIELD INTENSITY AT HEATER SURFACE

Electric Field Intensity At Heater Surface (E_s) kv/cm	Run Number	Measured Bubble Departure Diameters (in.)
0	1	0.02-0.03
	7	0.02-0.03
28	7B	0.02-0.024
46	7C	0.015-0.02
64	7D	0.01-0.015
92	7E	0.007-0.008
	5	0.004-0.005
120	7F	0.005-0.006
	4	0.003-0.004
137	7G	0.004

TABLE 6

BUBBLE DEPARTURE DIAMETER RANGE FOR DICHLORO-MONOFLUOROMETHANE AS A FUNCTION OF ELECTRIC FIELD INTENSITY AT HEATER SURFACE

Electric Field Intensity At Heater Surface kv/cm	Run Number	Measured Bubble Departure Diameter (in.)
0	1	0.02-0.03
9	1	0.015-0.020
18	7	0.01-0.02
28	3	0.008-0.0012
37	3	0.004-0.007

TABLE 7

BUBBLE DEPARTURE DIAMETER RANGE FOR CHLOROFORM
AS A FUNCTION OF ELECTRIC FIELD INTENSITY AT HEATER SURFACE

Electric Field Intensity At Heater Surface kv/cm	Run Number	Measured Bubble Departure Diameter (in.)
28	3	0.01-0.02
46	2, 2A	0.004-0.006

TABLE 8

RELATIONSHIP OF ELECTRIC FIELD INTENSITY AT HEATER SURFACE (E_S) AND BUBBLE DEPARTURE DIAMETER

Carbon Tetrachloride			Trichloro-Trifluoroethane			Dichloro-monofluoromethane			Chloroform		
Electric Field Intensity at Heater Surface E_S kv/cm	Bubble Departure Diameter (D) cm	D x E_S	Electric Field Intensity at Heater Surface kv/cm	Bubble Departure Diameter cm	D x E_S	Electric Field Intensity at Heater Surface kv/cm	Bubble Departure Diameter cm	D x E_S	Electric Field Intensity at Heater Surface	Bubble Departure Diameter cm	D x E_S
9	0.064	0.57	9	0.056	.51	9	0.051	.46	9	-	-
28	0.053	1.5	28	0.033	.92	18	0.036	0.64	28	0.025	.70
46	0.038	1.7	46	0.022	.99	28	0.025	0.71	46	0.013	0.60
92	0.015	1.4	92	0.01	.94	37	0.018	0.66			
137	0.01	1.4	137	.0076	1.04						
			164	.0064	1.04						

From the data of Table 8 the following relationship is hypothesized:

$$DE_s = K_1 \tag{25}$$

where D = diameter of departure size

where E_s = surface electric field intensity

where K_1 = a constant

Equation 11 and 23 as derived for the effect of an electric field on the peak heat flux shows that near the peak heat flux the velocity of vapor or bubble removal would be proportional to the electric field intensity at the heater surface, namely

$$V_g = K_2 E_s \tag{26}$$

where V_g = bubble departure velocity

where E_s = surface electric field intensity

where K_2 = a constant

The velocity of any bubble departing from the surface may be defined as shown below:

$$V_g = fD \tag{27}$$

where V_g = bubble departure velocity

where f = frequency of bubble removal

where D = diameter of departing bubble

Combining equations 26 and 27 then gives:

$$V_g = fD = K_2 E_s \tag{28}$$

and since

$$E_s = \frac{K_1}{D} \tag{25}$$

then

$$fD = V_g = \frac{K_2 K_1}{D} \tag{29}$$

or,

$$fD^2 = K \tag{29}$$

Conclusions

Equation 29 therefore states that the velocity of vapor or bubble removal for a fluid under electric stress should be inversely proportional to the bubble departure size. We might also infer that at conditions away from the peak heat flux higher vapor velocities will exist for the specific case of a fluid stressed by an electric field. However, since no frequency measurements were possible from the still bubble photographs, Equation 29 can only be considered a hypothesis lacking experimental verification.

CHAPTER VI

CONCLUSIONS AND RECOMMENDATIONS

Conclusions

The effect of a non-uniform electric field on the boiling heat transfer mechanisms studied in this thesis may be summarized as follows:

1. The increase in the normal peak heat flux may be explained and quantitatively defined by the postulation of an electrically stabilized Helmholtz-Taylor hydrodynamic condition.
2. An electric field increases the peak heat flux. Large increases over the normal peak heat flux can be expected, with applied voltage and dielectric strength of the fluid seemingly the only limitations to further increased heat transfer rates.
3. An electric field will have a significant effect in the natural convection heat transfer regime. In this region heat fluxes may be maintained with correspondingly lower heat transfer surface temperatures at increased electric field strengths.
4. The variation of heat transfer surface temperatures in the region of nucleate boiling in the presence of a non-uniform electric field will be minor.

5. The effect of an electric field on bubble formation and departure is to reduce the bubble departure size and to increase the rate or frequency of bubble removal.
6. A hypothetical expression for the frequency and diameter of bubble removal in the presence of an electric field may be described as the product of the frequency of removal and the bubble departure diameter squared.
7. Applied voltage effects will be more efficient with higher dielectric constant fluids.

Recommendations

1. A study of particular importance would be that of the effect of uniform electric fields on fluids of varying dielectric constants. Up to the present time, only non-uniform fields have been investigated. A suitable electric geometry for these studies might be two uniform flat plates.
2. Various heat transfer surfaces should be studied, to further test and expand the postulation of the stabilized hydrodynamic condition for the increase in the normal peak heat flux with attendant electric fields.
3. The electric effect on bubble shapes, comprising the study of the frequency and diameter of departing bubbles, should be investigated to develop a more fundamental understanding of the exact nature of the hydrodynamic conditions existing at or near the peak heat flux.

4. A study not developed here would be the investigation of film boiling in a uniform or non-uniform electric field with various dielectric constant fluids.

APPENDIX I

SAMPLE CALCULATION

The necessary current and voltage readings were taken during a run to ascertain the following values:

1. Heat flux
2. Electric field intensity at heater surface

With the data available to calculate the above quantities, a typical sample calculation was as follows:

Electric Field Intensity

The electric field intensity between a coaxial arrangement of conductors is well known. The equation relating the electric field intensity for one experimental system is given below:

$$E = \frac{1}{r} \quad \frac{V_o}{} \quad \left(1/\ln \frac{r_o}{r_i}\right)$$

where E = electric field intensity, kv/cm

where V_o = voltage between cylinders, volts

where r_o = outer cylinder radius, in.

where r_i = inner cylinder or heater wire radius, in.

where r = distance from center of inner electrode, to point at which calculation of E is desired, cm

The electric field intensity vector for this particular case is always directed towards the inner cylinder regardless of voltage polarity.

The following calculations are for the run 2 with carbon tetrachloride.

Test conditions:

V_o = 5.00 kv ± 0.05 kv

r_i = 0.010 in. ± 0.0001 in.

r_o = 0.75 in. ± 0.01 in.

r = 0.010 in. ± 0.0001 in.

$$E_s = \frac{1}{2.54\ (0.01)} \quad \frac{5000}{0.75/0.01} = 45.6 \text{ kv/cm} \pm 1$$

Heat Flux

The heat flux for the test section in the experiment system is calculated by dividing the heat loss through the wire by the surface area of the section. The heat flux may be written as:

$$\frac{Q}{A} = \text{heat flux, Btu/hr.ft}^2$$

where Q = heat transfer rate, Btu/hr

where A = area, ft^2

specifically for this case:

$$A = 2\pi r_w L$$

where π = constant

where r_w = radius of wire, ft.

where L = length of test section, ft.

The heat dissipated in the test section of the wire equals:

$$Q = V_o I, \text{ watts}$$

where Q = heat transfer rate, watts

where V_o = voltage, volts

where I = current, amps

then,

$$Q/A = \frac{V_o I}{2\pi r_w L}$$

The test conditions for run 2 were:

V_o = 1.155 volts $\pm$ 0.0001 volts

I = 33.62 amp $\pm$ 0.01 amp

r_w = 0.01 in. $\pm$ 0.0001 in.

L = 4.80 cm $\pm$ 0.02 cm

then,

$$Q/A = \frac{(3.41)(33.62)(1.155)}{2(3.1416)\left(\frac{0.01}{12}\right)\left(\frac{4.80}{2.54/12}\right)} = 159{,}000 \frac{\text{Btu}}{\text{hr ft}^2} \pm 2320.$$

APPENDIX II

TEMPERATURE MEASUREMENT

The surface temperature of the platinum wire test section was determined by the use of the well known Callendar equation[22] for platinum resistance thermometry as given below:

$$R_T - R_o = \frac{(R_{100}-R_o)\ T}{100} \left(1 + \sigma' \left(\frac{T}{100} - 1\right)\right)$$

where R_t = resistance of platinum wire at temperature T

where R_o = resistance of platinum wire at zero degrees centigrade

where R_{100} = resistance of platinum wire at one hundred degrees centigrade

where T = temperature of platinum wire, °C

where σ' = empirical constant

The Callendar equation is a quadratic in temperature and was solved by the use of a digital computer. The resistance of the platinum wire at the ice and at the steam points was obtained by passing a small current through the test section of the wire while the section was immersed in an ice-water bath and in boiling water respectively. For the platinum wires used in this study, the ratio R_{100}/R_o was found to be 1.392, with sigma prime σ' being taken as 1.493.

The computer program is given below:

```
      READ, R0,R1
      READ, N
      DO   4  I=1, N
      READ, CUR, VOL
      RT= VOL/CUR
      A= (1.493/100.) + 1.
      B= (((1.493/100.) + 1.)**2)-(4.* 1.493/100.)*(RT-R0)/(R1-R0)
      B2= B** (1./2.)
      C= 2.* 1.493/10000.
      TN= (A-B2)/C
      TNF= 1.8*TN-142.16
      TNFD= TNF-142.16
      PUNCH, CUR, VOL, RT
4     PUNCH, TNF TNFD
      END
```

where CUR = current through test section

where VOL = voltage across test section

where N = number of data sets of current and voltage

where RT = resistance of test section at temperature T

where R0,R1 = resistance of test section at ice and steam points

where TN = temperature of test section surface °F

where TNF = temperature of test section surface °C

where TNFD = temperature difference between test section surface and saturated liquid temperature

where A,B,B2, C = fixed and variable constants

A sample calculation for run 2 for the carbon tetrachloride series is shown below with the following input data:

VOL = 1.155 volts

CUR = 33.62 amps

Ro = 0.023949 ohms

Rl = 0.033338 ohms

saturated liquid boiling point = 142.16°F

The following computer results were obtained:

TN = 231.82°F

ΔT = 61.67°C

APPENDIX III

PEAK HEAT FLUX CALCULATIONS

The final predictor equation developed in this study for the effect of non-uniform A.C. and D.C. electric fields on the peak heat flux in boiling heat transfer is shown below:

$$\frac{(Q/A)_{max}}{h_v \rho_v (0.18)} = \left(\frac{\sigma g (\rho_L - \rho_v)}{\rho_v^2}\right)^{1/4} \left(\frac{\rho_L}{\rho_L + \rho_v}\right)^{1/2} + \left(\frac{\varepsilon_o (K-1)^2 (C_o E_s)^2}{\rho_v (K+1)}\right)^{1/2}$$

The computer program to evaluate this equation is:

```
      READ, SIG, G, EO, XK
      READ, P, DV, DL
      D= P* DV* 0.180
      A= (SIG*(G**2) * (DL-DV))/(DV**2)
      B= ((EO*G*0.020088* (XK-1.) **2)/(DV*(XK+1.)))
      READ, N
      DO 5 I = 1, N
      READ, C, E
      Q= D*(A)** 0.25 + D*(C*B*E**2) **0.5
    5 PUNCH    Q, E
      END
```

where:

SIG = surface tension of fluid at saturated boiling point, $lb_f/ft.$

G = acceleration of gravity, ft/hr^2

EO = inductive capacity of free space, $coul^2/newton\text{-}m.^2$

XK = dielectric constant, liquid

P = latent heat of vaporization, Btu/lb

DV = density of vapor, lb_m/ft^3

DL = density of liquid, lb_m/ft^3

A,B,D = fixed and variable constants

C = equivalent field coefficient

E = electric field intensity at wire surface, volts/m.

N = number of data sets

Q = peak heat flux, $Btu/hr.ft^2$

The following computer results were obtained for run 2 of the carbon tetrachloride series with the following inputs:

SIG = 140.005×10^{-5} lb_f/ft

G = 4.17×10^8 ft/hr^2

EO = 8.854×10^{12}, $coul^2/newton\text{-}m.^2$

K = 2.10

P = 83.5 Btu/lb

DU = 0.340 lb/ft^3

DL = 92.5 lb/ft^3

C = 0.235

E = 4,600,000 volts/meter

Computer Result

Q = peak heat flux = 159,000 Btu/hr.ft^2

This quantity is the value for the peak heat flux for carbon tetrachloride with an electric field intensity at the heater surface of 46kv/cm.

APPENDIX IV

TABLE 9

FLUID PROPERTIES

Fluid	Latent Heat of Vaporization Btu/lb	Surface Tension lbf/ft.	Liquid Density lb/ft^3	Vapor Density lb/ft^3	Dielectric Constant
Freon 113[1]	63.09	118.86	94.2	0.464	2.40
Carbon Tetrachloride[3,4]	83.5	140.00	92.5	0.340	2.10
Freon 21[1]	104.15	140.69	87.7	0.285	5.65
Chloroform[2,3]	106.3	149.13	88.02	0.272	4.20
Liquid N_2[2,3]	86.07	60.74	50.45	0.288	1.431
Benzene[2,3]	169.9	144.81	50.53	0.168	2.15
Hexane[2,3]	142.9	91.96	38.07	0.192	1.804
Toluene[2,3]	155.9	124.32	48.49	0.183	2.14
Water[2,3]	970.3	404.23	59.81	0.0373	55.33
Ethyl Ether[2,3,4]	153.7	104.32	44.51	0.183	4.10
Isopropanol[2,3]	286.5	115.29	45.5	0.135	11.60
Freon 12[1]	71.03	114.61	92.85	0.397	2.373

1. "FREON" Technical Bulletins[8].
2. International Critical Tables, Vol. 1-7, 1926-30.
3. Timmermans[23].
4. Chem. Eng. Prog. Vol. 50, No. 6, 1954, pp. 307.

APPENDIX V

FIGURE 29

EFFECT OF AN ELECTRIC FIELD ON BUBBLE
DEPARTURE DIAMETERS FOR TRICHLOROTRIFLUOROETHANE

E_s = 0 kv/cm
Heat Flux = 5,900 Btu/hr.ft^2
ΔT = 22.6°F

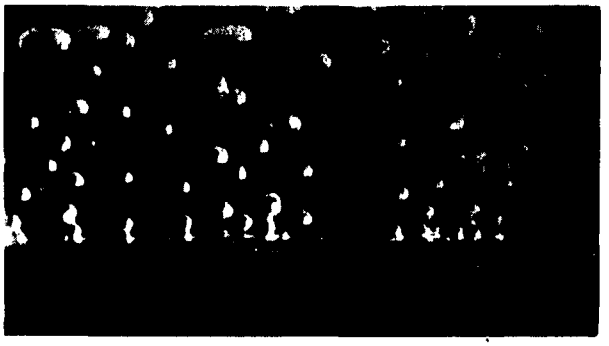

E_s = 45 kv/cm
Heat Flux = 5,960 Btu/hr.ft^2
ΔT = 23.6°F

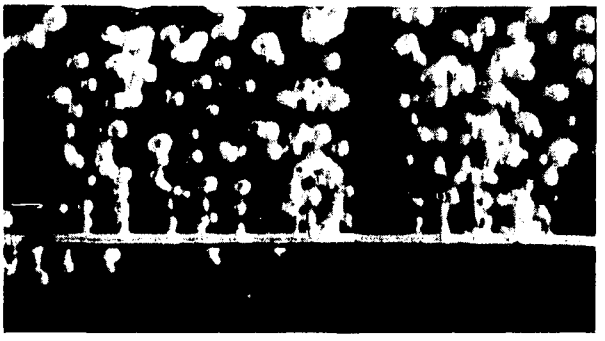

E_s = 92 kv/cm
Heat Flux = 5,940 Btu/hr.ft^2
ΔT = 20.4°F

FIGURE 30

EFFECT OF AN ELECTRIC FIELD ON BUBBLE
DEPARTURE DIAMETERS FOR TRICHLOROTRIFLUOROETHANE

E_s = 137 kv/cm
Heat Flux = 10,174 Btu/hr.ft^2
ΔT = 25.2°F

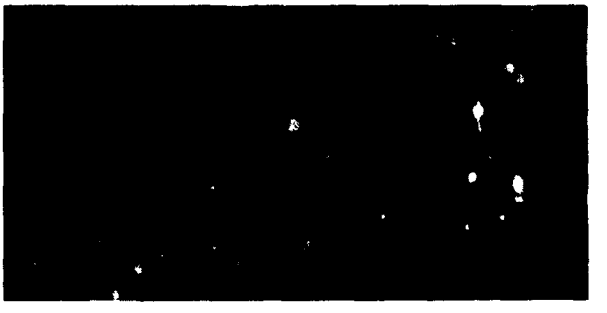

E_s = 184 kv/cm
Heat Flux = 16,500 Btu/hr.ft^2

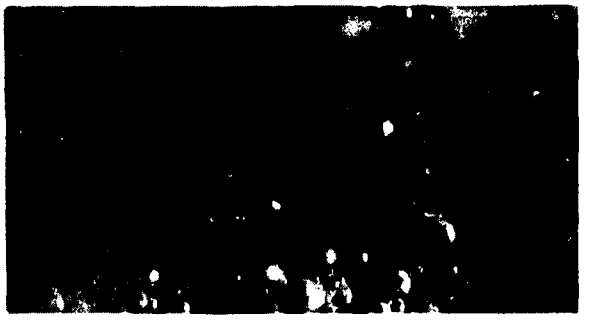

FIGURE 31

EFFECT OF AN ELECTRIC FIELD ON BUBBLE
DEPARTURE DIAMETERS FOR CARBON TETRACHLORIDE

E_s = 0 kv/cm
Heat Flux = 10,500 Btu/hr.ft^2
ΔT = 30°F

E_s = 9 kv/cm
Heat Flux = 10,688 Btu/hr.ft^2
ΔT = 32.9°F

E_s = 13 kv/cm
Heat Flux = 12,100 Btu/hr.ft^2
ΔT = 34.2°F

FIGURE 32

EFFECT OF AN ELECTRIC FIELD ON BUBBLE DEPARTURE DIAMETERS FOR DICHLOROMONOFLUOROMETHANE

E_s = 0 kv/cm
Heat Flux = 14,000 Btu/hr.ft^2

E_s = 9 kv/cm
Heat Flux = 14,000 Btu/hr.ft^2

E_s = 37 kv/cm
Heat Flux = 26,160 Btu/hr.ft^2

The data listed in Appendices VI through IX are computer results. Therefore, the significant figures associated with these data should be considered with respect to the following estimated measurement errors.

Voltage readings ± 0.01%

Current readings ± 0.04%

High Voltage Readings ± 1%

Wire Temperature readings ± 0.2°F

Length Measurements ± 0.4%

All of the current and voltage readings up to the peak heat flux were measured by the Leeds and Northrup potentiometer facility. The peak heat flux current and voltage reading was measured by the Autograf X-Y recorder. The error associated with this recorder was estimated at ± 0.2%.

APPENDIX VI

TABLE 10

1,2,2, TRICHLORO - 1,1,2, TRIFLUORO ETHANE RUN NO. 2

Test Section Length 2.00 in.
Test Voltage 0 kv

Test Section Voltage (volts)	Test Section Current (amps)	Wire Surface Temperature Tw (°F)	Wire Surface Temperature Minus Saturated Liquid Temperature Tw-Ts (°F)	Heat Flux Btu/hr. ft^2
0.085008	2.780	125.97	8.37	920.05
0.11406	3.680	133.52	15.91	1,634.13
0.13038	4.1737	137.94	20.34	2,118.54
0.22631	7.2462	137.81	20.2	6,384.39
0.25555	8.1680	138.82	21.22	8,126.37
0.30864	9.8390	140.32	22.72	11,822.5
0.33395	10.6320	141.058	23.46	13,822.9
0.36654	11.6486	142.085	24.49	16,622.6

TABLE 11

1,2,2, TRICHLORO - 1,1,2, TRIFLUORO ETHANE RUN NO. 4

Test Section Length 2.00 in.
Test Voltage 0 kv

Test Section Voltage (volts)	Test Section Current (amps)	Wire Surface Temperature Tw (°F)	Wire Surface Temperature Minus Saturated Liquid Temperature Tw-Ts (°F)	Heat Flux Btu/hr. ft^2
0.090386	2.9767	129.45	11.84	1,047.47
0.123839	4.0143	138.36	20.76	1,935.41
0.22721	7.3316	140.96	23.36	6,485.32
0.26175	8.4266	142.28	24.68	8,587.05
0.30235	9.7256	142.76	25.16	11,448.05
0.36070	11.5711	144.31	26.71	16,248.97
0.42165	13.480	146.28	28.69	22,128.25
0.46825	14.9386	147.49	29.89	27,232.85
0.51132	16.2760	148.79	31.19	32,400.04
0.54649	17.3770	149.41	31.81	36,971.08
0.57593	18.2730	150.68	33.08	40,971.77
0.65936	20.7860	154.43	36.83	53,357.89
0.72158	22.640	157.21	39.61	63,601.31

TABLE 12

1,2,2, TRICHLORO - 1,1,2, TRIFLUORO ETHANE RUN NO. 5

Test Section Length 2.00 in.
Test Voltage 0 kv

Test Section Voltage (volts)	Test Section Current (amps)	Wire Surface Temperature Tw (°F)	Wire Surface Temperature Minus Saturated Liquid Temperature Tw-Ts (°F)	Heat Flux Btu/hr. ft^2
0.124481	4.0364	138.18	20.58	1,956.15
0.097795	3.2106	131.20	13.60	1,222.38
0.106986	3.4932	134.27	16.67	1,454.97
0.11924	3.8839	135.63	18.03	1,802.99
0.18256	5.8936	140.69	23.09	4,188.82
0.15480	5.010	139.26	21.66	3,019.35
0.14305	4.6497	136.82	19.22	2,589.51
0.121305	3.9520	135.51	17.91	1,866.38
0.108532	3.5471	133.73	16.13	1,498.77

TABLE 13

1,2,2, TRICHLORO - 1,1,2, TRIFLUORO ETHANE RUN NO. 7

Test Section Length 2.00 in.
Test Voltage 0 kv

Test Section Voltage (volts)	Test Section Current (amps)	Wire Surface Temperature Tw (°F)	Wire Surface Temperature Minus Saturated Liquid Temperature Tw-Ts (°F)	Heat Flux Btu/hr. ft2
0.19121	6.1516	142.66	25.06	4,579.35
0.33614	10.796	143.63	26.03	14,128.24
0.48344	15.294	152.37	34.77	28,785.17
0.55466	17.525	153.11	35.51	37,843.38
0.62711	19.736	155.42	37.82	48,184.57
0.72448	22.635	159.71	42.11	63,842.82
0.8012	24.92	162.36	44.76	77,730.98

TABLE 14

1,2,2, TRICHLORO - 1,1,2, TRIFLUORO ETHANE RUN NO. 8

Test Section Length 2.00 in.
Test Voltage 0 kv

Test Section Voltage (volts)	Test Section Current (amps)	Wire Surface Temperature Tw (°F)	Wire Surface Temperature Minus Saturated Liquid Temperature Tw-Ts (°F)	Heat Flux Btu/hr. ft^2
0.81449	12.341	824.37	706.77	39,132.83
0.9020	12.84	913.42	795.82	45,089.63
1.000	13.332	1,014.93	897.33	51,903.95
1.252	14.489	1,266.78	1,149.18	70,623.28

TABLE 15

1,2,2, TRICHLORO - 1,1,2, TRIFLUORO ETHANE RUN NO. 9

Test Section Length 2.04 in.
Test Voltage 0 kv

Test Section Voltage (volts)	Test Section Current (amps)	Wire Surface Temperature Tw (°F)	Wire Surface Temperature Minus Saturated Liquid Temperature Tw-Ts (°F)	Heat Flux Btu/hr. ft^2
0.25318	8.0529	142.12	24.52	7,789.55
0.2000	6.3702	141.35	23.73	4,867.59
0.16727	5.3406	139.95	22.35	3,413.02
0.13657	4.3809	137.29	19.69	2,285.86
0.11926	3.8355	135.83	18.23	1,747.62
0.11215	3.6191	133.91	16.31	1,550.71
0.10433	3.3675	133.79	16.19	1,342.29
0.09678	3.1371	131.40	13.80	1,159.97
0.091616	2.9761	130.20	12.60	1,041.72
0.12436	4.0003	135.72	18.12	1,900.66
0.131655	4.2159	138.27	20.67	2,120.59

TABLE 16

1,2,2, TRICHLORO - 1,1,2, TRIFLUORO ETHANE RUN NO. 10

Test Section Length 2.04 in.
Test Voltage 0 kv

Test Section Voltage (volts)	Test Section Current (amps)	Wire Surface Temperature Tw (°F)	Wire Surface Temperature Minus Saturated Liquid Temperature Tw-Ts (°F)	Heat Flux Btu/hr. ft^2
0.23971	7.324	140.74	23.14	6,427.75
0.29103	9.2477	142.68	25.07	10,282.58
0.35531	11.2456	144.95	27.35	15,265.85
0.44085	13.8972	147.26	29.66	23,407.18
0.49909	15.663	149.85	32.25	29,866.53
0.58009	18.109	152.92	35.32	40,134.77
0.65601	20.353	156.54	38.94	51,011.70
0.75160	23.097	162.18	44.58	66,324.39
0.80072	24.493	164.93	47.33	74,929.63

TABLE 17

1,2,2, TRICHLORO - 1,1,2, TRIFLUORO ETHANE RUN NO. 12

Test Section Length 2.04 in.
Test Voltage 0 kv

Test Section Voltage (volts)	Test Section Current (amps)	Wire Surface Temperature Tw (°F)	Wire Surface Temperature Minus Saturated Liquid Temperature Tw-Ts (°F)	Heat Flux Btu/hr. ft^2
0.22109	7.0045	140.18	22.58	5,916.67
0.290205	9.1640	142.06	24.46	10,160.64
0.37021	11.6508	144.00	26.40	16,479.15
0.4344	13.6380	145.39	27.79	22,634.53
0.51366	16.056	147.91	30.31	31,509.68
0.59225	18.417	150.91	33.31	41,673.01
0.68046	21.076	153.23	35.63	54,792.57
1.5448	15.758	1,491.96	1,374.36	93,004.57
1.063	13,576	1,053.10	935.50	55,136.09

TABLE 18

1,2,2, TRICHLORO - 1,1,2, TRIFLUORO ETHANE RUN NO. 17

Test Section Length 2.16 in.
Test Voltage 0 kv

Test Section Voltage (volts)	Test Section Current (amps)	Wire Surface Temperature Tw (°F)	Wire Surface Temperature Minus Saturated Liquid Temperature Tw-Ts (°F)	Heat Flux Btu/hr. ft^2
0.30055	9.5936	144.61	27.01	10,393.93
0.41126	13.0390	148.51	30.91	19,330.40
0.51607	16.2570	152.25	34.65	30,243.38
0.61951	19.410	155.42	37.82	43,346.62
0.72819	22.666	159.28	41.68	59,497.81
0.63492	19.977	152.95	35.35	45,722.57
0.72842	22.680	159.10	41.50	49,553.36
0.7900	24.50	161.45	43.85	69,770.94
0.7800	24.10	163.66	46.06	67,763.06

TABLE 19

1,2,2, TRICHLORO - 1,1,2, TRIFLUORO ETHANE RUN NO. 22

Test Section Length 2.08 in.
Test Voltage 0 kv

Test Section Voltage (volts)	Test Section Current (amps)	Wire Surface Temperature Tw (°F)	Wire Surface Temperature Minus Saturated Liquid Temperature Tw-Ts (°F)	Heat Flux Btu/hr. ft2
0.31265	9.7049	145.96	28.36	11,365.39
0.47011	14.5124	149.14	31.54	25,554.87
0.65910	20.104	156.14	38.54	49,632.79
0.74998	22.702	160.64	43.04	63,774.74
0.8520	25.50	167.38	49.78	81,379.44
0.8610	25.70	169.00	51.40	82,884.09

TABLE 20

1,2,2, TRICHLORO - 1,1,2, TRIFLUORO ETHANE RUN NO. 20

Test Section Length 1.90 in.
Test Voltage 0 kv

Test Section Voltage (volts)	Test Section Current (amps)	Wire Surface Temperature Tw (°F)	Wire Surface Temperature Minus Saturated Liquid Temperature Tw-Ts (°F)	Heat Flux Btu/hr. ft^2
0.8200	26.40		-	88,715.4

TABLE 21

1,2,2, TRICHLORO - 1,1,2, TRIFLUORO ETHANE RUN NO. 23

Test Section Length 2.08 in.
Test Voltage 5.25 kv

Test Section Voltage (volts)	Test Section Current (amps)	Wire Surface Temperature Tw (°F)	Wire Surface Temperature Minus Saturated Liquid Temperature Tw-Ts (°F)	Heat Flux Btu/hr. ft^2
0.30784	9.4786	150.64	33.04	10,929.6
0.39603	12.1370	153.37	35.77	18,004.2
0.47131	14.3980	155.24	37.64	25,418.1
0.54736	16.7100	155.64	38.04	34,259.8
0.62466	19.044	156.43	38.83	44,559.1
0.70879	21.5450	158.17	40.57	57,200.4

TABLE 22

1,2,2, TRICHLORO - 1,1,2, TRIFLUORO ETHANE RUN NO. 23A

Test Section Length 2.08 in.
Test Voltage 5.25 kv

Test Section Voltage (volts)	Test Section Current (amps)	Wire Surface Temperature Tw (°F)	Wire Surface Temperature Minus Saturated Liquid Temperature Tw-Ts (°F)	Heat Flux Btu/hr. ft^2
0.38653	11.7299	159.15	41.55	16,982.9
0.70629	21.175	166.36	48.76	56,019.8
0.77230	23.0710	168.52	50.92	66,740.2
0.85610	25.472	170.93	53.33	81,681.3
0.92745	27.513	172.73	55.13	95,579.2
0.97879	28.967	174.17	56.57	106,200.8
1.02134	30.174	175.2	57.62	115,435.2
1.06795	31.450	177.2	59.8	125,807.5
1.150	33.50	183.8	66.3	144,303.7

TABLE 23

1,2,2, TRICHLORO - 1,1,2, TRIFLUORO ETHANE RUN NO. 12A

Test Section Length 2.04 in.
Test Voltage 5.25 kv

Test Section Voltage (volts)	Test Section Current (amps)	Wire Surface Temperature Tw (°F)	Wire Surface Temperature Minus Saturated Liquid Temperature Tw-Ts (°F)	Heat Flux Btu/hr. ft^2
0.22167	7.010	141.23	23.63	5,936.85
0.291353	9.1650	144.26	26.66	10,201.9
0.37194	11.6540	146.53	28.93	16,560.7
0.43605	13.6240	148.17	30.57	22,697.2
0.51461	16.032	149.85	32.25	31,520.8
0.59275	18.4095	151.64	34.04	41,691.2
0.66150	20.475	153.62	36.02	51,746.9
0.79680	24.5060	157.36	39.76	74,602.4

TABLE 24

1,2,2, TRICHLORO - 1,1,2, TRIFLUORO ETHANE RUN NO. 18

Test Section Length 2.00 in.
Test Voltage 5.25 kv

Test Section Voltage (volts)	Test Section Current (amps)	Wire Surface Temperature Tw (°F)	Wire Surface Temperature Minus Saturated Liquid Temperature Tw-Ts (°F)	Heat Flux Btu/hr. ft^2
0.30181	9.5520	142.74	25.14	11,223.6
0.30344	9.550	145.95	28.35	11,281.9
0.40480	12.6750	148.91	31.31	19,975.3
0.49786	15.536	150.88	33.28	30,112.8
0.58508	18.2105	152.39	34.79	41,480.3
0.69988	21.7055	154.49	36.89	59,142.3
0.52805	16.4520	151.80	34.20	33,821.9

TABLE 25

1,2,2, TRICHLORO - 1,1,2, TRIFLUORO ETHANE RUN NO. 2

Test Section Length 2.50 in.
Test Voltage 10.5 kv

Test Section Voltage (volts)	Test Section Current (amps)	Wire Surface Temperature Tw (°F)	Wire Surface Temperature Minus Saturated Liquid Temperature Tw-Ts (°F)	Heat Flux Btu/hr. ft^2
0.07367	2.4431	118.29	0.69	700.7
0.102125	3.3682	121.29	3.69	1,339.2
0.13275	4.3544	124.30	6.70	2,250.4
0.1588	5.1823	127.14	9.54	3,203.9
0.19431	6.2951	131.20	13.60	4,762.1
0.2177	7.0134	134.35	16.75	5,944.2
0.25081	8.0199	138.58	20.98	7,831.0
0.28865	9.1592	142.96	25.36	10,292.8
0.33225	10.4944	145.60	28.0	13,574.6
0.36195	11.4086	146.81	29.21	16,676.3
0.4915	15.43	149.12	31.52	29,525.3

TABLE 26

1,2,2, TRICHLORO - 1,1,2, TRIFLUORO ETHANE RUN NO. 7A

Test Section Length 2.00 in.
Test Voltage 10 kv

Test Section Voltage (volts)	Test Section Current (amps)	Wire Surface Temperature Tw (°F)	Wire Surface Temperature Minus Saturated Liquid Temperature Tw-Ts (°F)	Heat Flux Btu/hr. ft^2
0.18897	6.1498	136.13	18.53	4,524.4
0.24775	7.9814	141.89	24.29	7,698.4
0.33809	10.7211	150.99	33.39	14,111.6
0.40369	12.7357	153.99	36.39	20,015.9
0.48835	15.3320	156.84	39.24	29,149.8
0.55756	17.417	159.80	42.20	37,806.8
0.63438	19.80	160.30	42.70	48,901.2
0.72951	22.683	162.55	44.95	64,422.4

TABLE 27

1,2,2, TRICHLORO - 1,1,2, TRIFLUORO ETHANE RUN NO. 12B

Test Section Length 2.04 in.
Test Voltage 10.5 kv

Test Section Voltage (volts)	Test Section Current (amps)	Wire Surface Temperature Tw (°F)	Wire Surface Temperature Minus Saturated Liquid Temperature Tw-Ts (°F)	Heat Flux Btu/hr. ft^2
0.22055	7.014	138.02	20.42	5,910.2
0.29148	9.164	144.57	26.97	10,205.3
0.37291	11.650	148.23	30.63	16,598.2
0.4372	13.606	150.46	32.86	22,726.9
0.51627	16.012	152.45	34.85	31,583.0
0.59448	18.387	154.05	36.45	41,761.8
0.66250	20.448	155.28	37.68	51,756.8

TABLE 28

1,2,2, TRICHLORO - 1,1,2, TRIFLUORO ETHANE RUN NO. 24

Test Section Length 2.08 in.
Test Voltage 10.5 kv

Test Section Voltage (volts)	Test Section Current (amps)	Wire Surface Temperature Tw (°F)	Wire Surface Temperature Minus Saturated Liquid Temperature Tw-Ts (°F)	Heat Flux Btu/hr. ft^2
0.31783	9.766	151.84	34.24	11,626.4
0.50209	15.109	164.14	46.54	28,415.3
0.6730	20.124	167.94	50.34	50,729.9
0.84411	25.094	171.44	53.84	79,342.1
1.0158	30.04	174.62	57.02	114,299.2
1.19984	35.264	178.39	60.79	158,485.6
1.36	39.80	181.02	63.42	202,748.2

TABLE 29

1,2,2, TRICHLORO - 1,1,2, TRIFLUORO ETHANE RUN NO. 12C

Test Section Length 2.04 in.
Test Voltage 15.0 kv

Test Section Voltage (volts)	Test Section Current (amps)	Wire Surface Temperature Tw (°F)	Wire Surface Temperature Minus Saturated Liquid Temperature Tw-Ts (°F)	Heat Flux Btu/hr. ft^2
0.21938	7.010	135.33	17.73	5,875.5
0.2906	9.1640	142.84	25.24	10,174.5
0.37254	11.6450	147.90	30.30	16,574.6
0.43676	13.5880	150.64	33.04	22,674.1
0.51604	15.992	152.91	35.31	31,529.5
0.59436	18.365	154.64	37.04	41,703.4
0.55242	20.419	156.04	38.44	51.677.2
0.7992	24.551	158.05	40.45	74,964.5

TABLE 30

1,2,2, TRICHLORO - 1,1,2, TRIFLUORO ETHANE RUN NO. 25

Test Section Length 2.08 in.
Test Voltage 15.0 kv

Test Section Voltage (volts)	Test Section Current (amps)	Wire Surface Temperature Tw (°F)	Wire Surface Temperature Minus Saturated Liquid Temperature Tw-Ts (°F)	Heat Flux Btu/hr. ft^2
0.31494	9.5845	157.48	39.88	11,306.6
0.86064	25.512	173.18	55.58	82,243.4
1.02574	30.293	175.44	57.84	116,389.7
1.2057	35.462	177.95	60.34	160,153.9
1.46	42.2	188.69	71.09	230,781.1

TABLE 31

1,2,2, TRICHLORO - 1,1,2, TRIFLUORO ETHANE RUN NO. 27

Test Section Length 2.00 in.
Test Voltage 15.0 kv

Test Section Voltage (volts)	Test Section Current (amps)	Wire Surface Temperature Tw (°F)	Wire Surface Temperature Minus Saturated Liquid Temperature Tw-Ts (°F)	Heat Flux Btu/hr. ft^2
0.1081	3.6290	127.61	10.01	1,527.3
0.14824	4.9111	135.02	17.42	2,834.3
0.19915	6.539	140.09	22.49	5,069.9
0.25384	8.254	145.66	28.06	8,156.9
0.32212	10.364	151.79	34.19	12,997.2
0.47829	15.165	160.38	42.78	28,238.3
0.6390	20.230	161.28	43.68	50,327.1
1.49	44.8	192.75	75.15	259,877.9

TABLE 32

1,2,2, TRICHLORO - 1,1,2, TRIFLUORO ETHANE RUN NO. 3

Test Section Length 2.00 in.
Test Voltage 18.5 kv

Test Section Voltage (volts)	Test Section Current (amps)	Wire Surface Temperature Tw (°F)	Wire Surface Temperature Minus Saturated Liquid Temperature Tw-Ts (°F)	Heat Flux Btu/hr. ft^2
0.098511	3.2575	119.86	2.26	1,249.3
0.138954	4.5623	123.77	6.17	2,468.1
0.16752	5.4796	125.85	8.25	3,573.7
0.23505	7.5992	132.36	14.76	6,953.98
0.27241	8.7443	136.39	18.79	9,273.7
0.30939	9.8790	139.39	21.79	11,899.4
0.33265	10.5789	141.69	24.09	13,700.4
0.37026	11.7239	144.18	26.58	16,899.9
0.51926	16.232	151.61	34.01	32,814.2

TABLE 33

1,2,2, TRICHLORO - 1,1,2, TRIFLUORO ETHANE RUN NO. 14

Test Section Length 2.04 in.
Test Voltage 18.5 kv

Test Section Voltage (volts)	Test Section Current (amps	Wire Surface Temperature Tw (°F)	Wire Surface Temperature Minus Saturated Liquid Temperature Tw-Ts (°F)	Heat Flux Btu/hr. ft^2
0.15179	4.944	128.17	10.57	2,880.3
0.18286	5.93105	130.51	12.91	4,162.6
0.21470	6.9250	133.64	16.04	5,706.4
0.26021	8.3226	138.39	20.79	8,311.8
0.31193	9.8740	144.31	26.71	11,821.3
0.39430	12.350	150.42	32.82	18,689.9

TABLE 34

1,2,2, TRICHLORO - 1,1,2, TRIFLUORO ETHANE RUN NO. 15

Test Section Length 3.04 in.
Test Voltage 18.5 kv

Test Section Voltage (volts)	Test Section Current (amps)	Wire Surface Temperature Tw (°F)	Wire Surface Temperature Minus Saturated Liquid Temperature Tw-Ts (°F)	Heat Flux Btu/hr. ft^2
0.39438	12.343	150.87	33.27	18,683.1
0.49176	15.309	153.97	36.37	28,894.4
0.59526	18.470	155.91	38.31	42,197.5

APPENDIX VII

TABLE 35

DICHLORO-MONOFLUOROMETHANE RUN NO. 1

Test Section Length 2.02 in.
Test Voltage 0 kv

Test Section Voltage (volts)	Test Section Current (amps)	Wire Surface Temperature Tw (°F)	Wire Surface Temperature Minus Saturated Liquid Temperature Tw-Ts (°F)	Heat Flux Btu/hr. ft^2
0.08721	2.9487	57.27	9.17	918.6
0.097048	3.5231	60.27	12.17	1,319.6
0.10966	3.9613	62.66	14.56	1,676.5
0.12929	4.6285	67.06	18.96	2,309.6
0.14019	4.988	70.08	21.98	2,698.8
0.2125	7.3101	87.03	38.93	5,995.3
0.376	13.185	77.31	29.21	19,133.5
0.3120	10.810	83.38	35.28	13,016.8
0.25727	9.042	76.18	28.08	8,977.9
0.34148	12.006	75.99	27.89	15,823.0
0.42364	14.837	77.94	29.84	24,258.8
0.27921	9.777	78.03	29.93	10,535.7
0.086852	3.168	57.97	9.87	1,061.9
0.092825	3.3804	58.75	10.65	1,211.04

TABLE 36

DICHLORO-MONOFLUOROMETHANE RUN NO. 1

(Con't)

Test Section Length 2.02 in.
Test Voltage 0 kv

Test Section Voltage (volts)	Test Section Current (amps)	Wire Surface Temperature Tw (°F)	Wire Surface Temperature Minus Saturated Liquid Temperature Tw-Ts (°F)	Heat Flux Btu/hr. ft^2
0.096881	3.5210	59.72	11.62	1,316.5
0.15814	5.576	74.56	26.46	3,403.2
0.37365	13.106	77.18	29.08	18,899.97
0.48792	17.058	78.83	30.73	32,122.1
0.54636	19.026	80.82	32.72	40,119.2
0.60362	20.968	82.06	33.97	48,847.9
0.6497	22.481	84.04	35.94	56,370.8
0.70584	24.504	82.37	34.27	66,752.8
0.7642	26.295	86.90	38.80	77,554.3
0.83072	28.510	88.23	40.13	91,406.6
0.9070	30.80	93.69	45.59	107,816.2

TABLE 37

DICHLORO-MONOFLUOROMETHANE RUN NO. 2

Test Section Length 2.02 in.
Test Voltage 1 kv

Test Section Voltage (volts)	Test Section Current (amps)	Wire Surface Temperature Tw (°F)	Wire Surface Temperature Minus Saturated Liquid Temperature Tw-Ts (°F)	Heat Flux Btu/hr. ft^2
0.26599	9.520	71.04	22.94	9,724.4
0.09630	3.5523	56.35	8.25	1,313.7
0.10801	3.9795	56.92	8.82	1,650.6
0.12742	4.6850	57.90	9.80	2,292.5
0.16823	6.1504	60.65	12.55	3,973.5
0.22416	8.0794	67.58	19.48	6,955.0
0.31169	11.076	74.59	26.49	13,257.7
0.39838	14.009	79.84	31.74	21,432.2
0.49086	17.209	81.37	33.27	32,439.6
0.57673	20.106	84.22	36.12	44,530.7
0.66512	23.099	86.17	38.07	59,000.4
0.7593	26.229	88.92	40.82	76,481.6
0.980	33.2	99.03	50.93	124,946.9

TABLE 38

DICHLORO-MONOFLUOROMETHANE RUN NO. 3

Test Section Length 2.00 in.
Test Voltage 4 kv

Test Section Voltage (volts)	Test Section Current (amps)	Wire Surface Temperature Tw (°F)	Wire Surface Temperature Minus Saturated Liquid Temperature Tw-Ts (°F)	Heat Flux Btu/hr. ft^2
0.12154	4.6324	49.67	1.57	2,191.9
0.09246	3.527	49.28	1.18	1,269.6
0.19145	7.198	56.16	8.06	5,365.0
0.34139	12.383	73.66	25.56	16,458.2
0.43338	15.504	80.58	32.48	26,158.8
0.5855	20.770	84.86	36.76	47,344.4
1.370	47.770	102.22	54.12	250,682.2

TABLE 39

DICHLORO-MONOFLUOROMETHANE RUN NO. 4

Test Section Length 1.98 in.
Test Voltage 4 kv

Test Section Voltage (volts)	Test Section Current (amps)	Wire Surface Temperature Tw (°F)	Wire Surface Temperature Minus Saturated Liquid Temperature Tw-Ts (°F)	Heat Flux Btu/hr. ft^2
0.097954	3.8020	49.43	1.33	1,467.2
0.20161	7.676	58.60	10.50	6,096.9
0.23888	9.0492	61.04	12.94	8,516.4
0.37708	13.842	76.52	28.42	20,563.5
0.55130	20.126	79.29	31.19	43,712.9
0.75811	27.392	84.51	36.41	81,812.8

TABLE 40

DICHLORO-MONOFLUOROMETHANE RUN NO. 5

Test Section Length 2.04 in.
Test Voltage 3 kv

Test Section Voltage (volts)	Test Section Current (amps)	Wire Surface Temperature Tw (°F)	Wire Surface Temperature Minus Saturated Liquid Temperature Tw-Ts (°F)	Heat Flux Btu/hr. ft^2
0.09870	3.697	51.21	3.11	1,394.4
0.19807	7.327	56.72	8.62	5,540.9
0.17710	6.559	56.16	8.06	4,435.0
0.10986	4.110	51.36	3.26	1,723.9
0.08787	3.294	50.39	2.29	1,105.1
0.31312	11.332	67.34	19.24	13,547.4
0.43121	15.438	72.67	24.57	25,416.7
0.5741	20.260	79.87	31.77	44,408.5
0.73161	25.584	84.49	36.39	71,463.9
1.330	45.00	101.59	53.49	228,508.9
0.12681	4.7305	52.72	4.62	2,290.3
6.136	0.16498	54.14	6.04	3,865.1

TABLE 41

DICHLORO-MONOFLUOROMETHANE RUN NO. 6

Test Section Length 2.00 in.
Test Voltage 2 kv

Test Section Voltage (volts)	Test Section Current (amps)	Wire Surface Temperature Tw (°F)	Wire Surface Temperature Minus Saturated Liquid Temperature Tw-Ts (°F)	Heat Flux Btu/hr. ft^2
0.08730	3.3102	50.99	2.89	1,125.1
0.12715	4.7999	53.09	4.99	2,376.0
0.1695	6.324	58.71	10.61	4,173.2
0.21074	7.825	61.02	12.92	6,420.0
0.14816	5.546	57.13	9.03	3,199.0
0.18474	6.891	58.82	10.72	4,956.2
0.09462	3.584	51.49	3.39	1,320.2
0.27612	10.061	70.24	22.14	10,815.4
0.35136	12.7504	72.26	24.16	17,441.4
0.45058	16.336	72.72	24.62	28,656.5
0.55209	19.845	77.00	28.90	42,654.6
0.6975	24.915	80.15	32.05	67,656.6
1.01	35.20	92.74	44.64	138,410.5

TABLE 42

DICHLORO-MONOFLUOROMETHANE RUN NO. 7

Test Section Length 2.00 in.
Test Voltage 2 kv

Test Section Voltage (volts)	Test Section Current (amps)	Wire Surface Temperature Tw (°F)	Wire Surface Temperature Minus Saturated Liquid Temperature Tw-Ts (°F)	Heat Flux Btu/hr. ft^2
0.31594	11.624	68.97	20.87	14,297.7
0.3990	14.569	72.72	24.62	22,631.2
0.47081	17.085	75.81	27.71	31,315.9
0.63888	22.955	80.79	32.69	57,095.5
1.00	34.7	98.72	50.62	135,093.6

TABLE 43

DICHLORO-MONOFLUOROMETHANE RUN NO. 8

Test Section Length 2.00 in.
Test Voltage 2 kv

Test Section Voltage (volts)	Test Section Current (amps)	Wire Surface Temperature Tw (°F)	Wire Surface Temperature Minus Saturated Liquid Temperature Tw-Ts (°F)	Heat Flux Btu/hr. ft^2
1.12	37.8	111.55	63.45	164,821.91

APPENDIX VIII

TABLE 44

CHLOROFORM RUN NO. 1

Test Section Length 2.00 in.
Test Voltage 0 kv

Test Section Voltage (volts)	Test Section Current (amps)	Wire Surface Temperature Tw (°F)	Wire Surface Temperature Minus Saturated Liquid Temperature Tw-Ts (°F)	Heat Flux Btu/hr. ft^2
0.30976	9.3722	170.54	27.29	11,358.9
0.39652	11.949	172.97	29.72	18,538.1
0.10420	3.2545	151.71	8.46	1,326.8
0.097364	3.0474	150.48	7.23	1,160.9
0.1167	3.6346	153.36	10.11	1,659.6
0.13562	4.1978	156.99	13.74	2,227.5
0.1680	5.1303	164.99	21.74	3,372.3
0.18869	5.7811	163.03	19.78	4,268.0
0.2530	7.6930	167.55	24.30	7,615.3
0.49444	14.859	174.64	31.39	28,745.7
0.61471	18.385	177.56	34.31	44,218.4
0.71446	21.262	180.61	37.36	59,436.3
0.80509	23.849	183.45	40.20	75,124.9
0.961	28.0	193.77	50.52	105,281.2

TABLE 45

CHLOROFORM RUN NO. 3

Test Section Length 1.97 in.
Test Voltage 2.5 kv

Test Section Voltage (volts)	Test Section Current (amps)	Wire Surface Temperature Tw (°F)	Wire Surface Temperature Minus Saturated Liquid Temperature Tw-Ts (°F)	Heat Flux Btu/hr. ft^2
0.131724	4.2471	148.24	6.08	2,210.3
0.17069	5.4861	149.39	7.23	3,703.9
0.22866	7.2962	153.61	11.45	6,599.1
0.29581	9.3282	160.55	18.39	10,914.6
0.33269	10.411	165.11	22.95	13,700.3
0.38729	12.009	170.61	28.45	18,396.8
0.48095	14.841	173.54	31.38	28,233.3
0.58629	17.993	176.87	34.71	41,726.8
0.68789	20.98	180.68	38.57	57,085.2
0.80472	24.472	182.47	40.31	77,895.6
0.8980	27.150	186.07	43.91	96,437.3
1.150	33.50	209.61	67.45	152,384.7

TABLE 46

CHLOROFORM RUN NO. 4

Test Section Length 1.97 in.
Test Voltage 4 kv

Test Section Voltage (volts)	Test Section Current (amps)	Wire Surface Temperature Tw (°F)	Wire Surface Temperature Minus Saturated Liquid Temperature Tw-Ts (°F)	Heat Flux Btu/hr. ft^2
0.113672	3.6766	146.29	3.04	1,653.1
0.15813	5.1030	147.59	4.34	3,191.8
0.22783	7.283	153.09	9.84	6,563.2
0.3486	10.944	163.75	20.50	15,090.4
0.5781	17.70	178.88	35.63	40,473.8
1.36	39.6	210.50	67.25	213,025.5

TABLE 47

CHLOROFORM RUN NO. 2

Test Section Length 2.00 in.
Test Voltage 5 kv

Test Section Voltage (volts)	Test Section Current (amps)	Wire Surface Temperature Tw (°F)	Wire Surface Temperature Minus Saturated Liquid Temperature Tw-Ts (°F)	Heat Flux Btu/hr. ft^2
0.116481	3.6826	144.67	1.42	1,678.3
0.138456	4.3660	146.16	2.91	2,365.2
0.17266	5.4366	147.01	3.76	3,672.7
0.23334	7.2523	154.57	11.32	6,621.2
0.29007	8.9006	162.13	18.88	10,101.6
0.30501	9.3459	162.97	19.72	11,153.3
0.40675	12.2483	173.42	30.17	19,492.7
0.49859	14.9715	175.13	31.88	29,206.4
0.59830	17.876	178.18	34.93	41,846.5
0.69011	20.516	181.25	38.00	55,396.3
0.81505	24.156	183.15	39.90	77,033.3
0.495	41.9	218.71	75.46	245,089.5

APPENDIX IX

TABLE 48

CARBON TETRACHLORIDE RUN NO. 1

Test Section Length 1.90 in.
Test Voltage 0 kv

Test Section Voltage (volts)	Test Section Current (amps)	Wire Surface Temperature Tw (°F)	Wire Surface Temperature Minus Saturated Liquid Temperature Tw-Ts (°F)	Heat Flux Btu/hr. ft^2
0.30619	9.3098	203.27	33.12	11,745.2
0.36641	11.099	205.67	35.52	16,756.3
0.43975	13.291	207.10	36.95	24.081.9
0.5023	15.147	208.57	38.42	31,348.6
0.56645	17.038	210.21	40.06	39,765.6
0.64691	19.400	212.15	42.00	51,709.8
0.097116	3.0409	184.78	14.63	1,216.8
0.11249	3.4908	190.37	20.22	1,617.9
0.125835	3.900	191.16	21.01	2,022.1
0.15460	4.7354	198.58	28.43	3,016.4
0.16523	5.0893	195.05	24.90	3,464.8
0.1387	4.2919	192.15	22.00	2,452.8
0.67674	20.2490	213.61	43.46	56,461.6
0.72614	21.684	214.91	44.76	64,876.5
0.76323	22.749	216.13	45.98	71,539.4
0.9310	27.30	226.90	56.75	104,722.5

TABLE 49

CARBON TETRACHLORIDE RUN NO. 2

Test Section Length 1.90 in.
Test Voltage 5 kv

Test Section Voltage (volts)	Test Section Current (amps)	Wire Surface Temperature Tw (°F)	Wire Surface Temperature Minus Saturated Liquid Temperature Tw-Ts (°F)	Heat Flux Btu/hr. ft^2
1.155	33.62	231.82	61.67	159,995.3

TABLE 50

CARBON TETRACHLORIDE RUN NO. 3

Test Section Length 1.90 in.
Test Voltage 9 kv

Test Section Voltage (volts)	Test Section Current (amps)	Wire Surface Temperature Tw (°F)	Wire Surface Temperature Minus Saturated Liquid Temperature Tw-Ts (°F)	Heat Flux Btu/hr. ft^2
1.34	38.70	237.11	66.96	213,669.9

TABLE 51

CARBON TETRACHLORIDE RUN NO. 5

Test Section Length 2.03 in.
Test Voltage 9 kv

Test Section Voltage (volts)	Test Section Current (amps	Wire Surface Temperature Tw (°F)	Wire Surface Temperature Minus Saturated Liquid Temperature Tw-Ts (°F)	Heat Flux Btu/hr. ft^2
0.30932	8.98149	203.02	32.87	10,668.9
0.19703	5.8408	189.93	19.78	4,419.4
0.15911	4.7410	186.73	16.58	2,896.9
0.12578	3.7715	182.84	12.69	1,821.7
0.10391	3.1265	180.71	10.56	1,247.6
0.3467	10.039	204.79	34.64	13,366.2
0.47031	13.482	211.27	41.12	24,350.1
0.57649	16.526	211.26	41.11	36,586.5
0.77831	22.361	209.83	39.68	66,835.2
0.8911	25.411	214.67	44.52	86,958.1
0.98413	28.011	215.91	45.76	105,862.6
1.1078	31.391	218.82	48.67	133,545.1
1.2486	35.190	222.38	52.23	168,734.6
1.410	39.20	231.56	61.31	212,259.3

TABLE 52

CARBON TETRACHLORIDE RUN NO. 4

Test Section Length 2.00 in.
Test Voltage 13 kv

Test Section Voltage (volts)	Test Section Current (amps)	Wire Surface Temperature Tw (°F)	Wire Surface Temperature Minus Saturated Liquid Temperature Tw-Ts (°F)	Heat Flux Btu/hr. ft^2
0.25516	7.4845	195.85	25.70	7,434.9
0.16329	4.8709	185.35	15.20	3,096.5
0.13544	4.0569	182.79	12.64	2,139.2
0.1164	3.4983	180.73	10.58	1,585.3
0.099501	2.9976	179.25	9.10	1,161.2
0.32774	9.4866	204.30	34.15	12,104.5
0.41615	11.930	210.51	40.36	19,328.4
0.52331	14.935	213.42	43.27	30,427.7
0.6325	17.953	216.98	48.83	44,208.2
0.78950	22.376	217.95	47.80	68,776.4
0.90615	25.416	224.82	54.67	89,662.8
1.0285	28.984	221.70	51.55	116,056.0
1.1505	32.338	223.41	53.26	144,845.5
1.2651	35.461	225.25	55.10	174,654.9
1.4160	39.41	229.97	59.82	217,257.5
1.48	40.40	243.09	72.94	232,781.4

TABLE 53

CARBON TETRACHLORIDE RUN NO. 6

Test Section Length 2.03 in.
Test Voltage 15 kv

Test Section Voltage (volts)	Test Section Current (amps)	Wire Surface Temperature Tw (°F)	Wire Surface Temperature Minus Saturated Liquid Temperature Tw-Ts (°F)	Heat Flux Btu/hr. ft^2
1.540	42.50	236.42	66.27	251,345.6

APPENDIX X

Calculation of Maximum Probable Error

I. Heat Flux, Q/A

$$Q/A = \frac{V_o I}{2\pi r_w L}$$

$$d(Q/A) = \frac{I}{2\pi r_w L} dV_o + \frac{V_o}{2\pi r_w L} dI + \frac{V_o I}{2\pi L}\left(\frac{-1}{r_w^2}\right) dr_w + \frac{V_o I}{2\pi r_w}\left(\frac{-1}{L^2}\right) dL$$

$$\frac{d(Q/A)}{(Q/A)} = \frac{dV_o}{V_o} + \frac{dI}{I} - \frac{dr_w}{r_w} - \frac{dL}{L}$$

Maximum Probable Error is obtained without regard for sign.

Therefore,

$$\frac{d(Q/A)}{Q/A} = \frac{dV_o}{V_o} + \frac{dI}{I} + \frac{dr_w}{r_w} + \frac{dL}{L}$$

For example,

V_o = 1.155 volts $\pm$ 0.0001 volts

I = 33.62 amp $\pm$ 0.01 amps

r_w = 0.01 inch $\pm$ 0.0001 inch

L = 4.80 cm $\pm$ 0.02 cm

$$\frac{d\,(Q/A)}{Q/A} = \frac{.0001}{1.155} + \frac{.01}{33.62} + \frac{.0001}{.01} + \frac{.02}{4.80}$$

$= .0000866 + .000298 + .01 + .00417$

$= .01455$

or % Error = 1.46

$Q/A = 159{,}000 \pm 1.46\%$

$= 159{,}000 \pm 2320$

II. Electric Field Intensity, E_s

$$E_s = \frac{V_o}{r \ln (r_o/r_i)}$$

Let $R = \ln (r_o/r_i)$

$$E_s = r_i \frac{V_o}{R}$$

$$dE_s = \frac{1}{r_i R} dV_o + \frac{V_o}{R}\left(\frac{-1}{r_i^2}\right) dr_i + \frac{V_o}{r_i}\left(-\frac{1}{R^2}\right) dR$$

$$\frac{dE_s}{E_s} = \frac{dV_o}{V_o} - \frac{dr_i}{r_i} - \frac{dR}{R}$$

$R = \ln r_o - \ln r_i$

$$dR = \frac{1}{r_o} dr_o - \frac{1}{r_i} dr_i$$

$$\frac{dE_s}{E_s} = \frac{dV_o}{V_o} - \frac{dr_i}{r_i} - \frac{dr_o}{R_o(R)} + \frac{dr_i}{r_i(R)}$$

Therefore, maximum probable error is:

$$\frac{dE}{E} = \frac{dV_o}{V_o} + \frac{dr_i}{r_i} + \frac{dr_o}{r_o\left[\ln (r_o/r_i)\right]} + \frac{dr_i}{r_i\left[\ln (r_o/r_i)\right]}$$

For example,

V_o = 5000 volts $\pm$ 50 volts

r_i = 0.010 inch $\pm$ 0.0001 inch

r_o = 0.75 inch $\pm$ 0.01 inch

$$\frac{dE}{E} = \frac{50}{5000} + \frac{.0001}{.01} + \frac{.01}{(.75)\left[\ln\left(\frac{.75}{.01}\right)\right]} + \frac{.0001}{.01\left[\ln\left(\frac{.75}{.01}\right)\right]}$$

$$= .01 + .01 + \frac{.01}{.75\ (4.31)} + \frac{.01}{4.31}$$

$$= .01 + .01 + .00309 + .00232$$

$$= .02541$$

$$= 2.54\%$$

E_s = 45.6 kv $\pm$ 2.54%
45.6 kv $\pm$ 1.2 kv

APPENDIX XI

Derivation of Equation 12

Helmholtz Instability

The maximum heat flux occurs when the Helmholtz hydrodynamic instability occurs. The Helmholtz criterion[10,25] for two fluids in relative motion is:

$$c^2 = \left(\frac{N}{M}\right)^2 = \frac{\sigma M}{\rho_L + \rho_V} - \frac{\rho_L \rho_V}{(\rho_L + \rho_V)^2}\left(V_g - V_L\right)^2 \qquad (4)$$

As stated in Chapter II the condition for a stable jet requires that the wave angular frequency be real, that is:

$$c^2 = \left(\frac{N}{M}\right)^2 > 0 \qquad (5)$$

The maximum relative vapor velocity which will be stabilized by the surface tension term can now be found by equating both terms of Equation 4, thus

$$\frac{\sigma M}{\rho_L + \rho_V} = \frac{\rho_L \rho_V}{(\rho_L + \rho_V)^2}\left(V_{g_{max}} - V_{L_{max}}\right)^2 \qquad (6)$$

For a steady state condition the equation of continuity gives:

$$V_{L_{max}} = -\frac{\rho_V V_{g_{max}}}{\rho_L} \qquad (7)$$

Substituting Equation 7 into Equation 6 gives:

$$\frac{\sigma M}{\rho_L+\rho_V} = \frac{\rho_L\rho_V}{(\rho_L+\rho_V)^2}\left(V_{g_{max}} - \left(-\frac{\rho_V}{\rho_L}V_{g_{max}}\right)\right)^2 \qquad (8)$$

simplifying

$$\frac{\sigma M}{\rho_L+\rho_V} = \frac{\rho_L\rho_V}{(\rho_L+\rho_V)^2}\left(V_{g_{max}}\left(1+\frac{\rho_V}{\rho_L}\right)\right)^2$$

$$\frac{\sigma M}{\rho_L+\rho_V} = \frac{\rho_L\rho_V}{(\rho_L+\rho_V)^2}\left(V_{g_{max}}\right)^2\left(\frac{\rho_L+\rho_V}{\rho_L}\right)^2$$

$$\frac{\sigma M}{\rho_L+\rho_V} = \frac{\rho_V}{\rho_L}V_{g_{max}}^2$$

$$V_{g_{max}} = \left[\frac{\sigma M \rho_L}{(\rho_L+\rho_V)\rho_V}\right]^{1/2} \qquad (8)$$

The peak heat flux may now be obtained by relating this maximum vapor velocity (Equation 8) to the peak heat flux.

Taylor Instability

For purposes of analysis we shall consider that the vapor-liquid interface is horizontal and postulate[25] that because of

Taylor instability the interface will fail resulting in a definite two dimensional pattern of vapor jets flowing upward and liquid flowing downward. The wavelength for which instability occurs by the Taylor instability analysis[10,25] is:

$$\lambda = 2\pi \left[\frac{\sigma}{g(\rho_L + \rho_V)} \right]^{1/2} \tag{9}$$

This wavelength is then postulated by Zuber[25] to correspond to that expressed in Equation 8. Therefore combining Equations 8 and 9 and noting that $\frac{2\pi}{\lambda} = M$, there results in the following expression for the maximum vapor velocity.

$$V_{g_{max}} = \left[\frac{\sigma g^{1/2} (\rho_L - \rho_V)^{1/2} \rho_L}{\sigma^{1/2} (\rho_L + \rho_V) \rho_V} \right]^{1/2} \tag{10}$$

$$V_{g_{max}} = \left[\frac{\sigma g (\rho_L - \rho_V)}{\rho_V^2} \right]^{1/4} \left[\frac{\rho_L}{\rho_L + \rho_V} \right]^{1/2} \tag{10}$$

Zuber[25] relates the critical heat flux to the maximum vapor velocity by assuming that the interface between liquid and vapor as governed by the Taylor instability analysis breaks at the nodes giving a "unit cell" of horizontal dimensions λ. Zuber further postulates that there are released two bubbles per wavelength squared, per period. Therefore relating the critical heat flux to the vapor generated results in the following equation.

$$(Q/A)\ \text{max} = h_v \rho_v \frac{4\pi}{3}\left(\frac{\lambda}{4}\right)^3 f \frac{2}{\lambda^2} \qquad (11)$$

$$\text{Therefore } (Q/A)\ \text{max} = h_v \rho_v \frac{\pi}{24}(\lambda f) \qquad (11)$$

The product λf is then defined[25] as the critical or maximum vapor velocity (Vg max). Combining then Equations 10 and 11 results in Equation 12.

$$\frac{(Q/A)_{max}}{h_v \rho_v} = \frac{\pi}{24}\left[\frac{\sigma g(\rho_L - \rho_v)}{\rho_v^2}\right]^{1/4}\left[\frac{\rho_L}{\rho_L + \rho_v}\right]^{1/2} \qquad (12)$$

Derivation of Equation 19

Helmholtz Analysis

The maximum heat flux occurs when the Helmholtz hydrodynamic crises occurs. The Helmholtz criterion for two fluids in relative motion stressed by an electric field postulate in this study is:

$$C^2 = \left(\frac{N}{M}\right)^2 = \frac{\sigma M}{\rho_L + \rho_V} - \frac{\rho_L \rho_V}{(\rho_L + \rho_V)^2}\left(V_g - V_L\right)^2 + \frac{(\varepsilon - \varepsilon_0)^2 E^2}{(\varepsilon + \varepsilon_0)\rho_L} \qquad (13)$$

Again stating the condition for stability, namely that the wave angular frequency be real,

$$C^2 = \left(\frac{N}{M}\right)^2 \qquad (5)$$

The maximum relative vapor velocity which will be stabilized by the surface tension and electric term can now be found by equating the three terms of Equation 13 in the following manner:

$$\frac{\sigma M}{\rho_L + \rho_V} + \frac{(\varepsilon - \varepsilon_0)^2 E^2}{(\varepsilon + \varepsilon_0)\rho_L} = \frac{\rho_L \rho_V}{(\rho_L + \rho_V)^2}\left(V_{g_{max}} - V_{L_{max}}\right)^2 \qquad (15)$$

For a steady state condition, the equation of continuity gives:

$$V_{L_{max}} = -\frac{\rho_V}{\rho_L} V_{g_{max}} \qquad (7)$$

Substituting Equation 7 into Equation 15 gives:

$$\frac{\sigma M}{(\rho_L+\rho_V)} + \frac{(\varepsilon-\varepsilon_0)^2 E^2}{(\varepsilon+\varepsilon_0)\rho_L} = \frac{\rho_L\rho_V}{(\rho_L+\rho_V)^2}\left(V_{g_{max}} - \left(-\frac{\rho_V}{\rho_L} V_{g_{max}}\right)\right)$$

simplifying

$$\frac{\sigma M}{(\rho_L+\rho_V)} + \frac{(\varepsilon-\varepsilon_0)^2 E^2}{(\varepsilon+\varepsilon_0)\rho_L} = \frac{\rho_L\rho_V}{(\rho_L+\rho_V)^2}\left(V_{g_{max}}\right)^2\left(\frac{\rho_L+\rho_V}{\rho_L}\right)^2$$

$$\frac{\sigma M}{(\rho_L+\rho_V)} + \frac{(\varepsilon-\varepsilon_0)^2 E^2}{(\varepsilon+\varepsilon_0)\rho_L} = \frac{\rho_V}{\rho_L} V_{g_{max}}^2$$

Therefore,

$$V_{g_{max}}^2 = \frac{\sigma M}{(\rho_L+\rho_V)\rho_V}\rho_L + \frac{(\varepsilon-\varepsilon_0)^2 E^2}{(\varepsilon+\varepsilon_0)\rho_V} \qquad (16)$$

and

$$V_{g_{max}} = \left[\frac{\sigma M \rho_L}{(\rho_L+\rho_V)\rho_V} + \frac{(\varepsilon-\varepsilon_0)^2 E^2}{(\varepsilon+\varepsilon_0)\rho_V}\right]^{1/2} \qquad (16)$$

The peak heat may now be obtained by relating this maximum vapor velocity for the electric field case (Equation 16) to the peak heat flux.

Taylor Instability

Melcher[15] states that the wave number remains unchanged with the addition of the electric field intensity. The result of the previous analysis of the Taylor instability[10,25] gives:

$$\lambda = 2\pi\left[\frac{\sigma}{g(\rho_L-\rho_V)}\right]^{1/2} \tag{9}$$

This wave length is then postulated in this study to correspond to that expressed in Equation 16. Therefore combining Equations 9 and 16 and noting that $2\pi/\lambda = M$ there results in the following expression for the maximum vapor velocity in the presence of an electric field.

$$V_{g_{max}} = \left[\frac{\sigma^{1/2} g^{1/2} (\rho_L-\rho_V)^{1/2}}{\rho_V}\left(\frac{\rho_L}{\rho_L+\rho_V}\right) + \frac{(\varepsilon-\varepsilon_0)^2 E^2}{(\varepsilon+\varepsilon_0)\rho_V}\right]^{1/2} \tag{16}$$

As before the critical heat flux is related to the maximum vapor velocity by Equation 11 as shown below:

$$(Q/A)_{max} = \frac{\pi}{24} h_{fg} \rho_V (\lambda f) \tag{11}$$

where the product λf is defined by Zuber[25] as the maximum vapor velocity ($V_{g\ max}$). Combining then Equations 11 and 16 results in Equation 19 shown below.

$$\frac{(Q/A)_{max}}{h_{fg}\rho_V} = C\left[\frac{\sigma^{1/2} g^{1/2} (\rho_L-\rho_V)^{1/2}}{\rho_V}\left(\frac{\rho_L}{\rho_L+\rho_V}\right) + \frac{\varepsilon_0 (K-1)^2 E^2}{\rho_V (K+1)}\right]^{1/2} \tag{19}$$

NOMENCLATURE

A	= area, ft^2
C	= wave velocity of propagation, ft/s
D	= diameter, ft.in.
E,Es,Eeq.	= electrical field intensity, kv/cm
f	= frequency, $\frac{1}{s}$ reciprocal seconds
g	= gravitational acceleration, ft/s^2
h_v	= latent heat of vaporization, Btu/lb
K	= dielectric constant, dimensionless
L	= length, ft., in.
M	= wave number, ft^{-1}
N	= wave angular frequency 1/s reciprocal seconds
Q	= heat transfer rate, $Btu/hr.ft^2$
r	= radius, in.
r_w, r_o	= wire radius, radius of outer electrode in.
T	= temperature, °F, °C
V	= velocity, ft/s
V_o	= voltage, volts

Greek Letters

ε = inductive capacity, $coul^2/newton\text{-}m.^2$

ε_o = inductive capacity of free space (vacuum), $coul^2/newt\text{-}m.^2$

μ = viscosity, $lb_m/ft.sec.$

ρ = density, $lb_m/ft.^3$

σ = surface tension, $lb_f/ft.$

Δ = difference

Subscripts

eq. = equivalent

max. = maximum

o = outer or reference value

s = surface

v,g = vapor, gas

1,2 = reference subscripts for constants

L = liquid

LITERATURE REFERENCES

1. Asch, V., "Electrokinetic Phenomena in Boiling Freon 113." Journal of Applied Physics, Vol. 37, June, 1966, pp. 2654-2658.

2. Baboy, N.F., Bologa, M.K., Semonev, K.N., "Effect of Electrical Fields on Heat Exchange in Liquids and Gases", Electronic Treatment of Materials, U.S.S.R., Vol. 1, 1965, pp. 57-71.

3. Bonjour, E., Verdier, J., Weil, L., Chemical Engineering Progress, Vol. 58, 1962, pp. 63-66.

4. Chandrasekhar, Hydrodynamics and Hydromagnetic Stability, Oxford Press, 1961, pp. 511.

5. Choi, H.Y., Electrohydrodynamic Boiling Heat Transfer Ph.D. Thesis, Massachusetts Institute of Technology, Cambridge, Massachusetts, April 5, 1962.

6. Devitt, E.B., Melcher, J.R., "Surface Electrohydrodynamics with High Frequency Fields", Physics of Fluids, Vol. 8, 1965, pp. 1193.

7. Durfee, R.L., Nichols, C.R., Spurdock, J.M., Markels Jr., M., Boiling Heat Transfer with Electrical Fields (EHD) NYO-2404-76, United States Atomic Energy Commission, Contract No. AT(30-1)-2404, Summary Report, (1960-1963), and Final Report.

8. "Freon" Technical Bulletins issued by Freon Products Division, E.I. Dupont de Nemours and Co., Wilmington, Delaware.

9. Kutateladze, S.S., Izo. Akod. Nauk. U.S.S.R., Otd. Tekh. Nauk, No. 4, 1951, pp. 529.

10. Lamb, H., Hydrodynamics, Cambridge University Press, 6th edition, 1932, pp. 461.

11. Leppert, G., Pitts, C.C., "Boiling", Advances in Heat Transfer, Vol. 1, Academic Press, 1964, pp. 232-240.

12. Lyon, J.F., Electrohydrodynamic Kelvin-Helmholtz Instability, S.M. Thesis, Massachusetts Institute of Technology, Cambridge, Massachusetts, 1962.

13. Malkus, W.V.R., Veronis, G., "Surface Electroconvection", Physics of Fluids, Vol. 4, 1961, pp. 13.

14. Markels Jr., M., Durfee, R.L., "The Effect of Applied Voltage on Boiling Heat Transfer", A.I.Ch.E. Journal, Vol. 10, No. 2, January 1964, pp. 106-10.

15. Melcher, J.R., Field Coupled Surface Waves; A Comparative Study of Surface Coupled EHD and MHD Systems, M.I.T., Press, Cambridge, Massachusetts, 1963.

16. Moisses, R., Berenson, P., A.S.M.E. Transactions, Journal of Heat Transfer, Vol. 85, 1963, pp. 221.

17. Ostrach, S., Koestal, A., "Film Instabilities in Two Phase Flows", Chemical Engineering Symposium Series 57, Vol. 61, 1965, pp. 153-163.

18. Pohl, H.A., "Some Effects of Non-Uniform Fields on Dielectrics", Journal of Applied Physics, Vol. 29, 1958, pp. 1182-8.

19. Rohsenow, W.M., "Heat Transfer with Boiling", Modern Developments in Heat Transfer, ed. Ibele, pp. 85-158.

20. Schmidt, E., Lindenfrost, W., Forsch, Gebiete Ingenieurev, Vol. 19, 1953, pp. 65.

21. Senftleben, H., Braun , W., Z. Physik, Vol. 102, 1936, pp. 480.

22. Temperature - Its Measurement and Control in Science and Industry, Reinhold, N.Y., 1941.

23. Timmermans, J., Physico - Chemical Constant of Pure Organic Compounds, Vol. II, Elsevier Publishing Co., 1965.

24. Tong, L.S., Boiling Heat Transfer and Two Phase Flow, John Wiley and Sons Inc., 1965, pp. 22-25, pp. 36-45.

25. Zuber, N., A.S.M.E. Transactions, Vol. 80 1958, pp. 711.

26. Zuber, N., Tribus, M., Report No. 58-5, U.C.L.A., Department of Engineering, January 1958.

27. Personal Communication.

VITA

Ronald Francis Lovenguth was born in , in . He received his B.S. Ch.E. from the Newark College of Engineering in 1963. Upon graduation in 1963 he was the recipient of a three year NDEA Fellowship at Newark. He received his M.S. Ch.E. at Newark in 1964. In 1966 he was awarded an American Cyanamid Fellowship. He is a member of Tau Beta Pi, and of Omega Chi Epsilon. He is married and has one daughter.

He is presently employed by the Celanese Plastics Company of Clark, New Jersey.